THESE

en cotutelle
Pour l'obtention du Grade de

DOCTEUR DE L'UNIVERSITE DE POITIERS
Faculté des Sciences Fondamentales et Appliquées
(Diplôme National - Arrêté du 7 août 2006)

Ecole Doctorale : Sciences et Ingénierie en Matériaux, Mécanique, Energétique et Aéronautique

et de

DOCTOR AL UNIVERSITATII TEHNICE « GHEORGHE ASACHI » IASI
Facultatea de Electronica, Telecomunicatii si Tehnologia Informatiei

Secteur de Recherche : Sciences pour l'ingénieur
Spécialité : Génie électrique

Présentée par :

.....................................**Angela VASILUT ANTONIU**......................................

****

CONTRIBUTIONS TO THE STUDY OF CERTAIN ELECTROSTATIC HAZARDS IN THE MANUFACTURING PROCESS OF ELECTRONIC DEVICES AND CIRCUITS

****

Directeurs de Thèse : Lucian DASCALESCU et Horia-Nicolai TEODORESCU

****

Soutenue le 17 novembre 2010 (date provisoire)

devant la Commission d'Examen

****

JURY

M. **Serge AGNEL**, Professeur, Université de Montpellier II	Rapporteur
M. **Adrian SAMUILA**, Professeur, Université Technique de Cluj-Napoca	Rapporteur
M. **Lucian DASCALESCU**, Professeur, Université de Poitiers	Examinateur
M. **Horia-Nicolai TEODORESCU**, Professeur, Université Technique de Iassy	Examinateur

La scris, gand bun si slobod trebuieste

Miron Costin

TABLE OF CONTENT

Everything should be made as simple as possible, but not simpler.

Albert Einstein

INTRODUCTION

I have frequently been questioned, especially by women, of how I could reconcile family life with a scientific career. Well, it has not been easy.

Marie Curie

The prevention of ElectroStatic Discharges (ESD) effects on electronic devices is a field of study that has reached maturity in the last three decades. These improvements in the control methods have been offset by the aggressive scaling of silicon technologies which presents a scenario where the component level ESD protection designs become more challenging. The researchers and engineers working in this field have been continuously and successfully developing new techniques that keep up with the emerging electronic circuit manufacturing technologies and architectures, characterized by shrinking chip areas, increasing component density and higher operating frequencies. Despite the remarkable advances achieved during the recent years, the adopted solutions and the present qualification testing standards leave room for ESD susceptibility with considerable consequences on the production yield and product failure in the field. [1]-[25] The characterization of such susceptibility is particularly important and not fully mastered in some manufacturing environments out of the clean room, where uncontrollable factors, combined with sources of high electrostatic charge levels, are inherently present. The need for constantly improving the control methods to keep up with the Integrated Circuits (IC) technologies is established by the ESD Technology Roadmap [1].

The scope of this thesis is three-fold. It primarily aims at bringing advances in the area of static charge characterization of non-woven textile materials in the manufacturing process, in view of the evaluation of the potentially hazardous effects their accumulated charge may have on the operation of nearby electronic equipment. Further, the thesis aims at proposing practical methods of static charge reduction for the situations in which the charge monitoring devices indicate hazardous levels. Last but not least, the present work aims at drawing attention to the routinely ignored ubiquitous electrostatic charging during the rather new field of manufacturing processing of Si-based Micro-Electro Mechanical Systems (MEMS) in clean rooms.

The orientation of the thesis to these topics was suggested by the author’s own experience in research laboratory, industrial research and by multiple professional contacts with electronic circuit manufacturers. Much too often, the researchers and engineers attribute the malfunctioning of their devices to “obscure” or inexplicable phenomena, without attempting a minimal characterization of the electrostatic charge accumulation during manufacturing or packaging processes. Based on this observation, the present work was driven by the belief that proper characterization methods of the electrostatic charging of materials during the manufacturing processes would be a major step forward in minimizing hazards to both the neighbouring electronic equipment and the final product into which such materials are incorporated. Last but not least, the implementation of rigorous characterization methods could, in some cases, open the path to further securing the safety protocols to be observed by the operators.

Driven by these believes, **Chapter 1** presents the state of the art in the field, as well as facts derived from author’s engineering practice that support the rationale of the work, and justify the angle of view from which the topic is approached.

Chapter 2 describes the measurement methods and scientific instrumentation employed for the experimental investigations. It also outlines several practice-based, methodological conclusions.

Chapter 3 exposes several techniques that have been used to assess the electrostatic charging and discharging of textile materials. The results are analyzed in relation to the measuring methods and setups previously detailed in Chapter 2.

Models for the charging and discharging of the textiles under various conditions are presented and discussed in **Chapter 4**. A couple of methods for monitoring and fast reduction of the electrostatic charge on non-woven materials during the industrial processing of air filters are tested, as the charge can easily exceed the “safe” levels in these cases.

In **Chapter 5**, the aforementioned example of charge accumulation during a common silicon wafer process is discussed, and the effect on a final microelectronic mechanical system product is shown.

The major contributions and achievements of this thesis are outlined in the general conclusion section. Finally, future work directions are suggested and discussed.

1. THESIS BACKGROUND

The triumph of science has been mainly due to its practical utility.

Bertrand Russell

The purpose of this chapter is to provide a succinct background of the present work, and explain its rationale. The last three decades of remarkable advances in chip technology, that is the increase the density of circuits on a device as well as the processing speed, demanded the engineering research in ESD protection design to keep up with these new challenges, in order to ensure reliability. Researchers all over the world, spanning from academia to industry, have been rallying their efforts to ensure circuit protection and environment static control solutions, more too often through overdesign, in order to meet the one decade old quality standards. For circuits to be protected, and for users to prevent apparatus overstress and failure, a considerable amount of literature has been published. [8]-[10], [13]-[14], [16]-[50] At the same time, a lot of solutions have been applied but not published by the chip industry.

1.1 ESD hazards in electronic industry

Static electricity became a problem for the film industry in the 40’s and 50’s and for the electronic industry in the 50’s and 60’s. It became more and more critical in the 70’s for advanced electronic circuits. The Official ESD Symposium was first organized only in the late 70’s. The ESD awareness started becoming prevalent with the introduction of thin gate oxide FET devices for high performance IC technologies. Today, ESD is a major issue for many electronic organizations.

As the state of the art brings us to the realm of nanotechnology, the importance of understanding and controlling electrical overstress and electrostatic discharge becomes increasingly important. The 1-mm line width devices, which were the standard in late 1990's, required that voltage buildup due to triboelectrification and charge accumulation be kept below levels in the tens of volts. As the size of devices decreased, this voltage limit fell as well. Some of the earlier estimates [5], [24]-[25], [28]-[29], [35]-[36], [44]-[47], [50]-[53] predicted that by 2010 voltage levels in excess of one volt will be considered detrimental to some classes of electronic devices, are becoming reality. This sub-chapter will define ESD, show the models and their associated standard voltage levels, and briefly exemplify the types of damages in electronic industry.

1.1.1 Definition of ESD

ESD is defined as the transfer of electrostatic charge between bodies at different caused by direct contact or induced by an electrostatic field. To understand ESD, we review a few concepts about static electricity.

Table 1-I. Electrostatic triboelectric series [8]-[10], [15]-[16], [19]

Most **positively charged**
+
Human skin (Hands), Leather
Glass
Human hair
Nylon, Wool, Silk
Aluminum
Paper (Small positive charge)
Cotton (No charge)
0
Steel (No charge)
Wood (Small negative charge)
Acrylic, Polystyrene
Nickel, Copper, Silver, Gold, Platinum
Rayon, Synthetic rubber
Polyester
Polyurethane, Polyethylene
Polypropylene
Vinyl (PVC)
Silicon
Teflon
–
Most **negatively charged**

We know that when two bodies are rubbed against each other, transfer of charge takes place very rapidly. The body that loses electrons becomes positively charged while the one that receives it becomes negatively charged. Since charge is transferred, one can say that electricity is generated. This generation of electricity due to transfer of charges is called triboelectric effect. Static electricity can also be generated when two objects in contact are suddenly separated from each other.

Activities such as walking across the floor, standing up from a chair, packaging of ICs can generate static electricity. In order to understand the generation of charge that takes place in the latter examples, a triboelectric series, as in Table 1, is considered. [8]-[10], [12]-[20], [22]-[23] The "positive" materials in the series will capture positive charge each time they come in contact with materials from the lower side of the scale.

1.1.2 ESD models

In the previous paragraph, we defined ESD as the sudden discharge of a charged body either through direct contact or through induced charging. The ESD damage is often caused by human handling of the chips (Human Body Model or HBM), robotic handling in assemblies (Machine Model or MM) and charge of the package itself (Charged Device Model or CDM). Although in this work only studies using the HBM model were performed, a review of the CDM is also important, as in the production line where high levels of static charge is present, the discharge through this mechanisms is equally possible. Therefore, it is important to show all the main mechanisms through which the charging in the textile material manufacturing can create electronic failure in the field. However, the MM model will not be discussed here, as the latest reports from industry [1]-[3] suggest the redefinition in the future of this particular model. The most relevant and important ESD models used by device manufacturers as part of the device qualification process are the HBM and CDM.

Human Body Model

A variety of human body models are presented in literature [2], [8]-[20], [22]-[25], [30], [36], [45], [47], [49]-[51], [54]-[65]. The RC series model has been found adequate for the present work. This model is simple and accurate enough to test our method and enable relevant results.

In this model, the human body is assumed a conductive media of electrolyte type, which is modeled as a resistor [66]. The body resistor in series with the equivalent capacitance of the person with respect to the ground represents the model of the personnel in the HBM. An example of HBM ESD mechanism is given in Figure 1.1. When a highly static charged person, or any object for that matter, approaches a piece of electronic equipment, (AE in Figure 1.1) a discharge can take place. This discharge creates a current pulse which can damage the devices in its path.

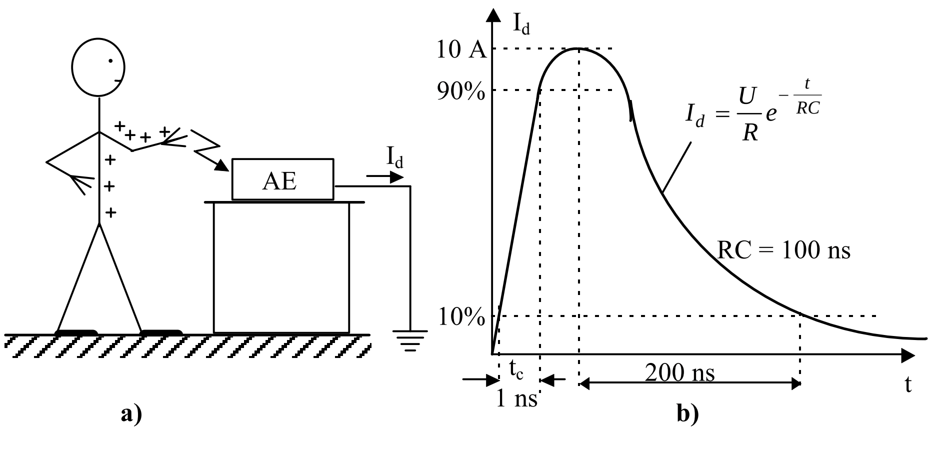

Figure 1.1. ESD. a) HBM discharge. b) Discharge current waveform. [67].

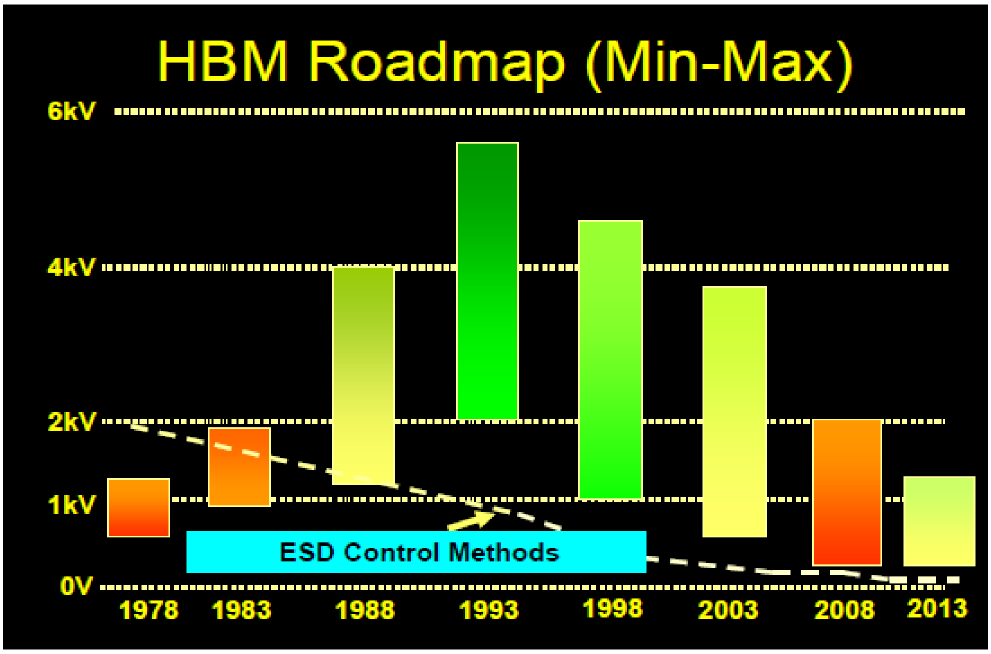

Figure 1.2. Human Body Model sensitivity limits projection. [1]

The graph in Figure 1.2 shows the present device ESD design sensitivity trends based on the HBM model [1]-[2].

The indicated min-max sensitivity limits are a projection by engineers from leading semiconductor manufacturers. Also shown is the progression of ESD control capability for HBM during the same time period. The max levels represent what is generally possible from technology scaling and min represents the constriction coming from meeting the circuit performance demands. It is interesting to observe that the gap between the ESD control and sensitive device HBM levels is closing in, and that the control of ESD for HBM is just barely below the minimum expected high sensitivity HBM designs at the beginning of this new decade. Therefore, implementation of advanced HBM controls using the limits and qualifications requirements in ANSI/ESD S2020 or IEC 61340-5-1 standards would become necessary within the next five years. [1]

The Charged Device Model

CDM damage occurs when a charged ESD sensitive device is grounded or when a neutral device is grounded in the presence of an electrostatic field. This makes the CDM model also valid for Field-Induced Model (FIM) for both field-induced charged device (FCDM or FICDM) and field-induced charged board (FCBM or FICBM). As previously mentioned, CDM is one of the two very useful models for ESD analysis in industry. Therefore, much literature is published each year regarding ESD analysis using this model. [1], [3], [7]-[25], [30], [36], [45], [47], [49]-[51], [58]-[59], [61]-[63], [68].

In recent years, arbitrary CDM protection levels have been specified as IC qualification goals with little background information on actual/realistic CDM event levels and the protection methods available in device design for safe production of IC components. The rapid advancement of IC technology scaling, coupled with the increased demand for high speed circuit performance, are making it increasingly difficult to guarantee the commonly customer “500V” CDM specification. At the same time, the required static control methods available for production area CDM protection at each process step have not been fully outlined. Therefore, a realistic CDM specification target must be defined in terms of available and commonly practiced CDM control methods, and also must reflect current ESD design constraints. [3]

Table1 -II. Recommended CDM classification based on factory CDM control. [3]

CDM classification level (tested acc. to JEDEC)	ESD control requirements
$V_{CDM} \geq 250V$	• **Basic ESD control methods** with grounding of metallic machine parts and control of insulators
$125V \leq V_{CDM} < 250V$	• **Basic ESD control methods** with grounding of metallic machine parts and control of insulators + • **Process specific measures** to reduce the charging of the device **OR** to avoid a hard discharge (high resistive material in contact with the device leads).
$V_{CDM} < 125V$	• **Basic ESD control methods** with grounding of metallic machine parts and control of insulators + • **Process specific measures** to reduce the charging of the device **AND** to avoid a hard discharge (high resistive material in contact with the device leads) + • **Charging/discharging measurements at each process step.**

The table above is the projection of CDM levels based on extensive manufacturing industry study. It is considered by the industry council that a safe and practical CDM passing level of 250V is realistic in the realm of increased processing speed and extended packaging size. The Council strongly recommends that products with a CDM level lower than 250V should implement additional process-specific measures for CDM control, especially during product ramp-up. [1], [3].

Again, this trend places increased responsibility in the hands of the users to both implement tighter control programs and to reduce the charging on the device/apparatus. This means that environment static charging control becomes more so important, which, again, justifies the pursuit of this work.

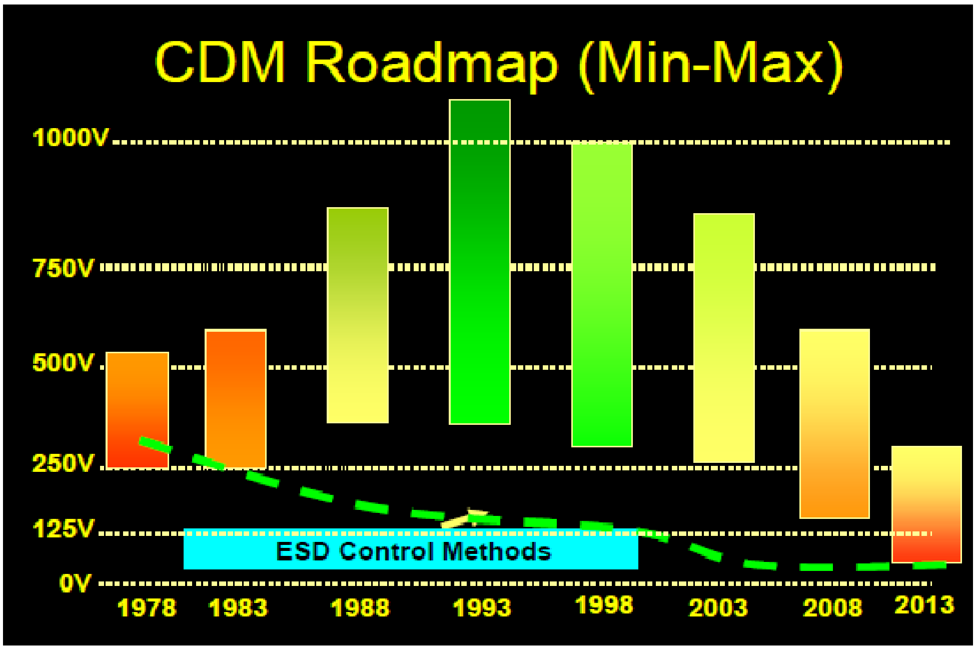

Figure 1.3. Charge Device Model sensitivity limit projection

In the projection of the CDM sensitivity levels (min and max) indicated in Figure 1.3, also shown is the progression of ESD control capability for CDM during the same time period. The same general arguments as given above for HBM also apply for CDM. However, the advanced designs will have a larger impact on CDM. This is because the HSS IOs (High Speed Serial Links) are generally used in high pin-count, hence larger capacitance, IC packages. This higher capacitance leads to relatively higher magnitude discharge peak current levels, and thus greater challenges in CDM protection design. A proactive implementation of advanced CDM controls would not only become necessary but would become mandatory within the next five years. [1], [3].

1.1.3 Types of damages and protection

Due to ESD pulses, usually the IC chips become damaged at the Input/Output (I/O) signal pins; the failure appears as thermal damage to the transistors. Other failures are due to:

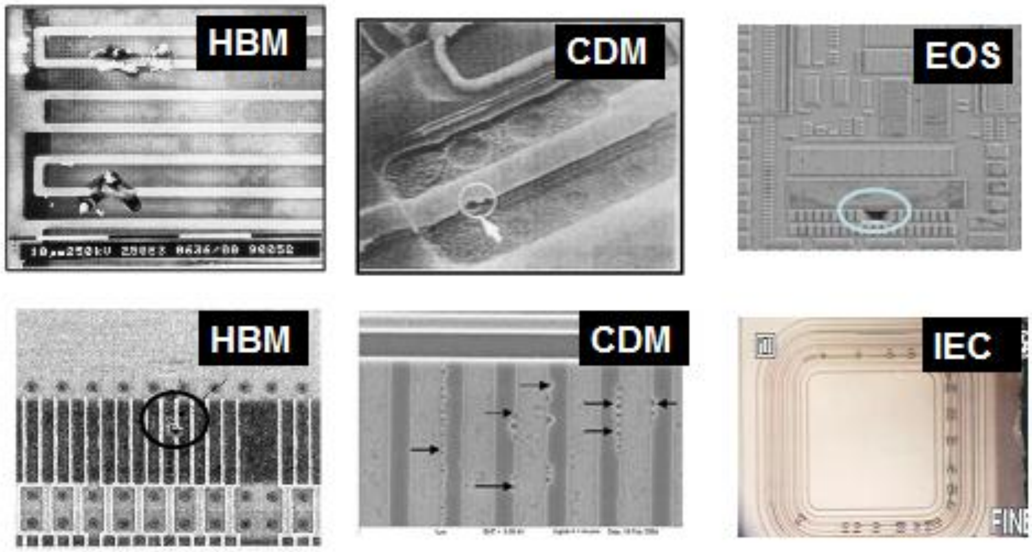

Figure 1.4. Examples of IC ESD damages. [5]

(1) oxide breakdown of the transistor gates;

(2) system board level ESD stress, known as IEC stress,

(3) customer application stress, known as electrical overstress or EOS. [1]-[3], [5], [8]-[11], [13]-[25], [34].

These two latter threats are of particular interest for further emphasizing the importance of this work, as they can occur in the production line where high levels of charge can be present.

In advanced CMOS technologies, circuitry which connects directly to I/O pads are often most at risk of damage during a CDM ESD event [1], [3]. Therefore, from the user's stand point, it is important to ensure charging and discharging at each manufacturing step and prevention measures should be taken to avoid the possibility of hard discharges, which is what this work attempts to accomplish for the particular case of the production line of the textile manufacturing.

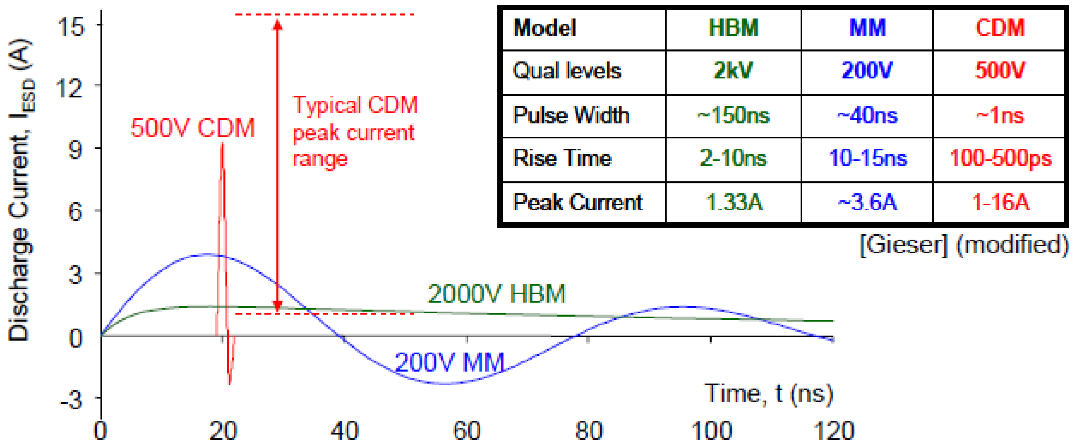

Model	HBM	MM	CDM
Qual levels	2kV	200V	500V
Pulse Width	~150ns	~40ns	~1ns
Rise Time	2-10ns	10-15ns	100-500ps
Peak Current	1.33A	~3.6A	1-16A

Figure 1.5. Comparison of current waveforms for CDM, MM, and HBM ESD events. [3]

While component ESD stress levels are typically defined in terms of a stress voltage (2000V HBM and 500V CDM), designers consider the ESD event in terms of the resulting current waveform (Figure 1.5). Elements in ESD protection circuits and ESD conduction paths are sized based on a target peak stress current and duration. In general, if the target peak current increases, the ESD elements and conduction paths must be increased in size accordingly. [3]

In the literature [8]-[20], the aforementioned types of stress or failures have been sub-classified, as not all failures are instantaneously damaging; some are latent/functional. In the immediate failure, the effect can be readily seen by the equipment manufacturer or user. In the delayed failure, the device is damaged only up to the point where it may pass quality control tests, or it may keep functioning for, but it wears out sooner than its rated time.

It is very difficult to determine the point at which the damage due to ESD occurs, since it can take place anytime during the manufacturing process, assembly, testing, packing and shipping. ESD control program that protects the device right from the manufacturing plant to the retailer and the user are therefore paramount. Some protective guidelines used in ESD control are established, [1]-[3], [7], [10], [12], [19]-[20], [69]-[72]:

a. Most workstations are provided with measures such as conductive table mats, wrist bands, conductive flooring, as protection of components from damage due to electrostatic charge on the body.

b. Air ionizers are operated in ESD protective areas to neutralize static charges on non-conductive materials used in the manufacturing lines.

c. All test and soldering equipment is provided with ground potential and is periodically inspected.

d. Anti-static foams are used during storage and transportation in order to protect ESD sensitive devices instead of ordinary plastic foams.

e. A number of monitoring devices, such as electrostatic alarms, electrostatic voltmeters and field meters are used to measure and control static charge on materials.

Despite high initial costs, most device and electronic apparatus companies have profited considerably by implementing ESD prevention programs. However, with the increase in device sensitivity, much of the responsibility in controlling the charging levels in the environment where the apparatus/devices are utilized is placed in the hands of the user.

1.2 Electrostatic measurements

1.2.1 ESD detection

ESD discharges induce voltages in the nearby circuits. When ESD occurs, the discharge time is usually 10 nanoseconds or less. Discharging energy in such a short interval results in the generation of broadband electromagnetic radiation, as well as in heat that damages electronic components. [3], [6]-[7], [10], [22]-[25], [29], [31], [33]-[34], [40], [47], [73]-[83]. This electromagnetic radiation—especially in the 10 MHz to 2 GHz frequency range—can affect the operation of production equipment. Much of today's complex equipment is controlled by microprocessors that operate in the same frequency range as the EMI from ESD events. ESD events cause a variety of equipment operating problems including stoppages, software errors, testing and calibration inaccuracies, and mishandling, all of which can cause physical component damage. To detect such events, EMI locators are used.

In the last years, with the advancements achieved in high frequency instrumentation, such as oscilloscopes of up to 20 GHz bandwidth, it has become easier to detect ESD events through a high frequency antenna connected at the input of a GHz bandwidth oscilloscope. A simple test at various distances from the field source could give a good indication of the ESD and EMI (Electromagnetic Interference) present in the respective environment. The schematic of the test is similar to the representation in Figure 1.5. A recorded set of waveform, obtained from three antennas, is depicted from literature. This aspect is not addressed in this work. However, since the manufacturing of filters is susceptible to ESD events, such testing can be important.

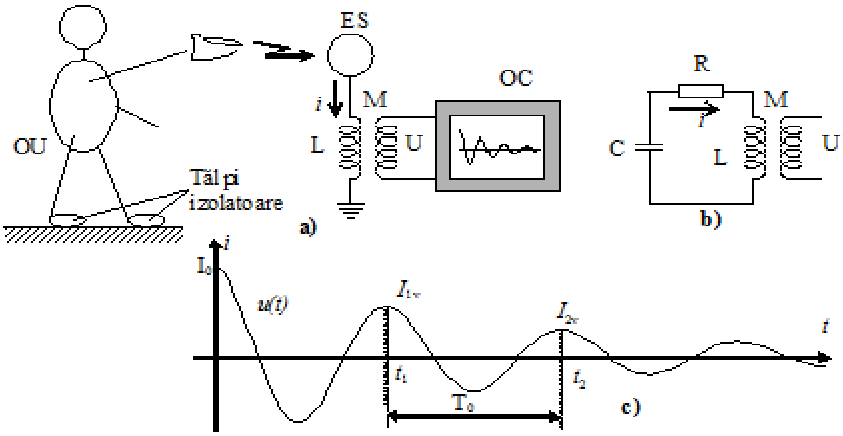

Figure 1.6. ESD and EMI; Discharge current measurement. [67]

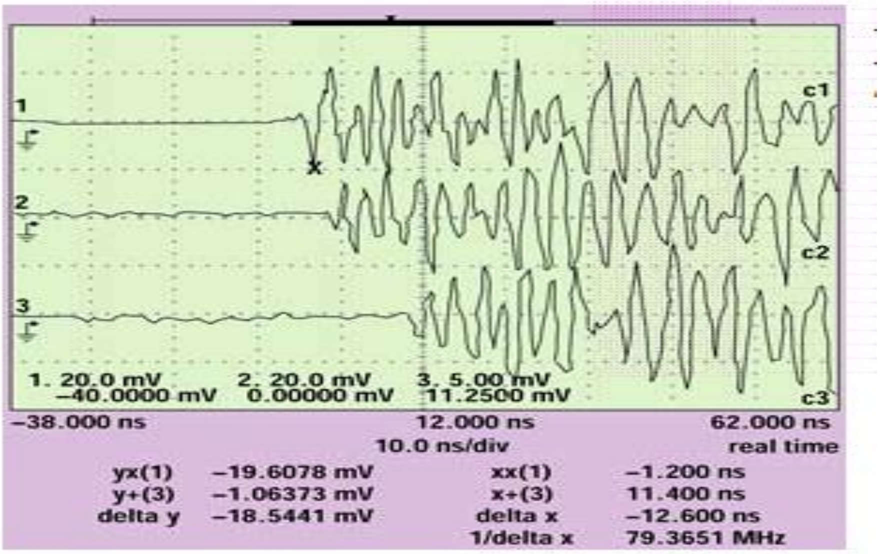

Figure 1.7. Example of radiated EMI from a CDM ESD event detected by a set of three antennas. Source: Joe Bernier at Intersil. Cited by [78]

1.2.2 Charge measurement

The Faraday pail is a shielded cup with attached electrometer for directly measuring the charge on any object dropped into it. This device is used for the measurement of the static charge on ICs, or on any charged object, including textile materials [16], [20], [78], [84]-[88].

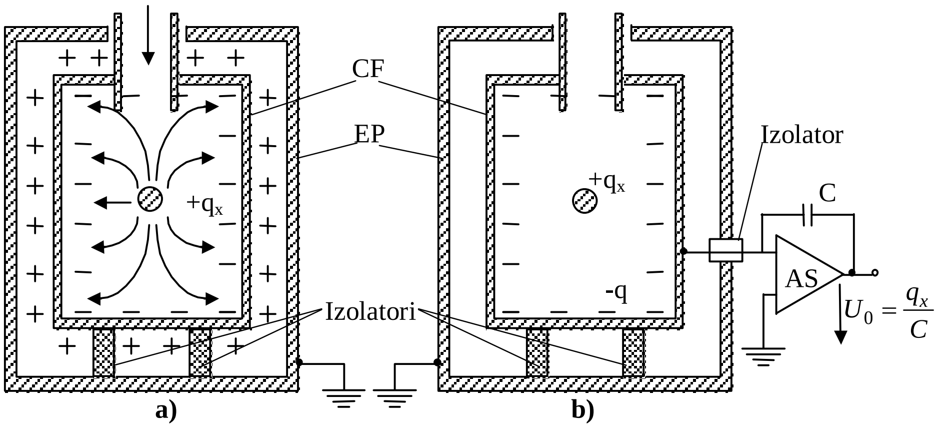

Figure 1.8. Faraday cup. a) principle b) measurement. [67]

The principle of the Faraday cup is illustrated in Figure 1.8. The cup CF is a metallic cylinder, insulated with respect to the ground, and EP is the protective shield. The charge to be measured, $+q_x$, induces negative charging at the interior of the metallic wall of the cup CF. Consequently, on the exterior surface of the cup positive charges appear. These charges can be measured with an electrometer.

1.2.3 Surface potential and electric field measurements

One of the very common methods of monitoring the static charge of a dielectric film is by measuring the potential decay at its surface [84], [87], [89]-[111]. The other method is by measuring the electric field created at the surface of the charged body [84], [87], [90], [93], [107]-[114].

Regardless of the particular circuitry solution employed [22]-[23], [62], [84], [87]-[91], [115]-[118], the instruments for the measurement of the electric field are built on the same basic principle (Figure 1.9).

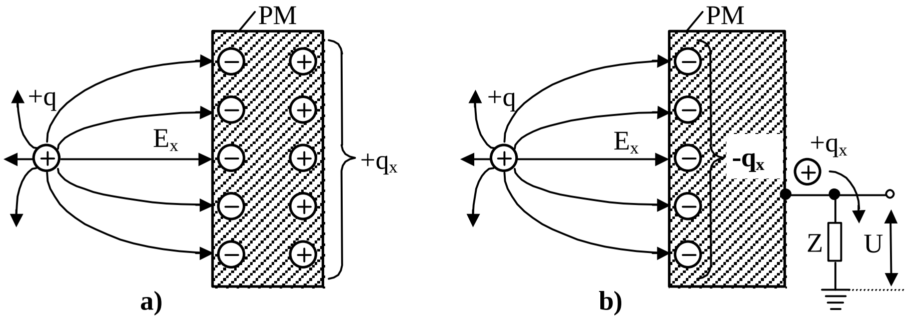

Figure 1.9. Metal plate charged through induction. a) insulated, b) induction probe. [67]

A metal plate (PM) placed in the electric field of a positive charge, +*q*, charges through induction as in Figure 1.9.a, with negative charge on the side towards the source +*q* and positive charge on the opposed side. However, if PM is connected to the ground as in Figure 1.8.b, the positive charges flow to the ground and only the negative charges are left. Thus, in a grounded metal plate in an electric field, positive charges induce negative charging and, reversely, negative charges induce positive charging. For a plate of surface *S*, the induced charge by the field of intensity E_x is given by the equation:

$$q_x = \sigma_x \cdot S \tag{1.1}$$

where

$$\sigma_x = \varepsilon_r \cdot \varepsilon_0 \cdot E_x \tag{1.2}$$

is the uniformly distributed charge density on the plate. In (1.2), ε_r is the relative permittivity of the material between the plate and the charged object under test and ε_0 = 8.86 10^{-12} F/m is the vacuum permittivity. As E_x propagates through air, ε_r = 1 and hence:

$$q_x = \varepsilon_0 \cdot S \cdot E_x \tag{1.3}$$

On the path through the ground, the charge q_x moves through the impedance (Z). This creates a voltage drop (U) proportional to q_x and hence with E_x. The recorded value for U~E_x [67], [119]-[121].

In the following examples [90] of fieldmeter and electrostatic voltmeters, the detecting element is a vibrating capacitive sensor. In this configuration, an electric current I is induced in the sinusoidally vibrating sensor. :

$$I = U\frac{dC}{dt} = U\frac{d}{dt}\left(\frac{\varepsilon_r\varepsilon_0 S}{d_0 + d_1\sin(\omega t)}\right) = -U\varepsilon_r\varepsilon_0 S\frac{d_1\omega\cos(wt)}{\left[d_0 + d_1\sin(\omega t)\right]} \tag{1.4}$$

U is the difference of potentials between the tested surface and the vibrating probe, [V],

d_0 is a constant representing the separation between the electrode and the charged surface under test when the electrode is not vibrating, [m],

d_1 is the amplitude of vibration, [m], and ωt is the circular frequency of vibrations, [rad/s].

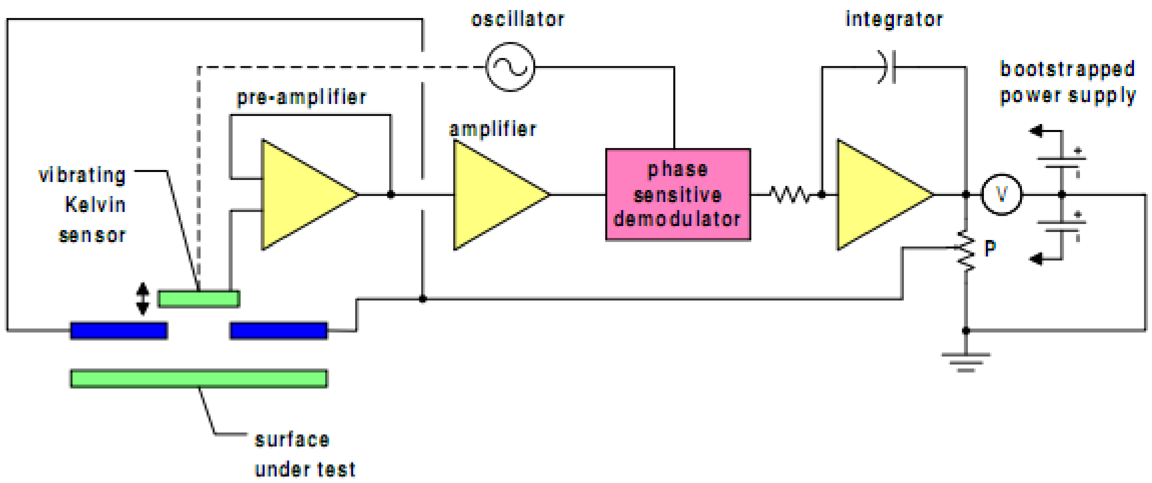

Figure 1.10. Electrostatic fieldmeter [90].

Figure 1.10 presents an electrostatic fieldmeter. A fraction of the detected and processed voltage V_p is inverted and fed back to a screening electrode. At this point the sensing electrode is influenced by two electric fields: one created by the tested surface and one generated by the screen. Therefore, the greater the surface voltage, the greater is the inverted voltage on the screen. Fields created by these two voltages cancel each other. Potentiometer P is used to establish a constant ratio between Vs and the measured voltage V_p. When the sum of the two fields equals zero, the stability of the signal detected by the vibrating sensor is greatly enhanced. However, the potential difference between the surface and the sensor can lead to the discharge and damage of the equipment if spacing d_0 becomes too small. The value of measured V_s is also sensitive to the changes of the distance d_0. [90] As mentioned before, other circuitry solutions are employed to ensure accuracy [116]-[117].

The following paragraphs are concerned with electrostatic voltmeters. Many voltage measurement applications cannot be made using conventional contacting voltmeters because they require charge transfer to the voltmeter, thus causing loading and modification of the source voltage. For example, when measuring voltage distribution on a dielectric surface, any measurement technique that requires charge transfer, no matter how small, will modify or destroy the actual data. In these types of applications a new approach to voltage measurement is needed [87], [90]

An instrument that measures voltage without charge transfer is called an electrostatic voltmeter. A primary characteristic of non-contact electrostatic voltmeters is that they accurately measure surface potential (voltage) on materials without making contact and, therefore, no electrostatic charge transfer and loading of the voltage source can occur [89],[90], [91].

In practice, an electrostatic charge monitoring probe is placed close to the surface to be measured. Electrostatic voltmeters function to drive the potential of the probe body to the same potential as the measured unknown. This achieves a high accuracy measurement that is virtually insensitive to variations in probe-to-surface distances, as well as preventing arc-over between the probe and measured surface. [90], [92], [93].

An example of the electrostatic voltmeter circuit is shown in Figure 1.11. In this voltage-follower device the output of the integrator drives a high voltage amplifier circuit to replicate the voltage on the tested surface. The amplified voltage is then applied to the sensor thus nullifying the electric field between the tested surface and the sensing electrode. Potential on the electrode "follows" the potential on the surface. In this case there is no threat of the eventual discharge between the probe and the surface under test, even at close spacing. This ability of following the voltage makes the electrostatic voltmeter measurement independent of the distance d_0 at least within a certain range of d_0. If the span between the surface and sensor is too big, the probe becomes influenced by other electric fields present in the vicinity [84], [87], [90].

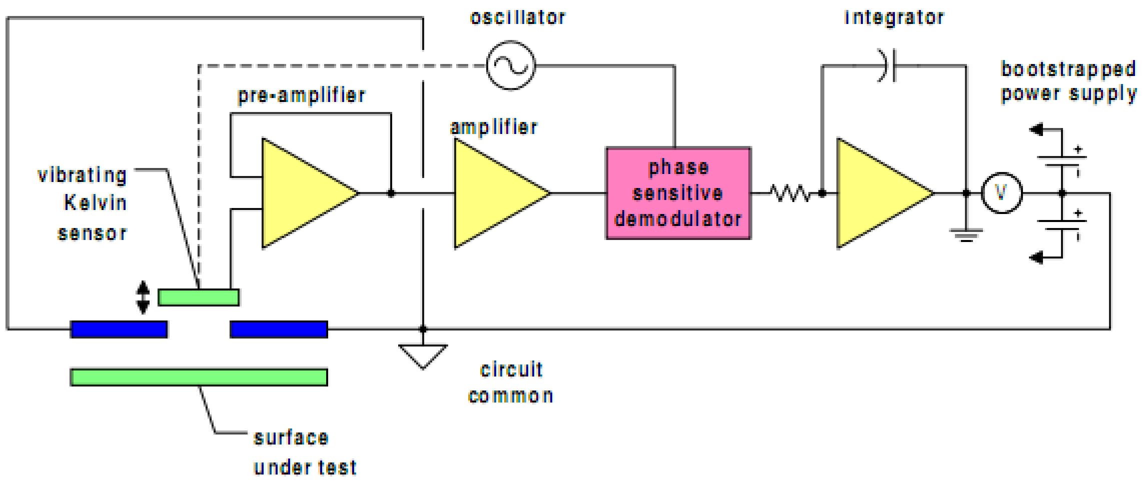

Figure 1.11. Electrostatic voltmeter (voltage follower). [90]

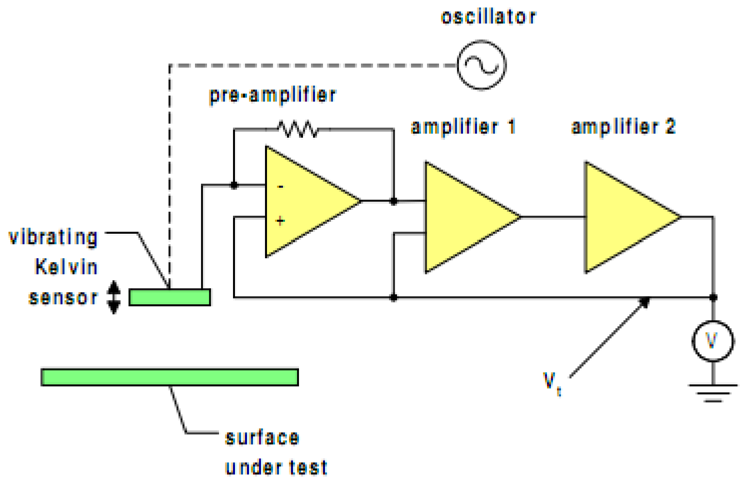

Figure 1.12. AC-feedback electrostatic voltmeter. [90]

The AC-feedback in voltmeter Figure 1.12 uses a different technique to achieve spacing independent surface voltage-charge measurements. Rather than cancelling the Kelvin current *I* by use of a feedback DC voltage which follows the surface test voltage to produce zero electric field, the AC feedback method utilizes a nullifying current I' to zero the Kelvin current *I*. The current I' is produced by external generator circuit tuned to the frequency of the Kelvin sensor oscillations:

$$I' = C\frac{dV_t}{dt} \tag{1.5}$$

Therefore, when currents I and I' cancel each other, $I = I'$,

$$U\frac{dC}{dt} = C\frac{dV_t}{dt} \tag{1.6}$$

As both I and I' currents are inversely proportional to spacing d_0, the ratio of the amplitude of V_t to U (the DC test surface voltage) remains constant over the large range of d_0. As shown in Figure 1.11, the Vt signal is obtained by amplification of the current I converted to a voltage at the preamplifier. At high gain, the current I is being cancelled to a very small value.

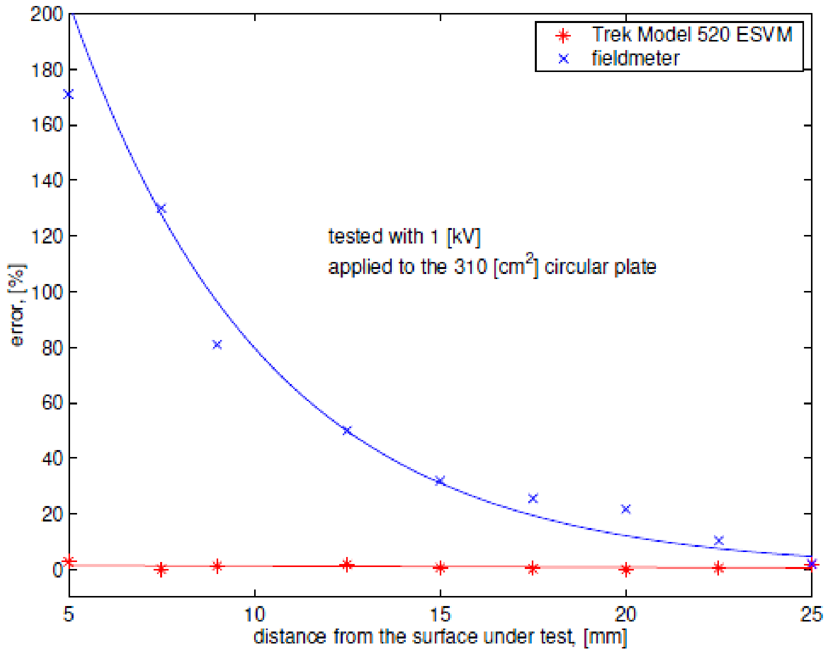

Figure 1.13. d_0 effect on fieldmeter and electrostatic voltmeter measurements. [90]

The graph in Figure 1.13 presents a comparison of measurement errors for a standard fieldmeter and the Trek model 520 electrostatic voltmeter. The experimental data was acquired from the factory-calibrated fieldmeter at one inch distance from the object that is being measured. The reason for the fieldmeter error is that the probe, a copper disk of 9.9 cm diameter (310 square cm surface area), connected to 1 kV DC source, was placed at distance different from the factory specifications. As you get closer to the surface, the field increases, with the surface potential being constant. The only way to make correct measurement with the fieldmeter is to re-calibrate it every time the distance of the fieldmeter vs. the surface is changed. The experiment indicates that it is important to keep the appropriate spacing between the fieldmeter sensor and the tested surface in order to consider the measurement reliable.

Table 1-III shows a brief comparison between fieldmeter, electrostatic voltmeter and AC feedback electrostatic voltmeter. Because of their principle of operation, the electrostatic fieldmeters are suitable for measurements conducted on relatively large areas. They are also not as accurate as electrostatic voltmeters. Since the results provided by the fieldmeters depend strongly on the probe-to-surface distance d_0, it is more convenient to read them as the electric field intensity values (thus the name, fieldmeter). Magnitude of fields measured this way is usually high.

Electrostatic voltmeters, particularly the voltage followers, can be employed for tests of relatively small charged areas - they have much better resolution than fieldmeters. Voltmeters are also very accurate over a certain range of distances d_0. Since the potential on the sensor during the measurement is theoretically equal to the potential of the tested surface, there is no hazard of discharge.

Table 1-III. Fieldmeter and electrostatic voltmeter comparison [90]

	Electrostatic fieldmeter	DC-feedback ESVM	AC-feedback ESVM
general recommendation	for tests of large surfaces	large and small surfaces	large and small surfaces
measured variable	electric field intensity	voltage	voltage
cost	low	high	medium
spatial resolution	poor	very good	good
accuracy	good at the large probe-to-surface distance	excellent at the small probe-to-surface distance	very good within the specified probe-to-surface distance
probe potential	ground (possibility of arcing)	potential of the tested surface	ground (possibility of arcing)
distance independent	no	within a certain, specified range (depends on the probe type)	within a broad range (depends on the probe type)

The above suggests the person conducting measurement has to be aware of the high voltage present on the probe and proceed with caution. AC-feedback voltmeter is a low-cost alternative for the voltage follower type voltmeter. It does not have high voltage circuitry and is accurate within a certain specified range of distances d_0. For example Trek's model 520 holds the 5% accuracy over the distance between 3 and 30 mm [90], [91].

1.3 Conclusions

With the physical limitations attained in the very last years in processing speed, and the industry’s stumble to find novel design solutions both at the circuit level and in circuit cooling, ESD susceptibility of electronic devices has increased significantly. As the industry council has recently proposed that the safe ESD voltage levels be lowered [1], new solutions should be found to ensure the equipment functionality, and personnel safety, justifying the importance of the present work.

The evaluation of ESD risks requires accurate measurement of the charge carried by the human operator or by the various objects on the manufacturing line. The fieldmeters and the electrostatic voltmeters enable the non-contact measurements required by ESD risk monitoring in an industrial environment. The literature-based comparison between these two classes of instruments indicates that they meet the methodological requirements of the present study.

2 INSTRUMENTS AND METHODS

I have no satisfaction in formulas unless I feel their arithmetical magnitude.

Baron William Thomson Kelvin

This chapter presents five proposed methods for the measurement of electrostatic charging on textile materials. The first method is linked to the HBM model discussed in chapter one, while the second involves a novel instrument for indirect measurement of the charge on the personnel. The last three measurement methods presented in this chapter are used for evaluating the charging state of non-woven textile materials that can attain hazardous levels of static charge during the manufacturing process.

2.1 Measurement method for static charge generated at walking on an insulating carpet

In the background chapter, the HBM was referred to as one of the two most important models for assessing the potential hazards to devices and electronic equipment. In fact, up to the point of the skyrocketing of high-speed circuit demand on device operation, the HBM model preceded the CDM model in hazard significance. The recent technology roadmap [1] does emphasize the continuing significance of assessing the personnel charging and exemplifies the signal monitored during walking. The roadmap, the extended previous industry council report on HBM [2], as well as publications [19], [55]-[56] and standards [70], [122]-[124] recognize that such monitoring continues to not only be important but also challenging to implement and control.

2.1.1 Mechanisms, phenomena and HBM

When two insulating materials A and B (eg. an operator's shoe sole and a textile or PVC floor covering) come in contact or rub against each other (Figure 2.1.a), charge transfer occurs between the two materials until the electrical balance at the contact surface is attained. If A loses electrons, it becomes positively charged while B, which receives these electrons, becomes negatively charged. If A is quickly separated from B, A remains positively charged and B keeps its negative charge (Figure 2.1.b).

Finally, if A keeps a contact point (or touches again) with B (Figure 2.1.c), the charge remains the same. Figure 2.1 shows the step-by step mechanism of personnel charging while walking on an insulating floor. In such process, the contact charging phenomenon is shown to always be accompanied by rubbing between the two contact surfaces, which causes tribocharging (Figure 2.1.c).

Personnel tribocharging may occur while: (1) Walking on insulating floor carpets (2) Changing synthetic fiber garments (3) Sitting on a chair (4) Dusting desk or apparatus

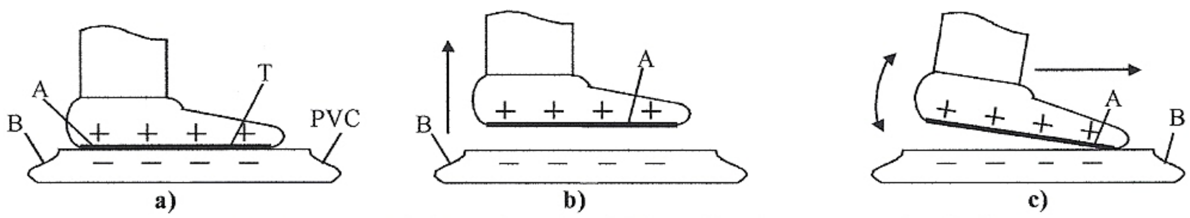

Figure 2.1. The shoe sole charging at walking: a, b) by contact c) through tribocharging

The concern with discharges produced by charged personnel when touching a device terminal or apparatus is that circuit damage can occur. The zapping effect is also unpleasant for the operator. Therefore, it is important to analyze the most frequent situations in which the charging of personnel (P) can occur. Figure 2.2 presents the personnel's typical charging at walking on an insulator floor-covering. Both positive and negative charges may appear on his clothes, depending on the fabric parts that came in touch (clothes, shoes, floor. etc). It is important to keep in mind that the charges are accumulated only on shoes and clothes, while the body, rather conductive, serves only for the charge transmission process (eg. through the fingers, as in Figure 2.2.b).

In 2.2.b, the typical tribocharging of the personnel at the workbench is shown. Here, the charging occurs at rubbing with the chair, as well as between the shoes-soles and the insulator floor-covering (CP). This charge is added to the charge accumulated while walking to the working area shown in Figure 2.2.a. Hence, due to the multiple sources of static charging that the personnel is exposed to, the charge accumulates on the body system and electrostatic discharge (ESD) may occur between the person's finger and an apparatus (Figure 2.2) or device (Figure 2.3).

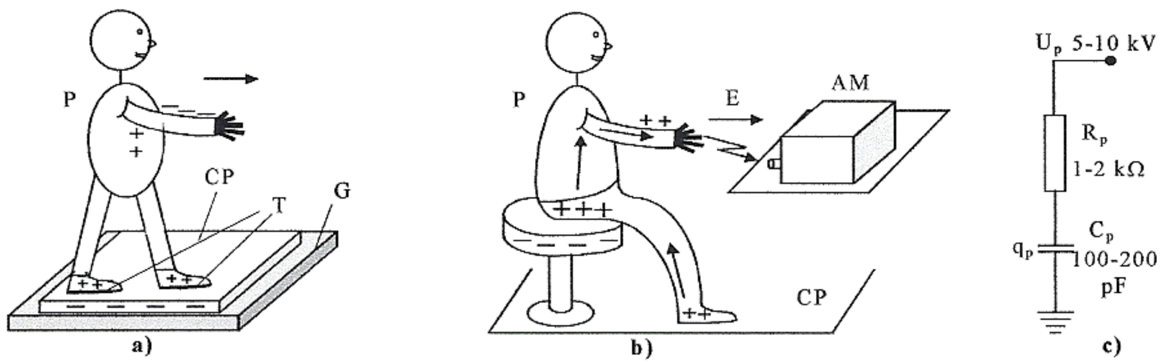

Figure 2.2. Typical personnel charging: a) walking b) at workplace c) human body model

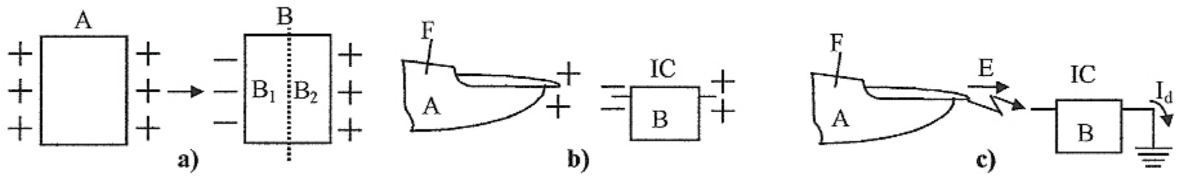

Figure 2.3. Induction charging a) phenomenon b) and c) practical examples

Besides the contact charging and tribocharging, charging through induction can occur in electronic industry and manufacturing lines, as stated in chapter 1. When a charged body, A, comes near a metallic non-grounded body (B) (Figure 2.3), the B_1 side positioned near to A charges with opposite charges. Only if A is moves far enough from B, the induced charge on B can decreases to zero. When the electric field intensity (between A and B)

$$E = \frac{U}{d} \tag{2.1}$$

is high (500–1000 kV/m) and the IC has a grounded pin (Figure 2..c), then an ESD can occur between A and B , which can cause destructive, latent or functional IC damage due to the induced voltage on the pin and the discharge current created on the path to the ground.

Finally, an operator's high tribocharging, to levels of over 5-15 kV, can also occur at changing a garment or piece of clothing. The tribocharging level depends on the speed of movement, as well as of the materials' positions in the triboelectric series.

As mentioned in the background chapter, throughout this work the simple HBM model, illustrated in Figure 2.c, is used. In this diagram, R_P represents the equivalent resistance of the body, and C_P the equivalent capacitance. C_P includes the capacitance between shoes and ground (C_{TG}), as well as the body capacitance with respect to the ground. In this simplified model, the assumption is that C_P is the capacitance of a sphere of surface equal to the body surface.

C_P varies in large limits (100-250 pF) depending on soles material (T) and floor-covering type (CP), as well as the body weight. [19], [56]. In the theoretical calculations, the standard values C_P = 200 pF and R_P = 1.5 KΩ are first assumed, and then C_P is determined experimentally. Theoretically, knowing C_P and the accumulated charge in C_P, q, the voltage on the body and the charging energy accumulated on C_P can be derived using the formulae:

$$q = C_P U_P \tag{2.2}$$

$$W = \frac{q^2}{2C_P} = \frac{1}{2} q U_P = \frac{1}{2} C_P U_P^2 \tag{2.3}$$

The scenario of personnel (P) charging at walking on an insulating floor-covering is further theoretically analyzed [14], [16], [30], in the methods paragraph and the results presented in Chapter 3. However, the involved mathematics is complex and, due the simplifying assumptions and constraints, as well as the uncontrollable parameters, such C_p, the results are not convincing enough. The simplest and most effective method to analyze this problem [16]-[17], [19], [64], [85], [125] is through experimental approach. In practice, U_P and C_P are first measured then q is computed. In the next paragraphs, the experimental setup for these measurements is presented, followed by the proposed measurement method [126].

2.1.2 Experimental setup and instrumentation

The experimental setup is presented in Figure 2.4.

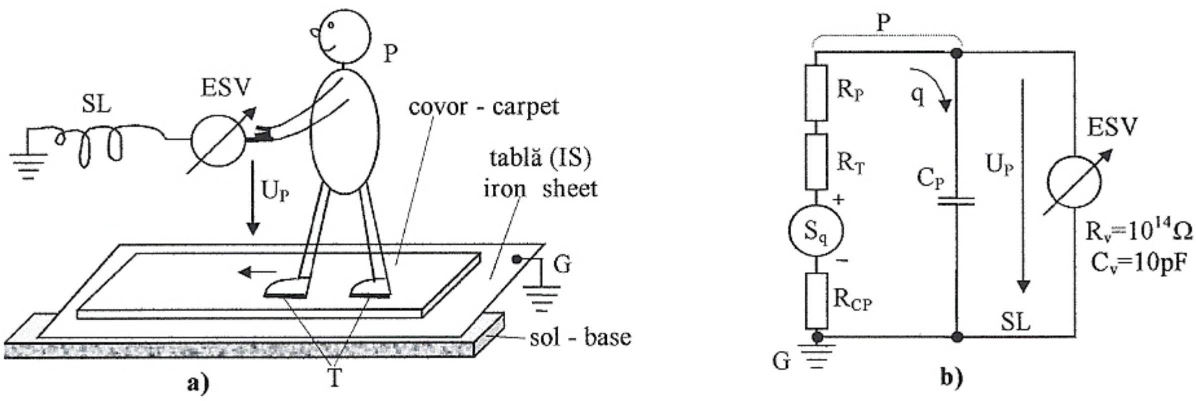

Figure 2.4. Proposed method for *Up* voltage measurements: a) physical setup b) equivalent diagram

The Electrostatic voltmeter (ESV) is a Field Mill type voltmeter [22]-[23], [125] with the following characteristics: nominal voltage 0.2 kV, 2 kV and 20 kV, input resistance R_V >10^{14} Ω and input capacitance C_V>>10 pF, accuracy 3 % end of scale. Starting from here on, $R_V > R_{CP} + R_T$ and $C_V << C_P$, which means that the voltage U_P indicated by ESV is accurate. The meter is equipped with the hygrometer function. Thus, the air humidity in the working area is constantly monitored. The physical setup in Figure 2.4.a was placed at constant temperature and humidity: 22°C and RH = 50% in an atmosphere with no air flow.

Two types of insulating floor coverings (CP) are used and tested:

- PCV, a typical material used in electronic areas and some assembly lines;
- Polypropylene carpet, a typical material used in many rooms in office and industrial setting.

Two shoe soles were tested:

- classic shoe type, with sole of man-made (synthetic) material(T_1);
- sport shoe type, with neoprene rubber sole (T_2).

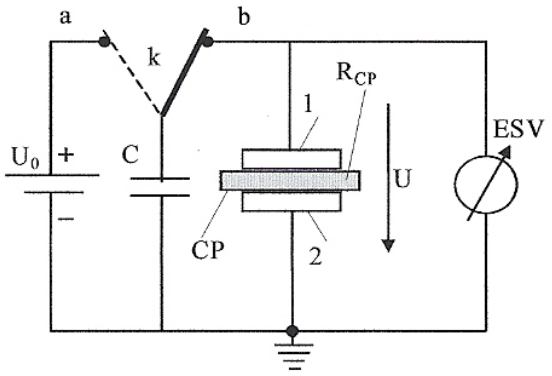

Figure 2.5. Diagram for carpet resistance measurement.

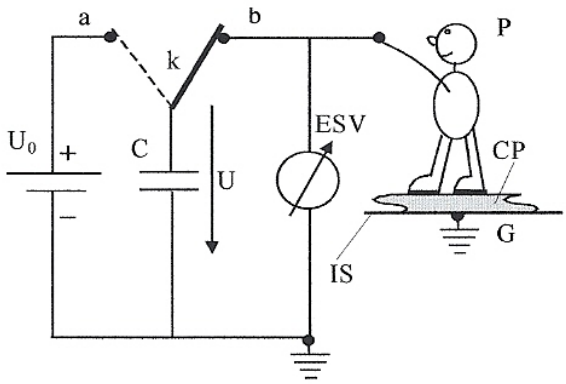

Figure 2.6. Measurement of capacitance C_P

Men of comparable bodyweight were chosen for the test, typically 75 kg, knowing that C_P increases with bodyweight [64]. Otherwise, this election was made based upon the most disadvantageous combination of conditions from amongst those shown above.

For both CP types, the insulating resistance R_{CP} is measured using the capacitor method [67]. The diagram for the carpet resistance and the body capacitance measurement is shown in Figure 2.5 and Figure 2.6, where 1, 2 are circular electrodes, C is a capacitor of known value and U_0 = 1 kV is the test voltage.

The personnel's (P) capacitance, C_p, was measured with both shoe types (T_1 and T_2). As support for the P's path, a PVC carpet (CP_1) and a polypropylene carpet (CP_2) were used. The results for the R_P and C_P measurements, derivation of the charge accumulated during walking at different combinations of materials, are presented in subchapter 3.1.

2.1.3 Proposed measurement method

The measurement methods for the personnel tribocharging during the first three activities mentioned in the previous paragraph are investigated here. The level of charging is expected to depend on the distance of the materials in the triboelectric series shown in chapter1. The experimental setup proposed for testing the method is shown in Figure 2.4, and is a modified and improved version of the classical method.

In order to explain the proposed method, first it is necessary to briefly overview the classical method, which we modified. In the classical measurement method [64], the test person walks on an insulating floor positioned onto a grounded conductive surface. During the measurement, the tested person is connected to an electrostatic voltmeter through a 5 m coaxial cable and a hand-held metal electrode. The test procedure is as follows. The test person walks on the floor at 2 steps/sec and the electrostatic voltmeter to which is connected measures the voltage on the equivalent capacitance of the parallel structure C_P, C_{CX} (coaxial cable capacitance), and C_V (input capacitance of the voltmeter). The main drawbacks of this classical method are introduced by the coaxial cable between the tested personnel and the voltmeter:

- *The capacitance* C_{cx} (500-600 pF) can be greater than C_P (≈ 200 pF), hence the voltage U indicated by the ESV can be smaller than the real parameter U_P. Obviously, using (2.1) and (2.3) we can still derive U_P:

$$q_P = U(C_P + C_{CX}); \ \ (C_V \ll C_P, C_{CX}) \tag{2.4}$$

However, the measurement method may be inconvenient, as all the theoretical verification is not the user preferred method and can be inefficient.

- *The capacitance C_{cx}*, (more than 5 m in length), may become a parasitic source due to the cable bending and torsion operations during the test.

The proposed method is an improvement of the above classical method. The experimental setup remains the same as in the classical solution, which means that the test person (P) walks on an insulator carpet (CP) positioned on a grounded conductive surface (IS).

The difference resides in eliminating the parasitic capacitance introduced by the coaxial cable. In the adopted solution shown in Figure 2.4.a, the ESV is grounded through a supple connection, a wire (SL), connected to the ESV ground terminal. This way, C_{CX} from the classical method is eliminated, and so is a big source of measurement error or uncertainty for the user. By comparison, the grounding wire, SL, in the proposed solution does not affect the U_P equation. Moreover, the voltage U_P at the body-system terminals is measured directly at the ESV input, which is another important advantage of the proposed method.

Figure 2.4.b shows the equivalent diagram of the experimental setup illustrated in Figure 2.4.a. In the equivalent diagram, S_q represents the electric charge source (q), that occurs at the friction between the shoe-sole (T) and the insulating carpet during walking. C_P, the P's capacitance, charges from S_q via the shoe sole resistance (R_T) and the body resistance (R_P =1.5 k ohms) which is negligible compared to R_T (10^9-10^{12} ohms). S_q is connected to the ground via the floor-covering resistance (R_{CP}), which is within the same range as R_T (or higher).

In an earlier paragraph, it was specified that body-system calculations for the resistance and capacitance can be performed if the voltage at the body-system terminal is known. The basic equations for these calculations are presented next.

At each step when the sole is lifted from the floor-covering, C_P is charging via the sole resistance R_T:

$$u_{Pi} = U_{Pm}(1 - e^{-\frac{t}{R_T C_P}}) \tag{2.5}$$

where

$$R_T C_P = \tau_i \tag{2.6}$$

represents the time constant and U_{Pm}-the maximmum value of U_P (Figure 3.1). Between two steps, C_P is discharged via carpet resistance R_{CP}:

$$u_{Pd} = U_{Pm} \cdot e^{-\frac{t}{R_{CP} C_P}} \tag{2.7}$$

where:

$$R_{CP} C_P = \tau_d \tag{2.8}$$

represents the charge decay time constant. From (2.4) and (2.5), if

$$R_T > R_{CP} \tag{2.9}$$

the human operator cannot charge (or charging is lower than for $R_T < R_{CP}$). This is because the C_p discharging speed is greater than its charging speed.

2.2 Faraday pail-based instrument for measurement of the electric charge of textile materials

This subchapter describes a Faraday cup based instrument designed to measure the electrostatic charge on textile materials, as well as protective clothing used in the electronics industry. The proposed Faraday instrument is different from the classically used type [126], as there is no direct electrical contact involved with the sensor electrode. This eliminates the cable between the electrode and the measuring instrument that is a main source of noise. The measurement method is explained (§ 2.2.1), its mathematical equation derived (§ 2.2.2) and the technical characteristics of the instrument detailed (§ 2.2.3). The characteristics of the built instrument are presented in § 3.1.2.

As mentioned in the previous subsection, the measurement of the accumulated charge (q) on a body system is typically performed through a “walking” circuit that includes the RC impedance of the HBM, as in Figure 2.2.c. The impedance of this RC model has considerable variations and instabilities, which contribute to errors in the measurement result. To avoid this limitation, a different method of measurement of the electrostatic charge is proposed. This proposed method not only can be used to measure the charge on the personnel, but also to measure the charge on either woven or non-woven textile materials of bigger size.

The method for the operator charge measurement consists of measuring the triboelectric charge accumulated on the piece of clothing (vest, pullover, etc.) that the person takes off in preparation to working at the workbench (and handling sensitive electronic components). To measure the value of the charge (q_x) the authors built a Coulombmeter-type Faraday Cup. The method is described in detail the next section.

2.2.1 Proposed method and diagram

As previously mentioned, when rubbing two objects (A and B, Figure 2.1.a) they charge with opposite sign charges of the same value ($+q_A=-q_B$). Figure 2.7 above suggests that after the object separation (Figure 2.7.b), the q_x measurement is possible by measuring the charge on either object A or B. Based on this observation, the charge accumulated on the personnel during the work preparation can be the same as the charge accumulated on the piece of removed clothing (q_{GP}, Figure 2.8). This charge will be designated as q_x.

A classic [22] Faraday Cup Instrument (Figure 2.8.a) can be used to measure the accumulated charge q_x. The active electrode (1) picks up the static charge ($+q_x$) accumulated on GP and transfers it to the electrometer (EM), which displays a value proportional to q_x.

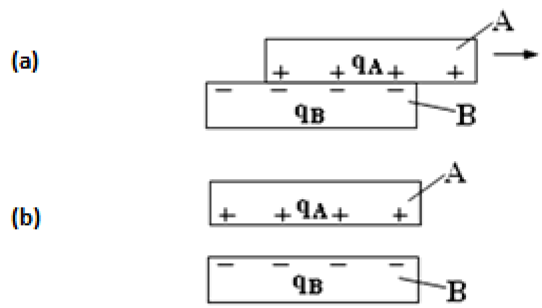

Figure 2.7. Triboelectric Phenomenon. a) Contact; b) Separation.

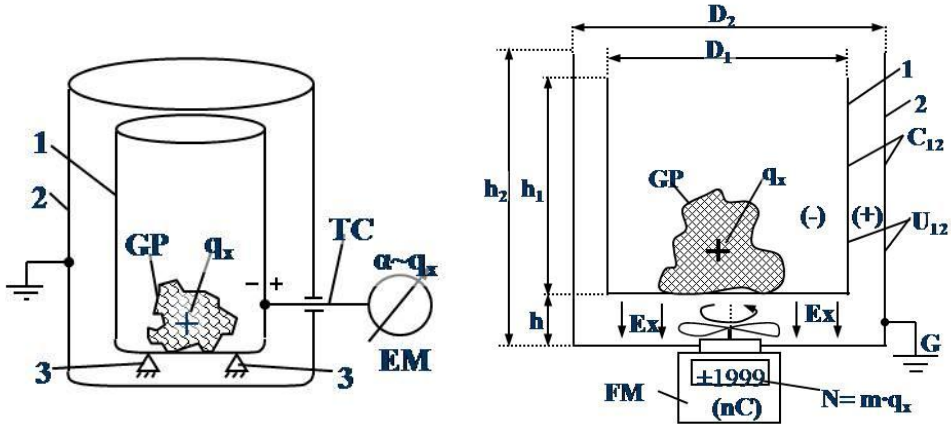

(a) (b)

Figure 2.8 Faraday Cup Instrument. (a) Classic instrument. (b) Functional diagram of the proposed instrument

However, the main limitation of this classical method is that the triaxial cable (TC) between the electrode and the electrometer can often cause important measurement errors during instrument handling [128].

The diagram of the proposed instrument is shown in Figure 2.8.b and the labeling previously assigned to the elements in Figure 2.8.a is preserved. For the sake of simplicity, the insulators 3 have been omitted from Figure 2.8.b. FM is a Field Mill type instrument [67], of the same characteristics as previously presented in subchapter 2.1, that measures the electric field E_x produced by the charge to be measured, q_x. The displayed number N is directly proportional to the charge q_x and, as shown, the measurement is made without direct contact with the electrode 1. Through this method, the triaxial cable (TC in Figure 2.8.a) is eliminated from the measurement circuit and, consequently, so is the main limitation associated with it [129].

2.2.2 Measurement equation

The measurement equation of the proposed instrument can be determined from the observation that when electrostatic charge (q_x) is present on the object GP, the potential between the two armatures 1 and 2 of the capacitor C_{12} is mathematically expressed by the formula:

$$U_{12} = \frac{q_x}{C_{12}} \tag{2.10}$$

Consequently, between the two bases of the cylinders 1 and 2, an electric field will occur:

$$E_x = \frac{U_{12}}{h} \tag{2.11}$$

where h is the distance between the two cylinder bases. The field intensity E_x is numerically displayed on the Field Meter FM:

$$N = a \cdot E_x \tag{2.12}$$

The letter a in Equation (2.12) symbolizes the fieldmeter sensitivity. The mathematical equation for the instrument is derived by substitution of (2.10) and (2.11) in (2.12):

$$N = m \cdot q_x \tag{2.13}$$

where the constant m is the instrument sensitivity:

$$m = \frac{a}{hC_{12}} \tag{2.14}$$

2.2.3 Instrument Calibration and Error Calculation

The instrument was designed as a two-range measurement system: 200 nC and 2000 nC. Since the charge q_x cannot be measured directly (unlike a voltage or a current for example), q_x was calculated using the mathematical expression (2.9). For a capacitance C_{12} of 140 pF, the two full ranges labeled "max" for future references correspond to the voltages U_{12} of 1.43 kV and 14.3 kV respectively.

The calibration diagram is shown in Figure 2.9, where VS is an adjustable voltage source and DV is a digital voltmeter of high precision (±0.02%). All the other notations from Figure 2.8 are kept. From the mathematical expression (2.13), it results that *m* can easiest be adjusted by modifying the fieldmeter sensitivity, *a.* The double range calibration was possible by adjusting the gain of the fieldmeter.

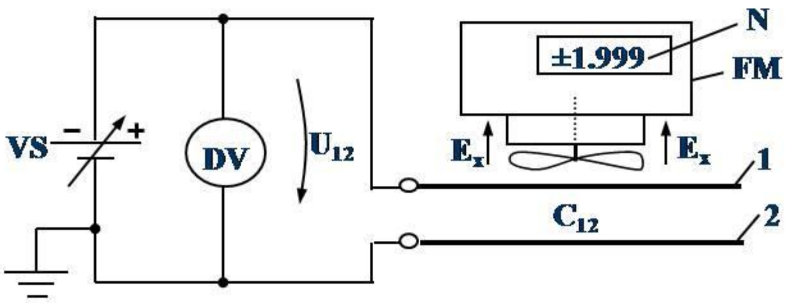

Figure 2.9 Instrument Calibration

From the elements in equation (2.14), the total error of the instrument in Figure 2.8.b is calculated through the method described in [67], vol. 1, pp. 33-239:

$$\frac{\Delta m}{m} = \frac{\Delta a}{a} + \frac{\Delta C_{12}}{C_{12}} + \frac{\Delta h}{h} \tag{2.15}$$

where, $\Delta a/a$ is the fieldmeter error ($\Delta a/a \leq 1.5\% \cdot \max$), $\Delta C_{12}/C_{12}$ the determined capacitor error ($\Delta C_{12}/C_{12} \leq 0.5$ %) and $\Delta h/h$ represents the relative error introduced by the distance *h* ($\Delta h/h \leq 0.2$ %). With this information, and, as required by the measurement equation (2.13), taking into account the simulation error $\Delta q_x/q_x \leq 0.5$ %), the calculated maximum error introduced by the instrument is 2.7%. This establishes the basic methodological index for the practical applications of this measuring instrument: the precision class 3. The physical and performance characteristics of this instrument are detailed in subchapter 3.2.

2.3 Measurement method for the personnel charge on the assembly line

The present subchapter describes a measurement method of the electrostatic charge on textile materials and personnel clothing. As described in subchapter 2.2, static charge can also be created on a garment as a result of removing it from a human body, usually before sitting at a workbench and handling PCBs, ICs, etc. The method is based on charging a capacitor of known value with the triboelectric charge accumulated on the garment placed in a Faraday cup (F_C) right after being removed off of the body system. The capacitor, charged with the charge to be measured, is part of the feedback loop of a circuit with operational amplifier with an Electrostatic Voltmeter as load. The charge is calculated as a function of the capacitor value and the voltage indicated by the output electrostatic voltmeter.

2.3.1 HBM testing method

As earlier stated, the measurement concerns the triboelectric charge (q) accumulated on the human operator (P, Figure 2.10.a) while removing a garment (GP: coat, jacket, sweater, etc.) as in Figure 2.10.b, before sitting and starting working at the workbench or worktable.

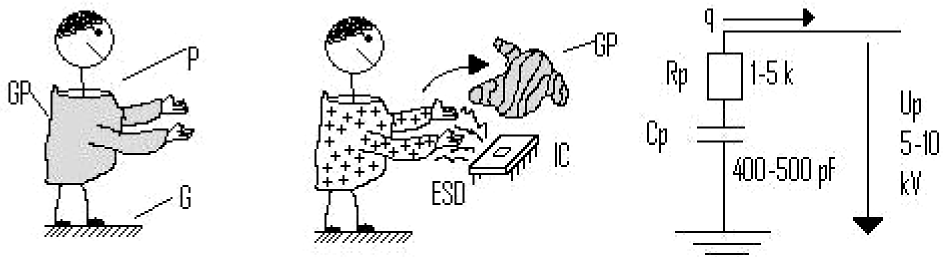

(a) **(b)** **(c)**

Figure 2.10. The Human Operator (P). a) Wearing a sweater (GP). b) Electrostatically charged from removing the sweater c) The model for the Human Body. [128]

Figure 2.10.c reiterates the HBM model for the purpose of present work. Here, C_P is the equivalent capacitance of the person with respect to the ground (G) before removing the piece of clothing. C_P is the sum between the capacitance of a sphere of surface equal to the surface of the operator body with respect to the ground, C_S, and additional parallel capacitors, C_Π [128]. Mathematically, that is:

$$C_P = C_S + C_\Pi \tag{2.16}$$

In practice, C_P varies within a wide range, as C_S depends on the size of the person P and the type of clothing worn. Moreover, C_Π is a function of the surrounding conductivities, thus calculating the two terms of C_P is a rather laborious task and the result insufficiently accurate. All these considered C_P is initially adopted as equal to 200 pF and then experimentally measured using the diagram shown in Figure 2.11. This setup is similar to that used in the already presented case of walking on a carpet.

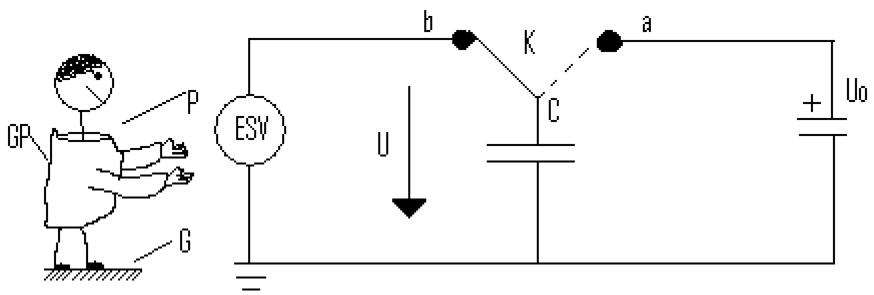

Figure 2.11. Diagram for the Human Body capacitance, C_P, measurement.

The capacitor C of known value is first charged to the voltage U_0, then is connected in parallel to the human body capacitance C_P. The voltage U indicated by the Electrostatic Voltmeter (ESV) is then used in the calculation of the person's capacitance, C_P:

$$C_P = \frac{C}{(U_0/U)-1} \tag{2.17}$$

This measured value is the value of the voltage that needs to be taken into account when evaluating the possibility of the ESD occurrence between the human operator P and an electronic board, integrated circuit or system, as previously stated

2.3.2 Direct method for human body charge measurement

The proposed method for the measurement of the triboelectric charge accumulated on the Human Body at the removal of a piece of clothing is based on the principle of charging a capacitor of known value (C) with the electrostatic charge to be measured (q_x). The method was experimented both by using direct and indirect measurements, cases in which the charge to be measured was named q_1 and q_2 respectively. Both methods, as well as the reason for finally choosing the indirect measurement method, are presented in the next paragraphs. The diagram for the direct measurement of the triboelectric charge (q_1) is shown in Figure 2.12.

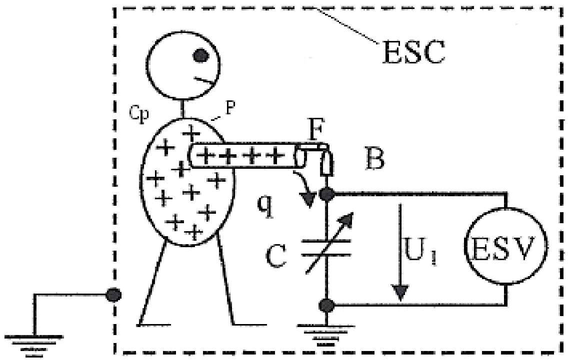

Figure 2.12. The direct method of measuring the static charge after garment removal.

The experimental setting showed in Figure 2.12 was placed in an environment of constant temperature and relative humidity, 22˚C and 50% (RH) respectively. The environment was specific to the computer and electronics laboratories.

The same Electrostatic Voltmeter, of fieldmill type and digital display, with the following characteristics: 0.2 kV, 2 kV and 20 kV scale, 2 % accuracy, 10^6 Ω input resistance and 100 pF input capacitance is used, as previous. The capacitor C is of high precision, specific for instrumentation, and adjustable within the range of 30 pF-500 pF.

The procedure for the direct measurement is performed as follows: the human subject (P), removes an outdoor piece of clothing (wool jacket, for example) as in Figures 2.10.a and 2.10.b, and then rapidly places it into a metallic container (Figure Figure 2.8 and Figure 2.13.b). With his index finger (F), the subject touches the free terminal (B) of the capacitor C (Figure 2.12).

As a result, the charge q_1 created on P at the removal of the piece of clothing, GP, is transferred to the capacitor C which, charges at its terminals with the voltage U_1. The

Electrostatic Voltmeter, ESV, of capacitance C_V<<C, C_P, indicates this voltage U_1. Since all three capacitors are in parallel, the measurement equation is of the form:

$$q_1 = (C + C_P) \cdot U_1 \tag{2.18}$$

Five students (A, B, C, D, E) were used as test subjects, all equipped with the same type of clothing: synthetic sweater (wool type) over synthetic fiber, cotton-type shirt. The synthetic materials of the two pieces of clothing were chosen such that they would be as far as possible on the triboelectric series, in order to obtain maximum triboelectric effect. Each subject was initially discharged by touching, with both hands, a metallic piece connected to ground.

2.3.3 Indirect method for human body charge measurement

According to the triboelectric charge conservation principle, and as suggested in § 2.2.1, the charge q_2 that accumulates on the personnel garment or piece of clothing at fast removal is equal and of opposite sign to the charge q_1 left on the operator body P. Consequently, the result of measuring the charge ($-q_2$) accumulated on the piece of clothing indirectly indicates the absolute value of the potentially damaging human body charge of interest, q_1.

The general diagram for the indirect measurement of the triboelectric charge (q_2) is shown in Figure 2.1.3 below. The Faraday Cup (FC) device is comprised of two cylinders, one for measurement 1 and the other one for shielding 2, insulated with respect to each other through the insulator 3. The switch K serves to discharge of the capacitor C before starting the experiment.

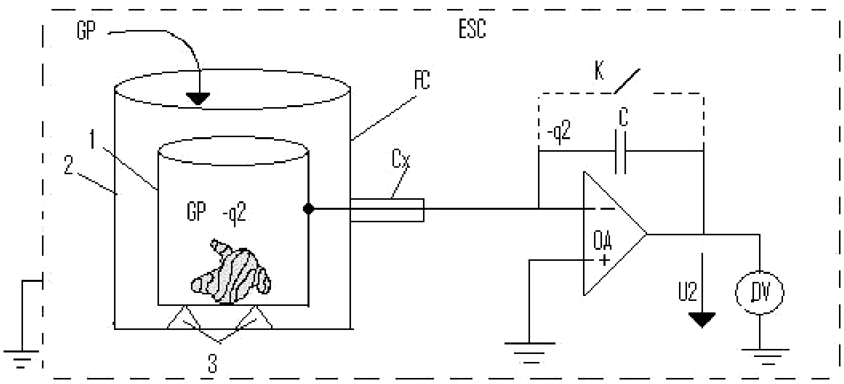

Figure 2.13. The indirect method of measuring the static charge after garment removal

In the indirect method, the subject/the operator, removes the piece of clothing (GP) and rapidly throws in cup 1. The triboelectric charge q_2 accumulated on GP is transferred to cup 1 and the voltage U_2 is measured..

The measurement equation is of the form:

$$q_2 = CU_2 \quad (2.19)$$

2.4 Surface potential versus electric field measurements for charging state characterization of non-woven fabrics

Surface potential and electric field measurement techniques are widely used for the investigation of the corona charging [107], [130]-[137] of dielectric surfaces in a wide range of industry applications [138]-[140]. The aim of the present work [141] is to estimate which of these techniques are the most appropriate for characterizing the charging state of non-woven fibrous dielectrics, and point out the "noise factors" that might distort the results of the measurements.

The experiments were performed on samples of non-woven polypropylene (PP) sheets, in contact with or at a well-defined distance from a grounded plane. The effect of the variability of the position of the probes with respect to the samples was also investigated. Several recommendations have been formulated regarding the use of these techniques for monitoring the charging state of non-woven fabrics in industry applications.

2.4.1 Materials and method

"Standard" square samples (100 mm x 100 mm) were cut from non-woven sheets of PP (sheet thickness: 400 μm, average fiber diameter: 20 μm, as a detail shows in Figure 2.14).

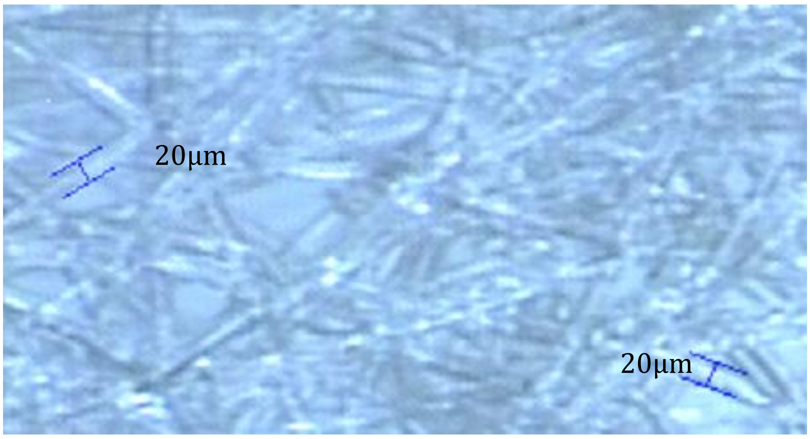

Figure.2.14 Photograph of the non-woven polypropylene media.

The samples shown in the previous figure were placed on an aluminum plate connected to the ground as shown in Figure 2.15.a and Figure 2.16. The sample carrier consisted of a PVC plate, to which the assembly plate electrode + non-woven fabric was firmly attached. A conveyor belt supported the sample carrier and transferred it from the charging position to the surface potential measurement and to the electric field measurement positions. The accuracy of horizontal positioning of the conveyor belt is 0.2 mm, and the positioning accuracy of the probes is 0.1 mm. The total geometrical error of the setup is less than 5%.

The samples were charged using the negative corona discharge generated by a high-voltage wire-type dual electrode as in [130], facing a metallic grid (Figure 2.15.b) distanced at 15 mm from it and located at a fixed distance (30 mm) above a grounded plate electrode (aluminum; 165 mm x 115 mm), as shown in Figure 2.15.

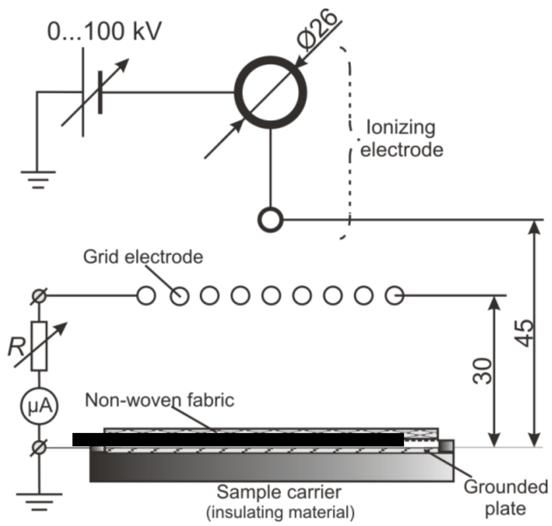

(a)

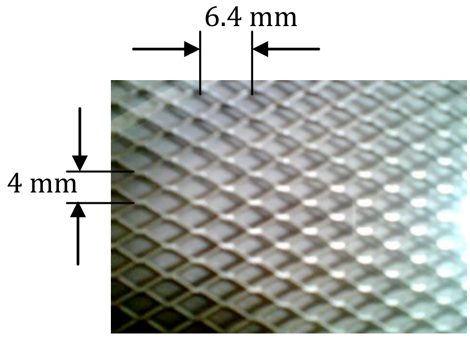

(b)

Figure 2 Electrode systems employed for the corona-charging of non-woven media (all dimensions are in millimeters); (a) triode-type arrangement; (b) aspect of the grid electrode (grid wire diameter: 1.18 mm).

The high-voltage electrode consisted of a tungsten wire (diameter 0.2 mm) supported by a metallic rod (diameter 26 mm) and distanced at 34 mm from its axis. The wire and the cylinder were energized for 10 s from an adjustable high-voltage supply 100 kV, 3 mA (model SL 300 SPELLMAN). The grid was connected to the ground through a series of calibrated resistors having a total resistance R. In this way, for the constant current I delivered by the power supply, a well-defined potential $V_g = RI$ was imposed between the grid and the grounded plate on which the samples were placed. For the purpose of the experiments in this paper, V_g = 1 kV. Thus, all the samples were similarly charged.

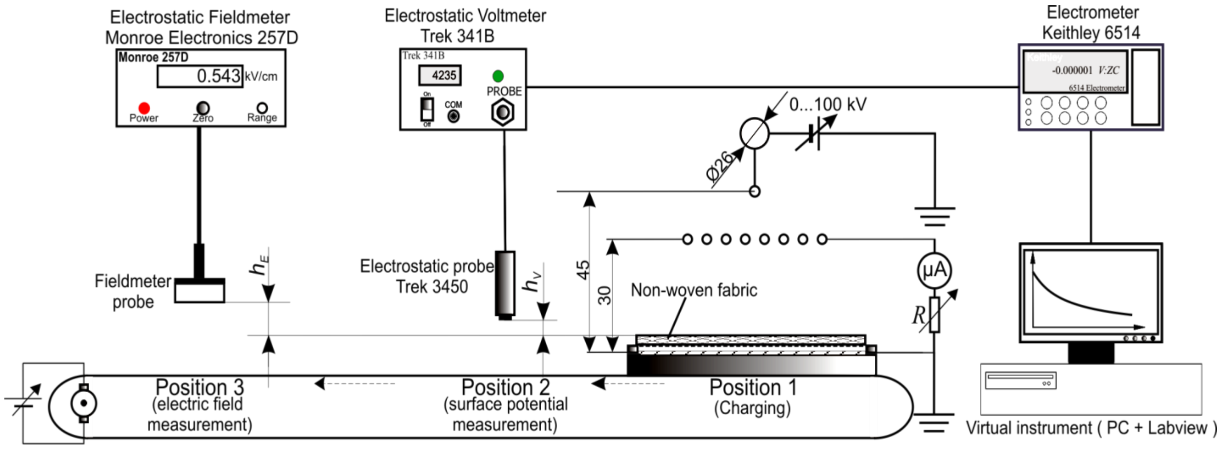

Figure 2.16. Experimental set-up for charge measurement.

As soon as the high-voltage supply of the corona charger was turned-off, the conveyor belt transferred the samples from Position 1 to Position 2 (Figure 2.16.), where the surface potential was measured with an electrostatic voltmeter (TREK, model 341B, equipped with a probe model 3450, accuracy on the 200 nC: ±(0.4% reading +50), temperature coefficient (0.04+10)/C). If not otherwise specified, the measured potential was monitored for 10 min via an electrometer (Keithley, model 6514), connected to a computer provided with data acquisition software as in [133]. The quasi-constant surface-potential value attained after 10 min was retained for data analysis.

When the surface potential measurement was over, the same conveyor belt transferred the sample to Position 3, beneath the properly screened probe of an electric fieldmeter (Monroe Electronics, model 527 D). In all but one experiment, the distance between the probe and the sample was h_E = 10 mm.

After each surface voltage and electric field measurement, the charged samples were introduced, using ESD-safe tweezers, into a custom-designed Faraday pail (different from the previously described), connected to an electrometer (Keithley, model 6514), as shown in Figure 2.17.

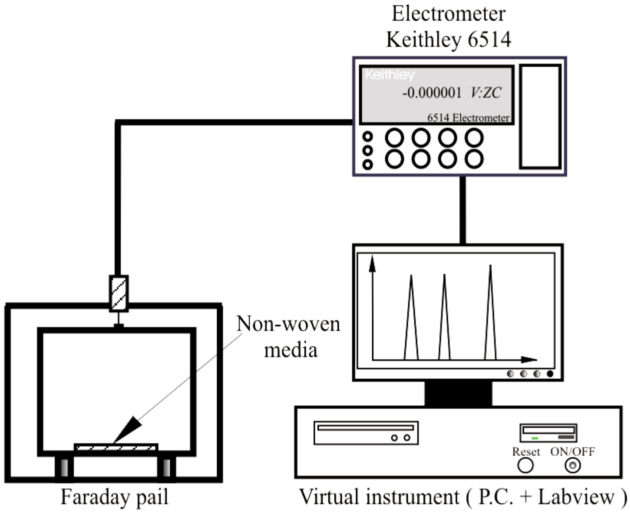

Figure 2. 17 Experimental set-up for charge measurement.

In the first two major sets of experiments (#1.1 and #1.2), the "standard" samples were in contact with the grounded electrode and the surface potential probes were located at either h_V = 5 mm or h_V = 10 mm above them.

Two additional set of experiments (#1.3 and #1.4), were carried out in the conditions of experiment #1.1, but with the field probe located at slightly larger distance, or, in a modified procedure, performing two consecutive V and E measurements on each sample. All the experiments were carried out in ambient air (temperature: 20°C to 25°C; relative humidity: 27% to 45%).

2.4.2 Measurement and comparison for the probe - sample distance of non-woven materials on a ground plate

The results of the first two sets of ten experiments are given in Table 2-I.

The difference between the surface potential measurements with the probe at h_V = 5 mm and at 10 mm respectively is statistically significant (Student's test: p = 0.00005). When the probe is at a larger distance from the sample, the measurement is likely to be perturbed by the presence of other bodies in the proximity. This is why the manufacturer recommends a distance $h_V = 3 \pm 1$ mm to be respected between the probe and the sample.

Table 2-I. Potential and Electric Field Measurements at the Surface of Non-Woven PP Fabrics in Contact with a Plate Electrode Experiments # 1.1 (h_V = 5 mm, h_E = 10 mm) and # 1.2 (h_V = 10 mm, h_E = 10 mm)

Sample No.	Experiment # 1.1 h_V = 5 mm; h_E = 10 mm		Experiment # 1.2 h_V = 10 mm; h_E = 10 mm	
	Surface Potential V (V)$_{bf}$	Electric Field E (V/cm)	Surface Potential V (V)$_{bf}$	Electric Field E (V/cm)
1	879	807	796	774
2	897	848	808	784
3	757	750	716	739
4	805	771	727	772
5	851	765	716	786
6	875	787	706	743
7	784	695	696	707
8	847	732	648	773
9	827	816	700	739
10	827	838	758	794
Average	834.9	780.9	727.1	761.1
Standard deviation	44.09	48.06	48.18	27.66

However, the standard deviations of the two series of data are practically the same. A wider dispersion of the results might have been expected in the case of the probe located at h_V = 5 mm from the sample, as it reflects the average potential on an area smaller than the one "viewed" when at a larger distance. This indicates that the non-homogeneity of the charge due to the variations in the local texture of the fibrous media cannot be detected with this type of probes located at relatively large distances from the samples. Surprisingly, the distribution of the values of the electric field is more asymmetric for the larger distance (median 772.5, average 761.1) than for the smaller distance (median 779, average 780.9). But, the number of values is too small to derive a conclusion.

As long as the manufacturer's recommendations are respected, the surface potential measurement is not affected by the small variations in the position of the probe. This might be an important advantage of this method in the various industrial applications where the distance between the probe of the electrostatic voltmeter and the non-woven material cannot be rigorously controlled.

Indeed, as the lack of rigidity of such materials is often accompanied by fluctuations in the momentary distance between the non-woven sheet and the probe, it is highly reassuring to note that the variability of the results due to this factor is negligible.

As expected, the difference between the values indicated by the electric field meter in the two experiments with h_E = 10 mm was not statistically significant (p = 0.229). In order to illustrate the sensitivity of this measurement method to the positioning of the probe, a first additional experiment was performed at h_E = 12 mm (Table 2-II).

The difference between the values of the electric field measured in the experiments #1.1 (h_E = 10 mm) and #1.3 (d_E = 12 mm) was statistically significant (p = 0.04), while the surface potential was practically the same (p = 0.728). In case that E is recalculated taking into account the factor 1.2 between the actual distance (h_E = 12 mm) and the one for which the field meter is calibrated (h_E = 10 mm), the average electric field in the experiment #1.3 becomes E = 832.3 V/cm, which is roughly the same as in the experiment #1.1: E = 834.9 V/cm.

Table 2-II. Potential and Electric Field Measurements at the Surface of Non-woven PP Fabrics in Contact with a Plate Electrode Experiment # 1.3 (h_V = 5 mm, h_E = 12 mm)

Sample No.	Experiment # 1.3 h_V = 5 mm; h_E = 12 mm		
	Potential V (V)	Electric Field E (V/cm)	Electric Charge Q (nC)
1	872	733	72
2	895	788	89
3	831	648	92
4	753	660	118
5	819	662	85
6	808	674	79
7	873	724	93
8	816	672	112
9	892	666	77
10	860	709	89
Average	841.9	693.6	90.6
Standard deviation	44.59	44.03	14.6

This observation points out the need of a strict control of the position of the probe with respect to the surface under examination, especially in the case of automated measurement systems, where no correction of the recorded data can be made. From this point of view, the surface potential measurements seem more appropriate for evaluating the charge state of non-woven fabrics, as it is less sensitive to the fluctuations of the probe – sheet relative position.

The present procedure of charge measurement is far from being satisfactory. The standard deviation of the ten values of Q measured in the experiment #1.3 represents 16.1% of the average charge. This variability could be caused in part by the manipulation of the charged samples between the grounded plate on the experimental setup and the Faraday cup, despite the precautions taken. The other source of variability might be due to the equipment itself, as the charge measurement equipment is significantly less accurate than the voltage and the field measuring equipment.

By comparison, the standard deviations of the corresponding ten values of the surface potential V and electric field E were only 5.3% and 6.35% of the respective averages. It can be concluded that both surface potential and electric field monitoring methods are more effective for evaluating the charging state of a non-woven fabric than the existing method of direct measurement of Q.

Table 2-III Potential and Electric Field Measurements at the Surface of Non-woven PP Fabrics in Contact with a Plate Electrode Experiment # 1.4 (h_V = 5 mm, d_E = 10 mm)

Sample No.	V_1 (V)	E_1 (V/cm)	V_2 (V)	E_2 (V/cm)	Q *) (nC)
1	800	754	801	753	55.7
2	800	815	803	808	78.4
3	800	840	780	828	99.4
4	800	860	798	859	71.7
5	800	732	787	728	90.8

*) The wide dispersion of Q values is due to the imperfections of the charge measurement method.

The experiment #1.4 was performed in order to point out a different aspect. Thus, the surface potential was monitored until the threshold – 800 V was attained. Then each sample was transferred under the electric field mill, for a first measurement. After that, a second voltage potential and a second electric field measurement were performed, without changing the position of the sample on the carrier. The results recorded in these experiments are given in Table 2-III.

The measured electric field E was close to the expected value E_e, calculated as $E_e = V/d$ only in the case of sample 2. Both values of electric field measured for each of the samples 1 and 5 were smaller than E_e. Similarly, both values measured for each of the samples 3 and 4 were higher than $E_e = V/d$. This can be simply explained by the fact that the equality of the values of the surface voltage V does not necessarily imply that the samples are similarly and uniformly charged. Because of the macroscopic textural distribution of the fibers in the material, one should expect an equivalent pattern in the electric field.

The samples 1 and 5 are likely to have smaller charges than samples 3 and 4, but located at a higher distance from the grounded plate, because of the difficulty to ensure a perfect planarity of the non-woven sheets on the surface of the grounded plate. Therefore, the potential V at their surface is the same. But the electric field E, which is not affected by the position of the charges with respect to the ground but by their value, can vary from one sample to the other. Consequently, whenever surface potential measurement is employed, special attention should be given to the sheet-to-ground relative position. This issue is especially critical in the situations when the position of the sample to the grounded plane is difficult to define.

2.4.3 Measurements and comparison for the influence of probe to sample distance on non-woven materials not in contact with the ground plate

The effect of the sheet-to-ground position was specifically examined in the experiments #2.1 and #2.2, the results of which are given in Table 2-IV. The difference between the surface potential measurements with the probe at hv = 5 mm and 10 mm was statistically significant (p = 0.000001), as it had also been the case when the samples were in contact with the grounded electrode.

These findings confirm the need of getting the surface potential probe closer to the sample, which might represent an unacceptable constraint in some industry applications. On the other hand, the values indicated by the electric field meter in the experiments #2.1 and #2.2 were practically the same (p = 0.379). This means that the electric field measurements can be confidently employed whenever the recommended probe-sample distance is strictly respected.

Table 2-IV Potential and Electric Field Measurements at the Surface of Non-woven Fabrics Distanced at h = 5 mm from a plate Electrode Experiments # 2.1 (hv = 5 mm, d_E = 10 mm) and # 2.2 (h_V = 10 mm, d_E = 10 mm)

Sample No.	Experiment # 2.1 h_V = 5 mm; d_E = 10 mm		Experiment # 2.2 h_V = 10 mm; d_E = 10 mm	
	Surface Potential V (V)	Electric Field E (V/cm)	Surface Potential V (V)	Electric Field E (V/cm)
1	1079	782	994	748
2	1034	822	1000	758
3	1074	783	1015	775
4	1069	768	1025	788
5	1053	752	1038	796
6	1082	780	999	748
7	1077	823	1000	756
8	1070	782	1017	774
9	1069	766	1022	786
10	1070	755	1047	796
Average	1067.7	781.3	1015.7	772.5
Standard deviation	14.24	24.41	17.79	18.91

2.5 Conclusions

(1) An improvement of the presently used method of charge monitoring while walking could be obtained by eliminating the parasitic capacitance due to the coaxial cable.

(2) The Faraday pail-based instrument designed for the measurement of the triboelectric charge on clothing worn by human operators in the electronic industry is a simpler solution of monitoring EDS risks than the “walking” solution that is presently in use [55].

(3) The dispersion of surface potential V and electric field E values recorded on similarly-charged samples of non-woven textiles is lower than that of direct charge Q measurements carried out with the Faraday cup method. Either V or E measurements can be confidently employed for assessing the charging state of a non-woven fabric

(4) The surface potential measurement is not significantly affected by the small variations (± 1 mm) in the position of the probe when it is close enough (< 5 mm) to the charged non-woven fabric. This might be an important advantage of this method in the various industrial applications where the probe of the electrostatic voltmeter can be placed in the proximity of the non-woven material but the distance between them cannot be rigorously controlled.

(5) In the conditions of the present experiments, the variability of the results partly due to uncontrollable fluctuations in the momentary distance between the non-woven sheet and the probe was negligible. However, the lack of rigidity of these materials, which largely accounts for these fluctuations, can impact the outcome of surface potential measurements. This aspect should be carefully examined prior to any industrial application of this indirect method of charge monitoring.

(6) The advantage of electric field measurements is that they are less affected by the fluctuations of the distance between the non-woven sheet and the probe. However, their main drawback is the need of a strict control of the position of the probe with respect to the surface under examination, especially in the case of automated measurement systems, where no correction of the recorded data can be made.

3 MEASUREMENTS ON PERSONNEL

If you cannot measure it, then it is not science.

Baron William Thomson Kelvin

In the previous chapter, novel instruments and methods have been proposed for the measurement of the electrostatic charge accumulated on the personnel during a manufacturing process. The results of the laboratory tests that were performed in order to validate the new techniques are described hereafter.

3.1 Direct measurement of the static charge on personnel

This sub-chapter exposes the results anticipated in subchapter 2.1. First, the preparatory measurement results that determine the diagram element values of the body system in Figure 2.2 are shown, followed by the results of the measurements performed on personnel while walking on insulating carpets and while at the workbench.

3.1.1 Footwear and carpet measurements

A first set of measurements were carried on in order to evaluate the electrical characteristics of floor carpet and personnel footwear. These body-system parameters were obtained using the experimental diagrams in Figure 2.5 and Figure 2.6 in § 2.1.2.

To obtain the carpet and shoe sole resistance, the switch K in Figure 2.5 was placed in the *a* position and the voltage U_0 recorded. Then K was switched in *b* position and the voltage U after the time decay time, t, was measured with the ESV. Finally, the carpet resistance R_{CP} was calculated using the two measured voltage values:

$$R_{CP} = \frac{t}{C \ln U_0/U} \tag{3.1}$$

The resulted data, averaged over five repeated measurements for each floor type (§ 2.1.2), as well as for both shoe-sole types (R_T), is illustrated in Table 3-I.

Table 3-I Shoe-sole and carpet resistance

Material	R_{T1}	R_{T2}	R_{CP1}	R_{CP2}
Resistance (Ω)	$3\ 10^{9}$	$5\ 10^{11}$	$5\ 10^{10}$	$2\ 10^{12}$

To determine personnel body-system capacitance C_P, the setup in Figure 2.6 was used and the averaged results are presented in Table 3-II. Similar to the precedent table, results from five repeated measurements for each combination were calculated with equation (2.17).

Table 3-I Body system capacitance C_P for different test conditions

Combination	T_1/CP_1	T_1/CP_2	T_2/CP_1	T_2/CP_2
Capacitance	$2.7\ 10^{-9}$	$2.4\ 10^{-10}$	$2.1\ 10^{-10}$	$2.5\ 10^{-10}$

The data in Table 3-II clearly shows higher C_P values for the combination of man-made leather shoe sole (T_1) on a PVC carpet (CP_1).

3.1.2 Measurement results at walking on an insulating floor

The physical setup for the proposed measurement method was presented in Chapter 2 (Figure 2.4.a). A few more experimental conditions need to be given here. The test carpet length was 8 m for both types (CP_1 and CP_2). In order to minimize the contact resistance, the person's skin in contact with the shoe and the electrode of the ESV was humidified. This also better simulated the skin conductivity during real working conditions.

The step duration during the walking test (T_P) is the time between sole lifting and sole returning on the floor. In order to obtain smooth experimental curves of $U_P(t)$, T_P was chosen such that C_P discharges as little as possible within T_P. That is:

$$Tp << \sigma_d \tag{3.2}$$

where τ_d represents the time constant at C_P discharging for the shoe-sole - floor-covering combinations. Table 3-III shows the τ_i and τ_d values, calculated using equation (2.6) and equation (2.8) for the combinations illustrated in Table 3-II.

Table 3-III Time constant for charging (τ_i) and discharging (τ_d) of C_P

Combination	T_1/CP_1	T_1/CP_2	T_2/CP_1	T_2/CP_2
τ_I (s)	0.84	0.72	115	169
τ_d (s)	140	480	0.7	456

The data in Table 3-III shows that with the exception of R_{T2}/C_{P1} combination, which indeed does satisfy the condition (2.9) derived in § 2.13, the τ_d values are hundreds of sec. Hence, if T_P is of fraction of second, the condition (3.2) above can be met. In full accord with the standards [2], [122], the choice of T_P = 0.5 s was made. Therefore, during these tests, the personnel walks at a speed of 2 steps/sec. Concerning the T_2/CP_2 combination, the values of τ_I and τ_d confirm the validity of the previous comments on equation (2.9).

Based on the results in Table 3-III, the experiments on the combinations T_2/CP_1 and T_2/CP_2 were not continued, because for the first the condition $R_{T2}>>R_{CP1}$ was satisfied, therefore the charging were insignificant. In the second case, the charging and discharging were very slow (τ_i and τ_d values are hundreds of sec). Therefore, only the T_1/C_{P1} and the T_1/C_{P2} combinations are further discussed.

Figure 3.1 shows the $U_P(t)$ curve based on the averaged experimental results of these combinations. In Figure 3.1.a, the case of walking with artificial leather soles on PVC foor, the personnel voltage, U_P, increases linearly in the first 10 seconds, then it reaches the saturation phase and settles to 3 kV after another 10 seconds. This value of $U_P(t)$ is close to the theoretical representation defined by equation (2.5).

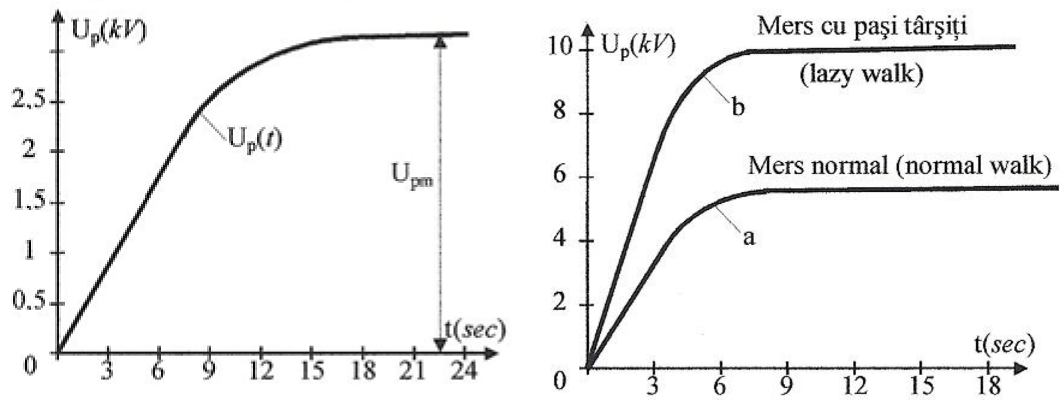

a) **b)**

Figure 3.1 Curve of *Up* voltage for walking a) T_1/C_{P1}: sole of artificial leather on PVC floor; b) T_1/CP_2: sole of artificial leather on carpet

For the artificial leather-carpet (T1/CP2) combination, the operator voltage was measured at normal walking and lazy walking speed. Figure 3.1.b shows the $U_P(t)$ curves for these cases. At normal walking, the tested personnel charges faster in average and more significantly than on the PVC floor-covering. One explanation can be that the friction is greater on the carpet than on the floor. At lazy walking U_P is higher compared to the normal walking. In order to avoid excessive charging, the recommendation is to avoid lazy walking on this type of polypropylene carpet.

Notes:

1. The tests were performed using the available polypropylene carpet, not treated antistatic, rather common in server rooms and many research and industrial facilities.

2. The charging levels at walking on the carpet Figure 3.1.b are important and may cause electrostatic discharges via operator that can be harmful to sensible electronic devices and equipment. For instance, assuming C_P = 200 pF in the normal walking case ($U_{Pm} \cong$ 5 kV) according to equation (2.2) the charging energy is 2.5 mJ and in the lazy walking case (U_P = 10 kV) it increases to 10 mJ. These values could generate hard damage, functional damage or latent damage. Although the charging level is not as high, these damages could also occur in the case of PVC floor coverings, as clearly the standard HBM levels under 100 V recommendation [2], [70]-[71], is evidently far from being satisfied. Moreover, if in this case C_P = 200 pF and U_P = 3.2 kV, the energy is W = 1 mJ. This energy is enough to generate hard damage or functional (soft) errors. If the discharge results in sparking, it could generate explosion in the presence of flammable vapors (e.g. from electro-insulating paint), as the flammability minimum energy in such environment is 0.25 mJ [22].

3.1.3 Measurements at sitting on a chair

As shown in subsection 2.1 (Figure 2.2.b), the personnel sitting at the workbench charges through frictions with chair, as well as at lifting from the chair. Again, a few experimental context considerations are seen as more fit to be referred to in this paragraph.

A textile tapestry chair with armrests covered by a vinyl foil was used. This mechanical protection foil simulated the worst possible conditions, as vinyl foil charges higher than the textile tapestry. Five volunteers (A-E) were used as test personnel, this time all of different weight, ranging between 50 kg to 80 kg, to illustrate the effect of this practical parameter in real working conditions in a production line. Otherwise, all the other conditions were kept the same and all the test personnel were equipped with the same synthetic fiber trousers type.

Similar to the case of walking, the charging capacitor method shown in Figure 2.11 was used to measure the body-system voltage. To make the proper measurements, the previously discharged test person (P) sits on the test chair facing a PC-based automation piece of equipment placed on the working table. The persons were asked to first rotate three times from left to right (simulating moving on chair during usual operator activity) and finally to stand up and finger touch the input terminal of the known capacitor C. The voltage U on the voltmeter (ESV) is recorded and the unknown charge q computed using:

$$q = (C + C_P) \cdot U \tag{3.3}$$

where C and C_P are the same as in equation (2.18). For every tested person (A, B, C, D, E), the measurement was repeated five times and the final result was then averaged and recorded. In order to draw significant conclusions on personnel charging in general, and since this particular set of data also concerns the effect of personnel body weight, the results for this personnel charging scenario will be presented in parallel with the results of indirect measurement data in § 3.2.3.

3.2 Indirect measurements of static charge on personnel

This sub-chapter shows the physical and the performance characteristics of the instrument presented detail in subchapter 2.2. This instrument can be used for both direct charge measurement of larger size textile materials and for indirect measurement of charging on personnel. The subchapter continues with the presentation of measurement results for both the indirect and direct method, with data in the direct method as control.

3.2.1 Faraday cup based instrument

The basic mechanical characteristics of the proposed and tested instrument shown in Figure 2.8.b are: size: h_1=230 mm, D_1=275 mm, h_2=250 mm, D_2=310 mm, h=18 mm.

The electrical characteristics of the instrument are given below:

- measured capacity C_{12} = 140 pF,
- insulation resistance $R_{12}>10^{14}\ \Omega$,
- breakdown voltage $U_{12}\cong 20$ kV.
- Measurement range: 200 nC and 2.000 nC.
- Accuracy: 3 %·max.
- Power: 4.5 V (batteries), current <50 mA.

The next table shows the comparison between a commercial instrument [127] and the proposed instrument. The volume of the Faraday cup in the proposed instrument is about five times larger while its accuracy remains comparable to the accuracy of the commercialized instrument. The proposed solution also has the advantage of measuring the charge q_x without direct contact with the measurement electrode of the Faraday Cup, as described in subchapter 2.2. The presented instrument (Nanocoulombmeter) is designated to measure the triboelectric charge either on larger size textile materials, on garments worn by human operators in the electronic industry, as well as on any charged object of larger size.

Table 3-IV Comparison with a classic Faraday instrument

Characteristic / Instrument	Input Volume (FC)	Accuracy	Output Instrument	Measurement Method
Commercial	3.2 dm3	2 %	Electrometer	Contact with q_x
Proposed instrument	17 dm3	3 %	Fieldmill	No contact

As indirect method, this instrument is a simpler solution for testing the charge on a human body system than the solution that is presently in use [55]. However, although comparable results were later obtained, the results on indirect HBM measurements using this particular instrument are not presented in this work, as at the time of proposing and testing the HBM indirect method [126], [128] this instrument [129] had not been built. For the sake of comparison, it is also important not to introduce variables such as different test subjects and slightly different environment conditions.

3.2.2 Measurement results on personnel

The same subjects, (A,…,E), environment conditions, initial discharge of the person before the experiment, as well as the same number of repetitions and sweater material as for the direct charging method at walking were used.

The indirect method of charge measurement on personnel at garment removal was described in § 2.3.3. However, to test the validity of the method, the direct method measurements described in § 2.3.2 are also performed here, and the results from both methods compared and discussed. As mentioned at the beginning of the subchapter, the direct method results are used as control to validate the proposed indirect method.

The direct measurement results on the statically charged operator at garment removal represent the averaging of five repeated measurements, made in the same conditions, for each subject. These averages are plotted in Figure 3.2. Although the subjects were of approximately the same weight and size, the charge q_1 is different from subject to subject. Subject C accumulated the highest charge ($q_{1\mathrm{C}}$=1.1 μC), and subject D accumulated the lowest charge ($q_{1\mathrm{D}}$=0.8 μC). This inconsistency can be due to the variation of C_{Π} in equation 2.16, term that is widely recognized as unstable [2], [55], [86], [125], as well as to the different speed at which each subject removes the garment during testing.

Figure 3.2.a shows that the highest charge level measured through the direct method is q_1 = 0.8 μC (D). For q_1 measurement, C was fixed at 200 pF. Using the energy described by equation (2.3) and equation (3.4), the energy range W results as between 6.4 mJ and 12.5 mJ. These levels are a higher compared to the energy at walking on insulator floor, hence more potentially damaging.

$$W = \frac{1}{2}CU^2 = \frac{1}{2}\frac{q^2}{C} \qquad (3.4)$$

The results of the measurements through the indirect method described in subsection 2.3 are shown in Figure 3.3.b. By comparison to the results for the direct method in Figure 3.3.a, the charge q_2 is smaller for most subjects except D and E.

By comparing the measurements of q_1 and q_2, it was determined that the difference

$$\Delta q = \left(q_{1A} + \ldots + q_{1E}\right) - \left(q_{2A} + \ldots + q_{2E}\right) \tag{3.5}$$

is approximately 8%.

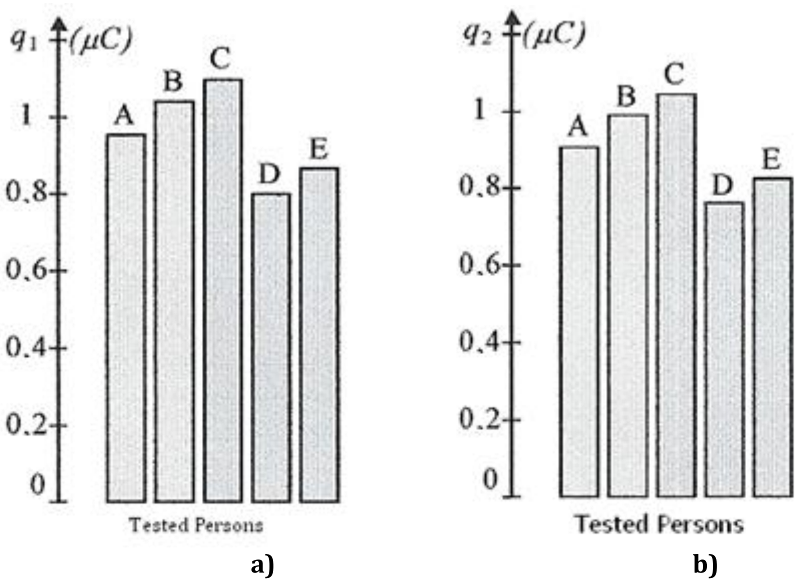

Figure 3.2 Electrostatic charge measurements on personnel at garment removal a) q_1 through the direct method; b) q_2 through the indirect method.

Based on the obtained error, acceptable for measurements in electrostatics, it results that the triboelectric charge on an operator at garment removal can also be tested indirectly. The indirect method is easier, more convenient, as well as more controllable, as the term C_p, which is unstable and needs to be measured for each individual before the direct measurement, is eliminated.

Based on this observation, the work proposes as measurement method of the electrostatic charge accumulated on the operator (P) as result of removing a piece of clothing (GP), the method illustrated in Figure 2.13. This diagram represents one of the original contributions in this work.

3.2.3 Comparison between indirect and direct charge measurement results

The results obtained for the experiments in § 3.1.3 for personnel of different weight, sitting on chair at the workbench, are presented in Figure 3.3. As expected, due to the fact that the personnel charging is influenced by his body weight (BW), the dispersion of q measurements is greater than the charge dispersion in the previous two test cases presented in Figure 2.4 and Figure 2.12. Therefore, it was deemed as useful to present the results in Figure 3.3 as sorted by values of q, rather than in subject order. In the latter figure, under the indicative A ... E, the body weight (kg) was mentioned for each person.

Both the charging level of P walking on insulator floor-covering, determined through voltage (U_p) measurement at P terminals, and the charging level of P at garment removal, determined through measurement of accumulated charge on garment at separation from the body system, are calculated as electrostatic energy using the appropriate-to-each case formula in equation (3.4). The energy levels are compared to the energy calculated for the case of P sitting on chair in order to determine which of them, in practice, poses more hazard to the equipment in the manufacturing line.

For each of the three activity types of P, a maximum and minimum value of W is obtained and plotted in Figure 3.4. Figure 3.4.a presents the minimum levels of accumulated electrostatic energy for each of the three regular personnel activities studied in this work. In Figure 3.4, these activities that the personnel ordinarily performs during working time in a normal work place, are designated by numbers: (1) walking on insulator floor-covering (PVC), (2) changing in preparation for work, taking a wool sweater off in our analyzed case, and (3) sitting on chair.

From this data comparison, one could note that the lowest electrostatic charging level (1 mJ) occurs at walking on PVC floor covering (1), and the highest level (6.4 mJ) is at taking a sweater off (2). An intermediate level (2.4 mJ) was determined for sitting on chair. Therefore, even in the most favorable case (minimum level) the accumulated energy is high enough to generate hard damage or soft errors as well as explosion of flammable vapors (the lowest flammable energy level is 0.25 mJ).

From Figure 3.4.a, it results that the worst case is for taking a wool garment piece off (2). Hence, this activity has to be seriously treated in terms of static charging: the personnel should discharge after changing into work garments and before handling/approaching devices or equipment.

The maximum levels of electrostatic energy that may be accumulated on the personnel are shown in Figure 3.4.b. By comparing this data to the data in Figure 3.4.a, the maximum levels of electrostatic energy accumulated during the three activities are twice of the minimum levels.

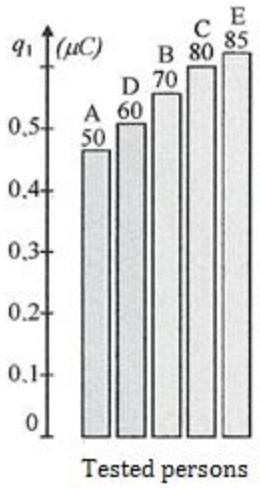

Figure 3.3 Electrostatic charging (q) for sitting on chair for persons of different weights

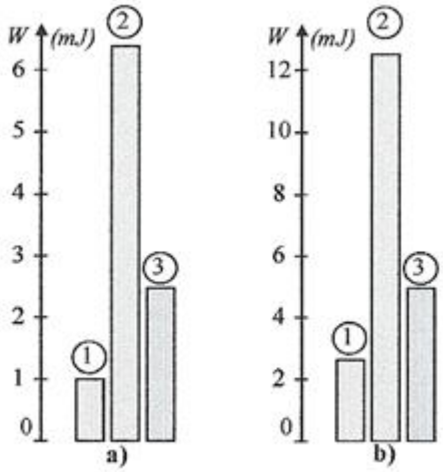

Figure 3.4 Comparisson of electrostatic energy for walking (1), at garment removal (2) and at sitting on a chair (3); a) minimum values; b) maximum values

3.3 Conclusions

(1) The level of accumulated charge on personnel is correlated to the body weight and varies in large range from the lowest level of energy (1 mJ), recorded at walking on PVC floor, to the highest (12.5 mJ), recorded at taking a sweater off. An intermediate value was obtained at sitting on a tapestried chair (4 mJ).

(2) Whenever the operator's preparation for work may involve removing off the outdoor clothing (such as sweater), the person can charge electrostatically with enough charge (0.5-1.1) μC to provoke damage to the equipment or the electronic components he will be touching.

(3) The indirect measurement method (i.e. measuring the charge on the removed clothing) is far more convenient than measuring the charge directly on the person, as it does not require the knowledge of the Human Body capacitance, which needs to be measured for each person every time before using the direct, classical method.

4 ELIMINATION OF STATIC CHARGE AT THE SURFACE OF NON-WOVEN TEXTILE MATERIALS

Let the experiment be made.

Benjamin Franklin

Static charge build-up at the surface of textile materials is a major nuisance, as seen in the previous chapter. In the manufacturing of air filters, where charging of non-woven fiber sheets is part of the last manufacturing steps, undesirable charging could also happen at previous steps in the process [142]-[147]. This accidental charging can pose problems to the apparatus around, as well as for the personnel.

A first step in avoiding this kind of hazards is the estimation of the maximum charge density attainable under various operating conditions [149] (subchapter 4.1). The second step consists in adopting technical solutions to reduce the charge at the surface of textile materials. Standard ion generators [150] (subchapter 4.2) and more sophisticated installations [151] (subchapter 4.3) could be employed in this purpose.

4.1 Estimation of the maximum charge density at the surface of non-woven fabrics

The experiments were performed on 100 mm x 85 mm samples of non-weaved sheets of PP (sheet thickness: 400 μm or 800 μm; average fiber diameter: 20 μm; Figure 2.14), in ambient air (temperature: 18°C to 22°C; relative humidity: 30% to 40%). The PP fibers represent roughly 15% of the volume of the media.

The samples were charged using a triode-type electrode arrangement described in subchapter 2.4, Figure 2.15. The high-voltage wire-type dual electrode [152] of the arrangement consisted in a tungsten wire (diameter 0.2 mm) supported by a metallic cylinder (diameter 26 mm) and distanced at 34 mm from its axis. The wire and the cylinder were powered from the same adjustable high-voltage supply 50 kV, 6 mA (model SL 300 SPELLMAN), operating as a constant current generator.

In a first set of experiments, the 0.3 mm thick PP sheets were deposed directly on the surface of the grounded plate electrode. In all the other experiments, the 0.8 mm thick PP sheets were suspended at 4.6 mm above the bottom electrode of the triode arrangement. In order to evaluate the effect of thermal conditioning on the charging and on the surface potential decay, in some experiments the samples were pre-heated at 75°C in an electric oven.

In all the experiments, the samples were charged for 10 s by exposing them to the corona discharge, at various grid potentials. The surface potential on the samples was then measured with an electrostatic voltmeter (TREK, model 341B, equiped with an electrostatic probe model 3450). The measured potential was monitored via an electrometer (Keithley, model 6514), connected to a PC. The acquisition and processing of the experimental data was performed using the ad-hoc virtual instrument, described in subchapter 2.4.

4.1.1 Samples in contact with a ground plate

The first set of experiments, carried out with the 0.3 mm thick PP sheets deposed directly on the surface of the grounded plate electrode, pointed out a phenomenon that has already been reported in the case of insulating films [94], [101], [106], [153]-[156]: at a higher initial value, such as the one obtained for V_g = 4 kV, the surface potential decreases faster than in the case when the sample is charged to a lower potential, such as V_g = 1.5 kV (Figure 4.1).

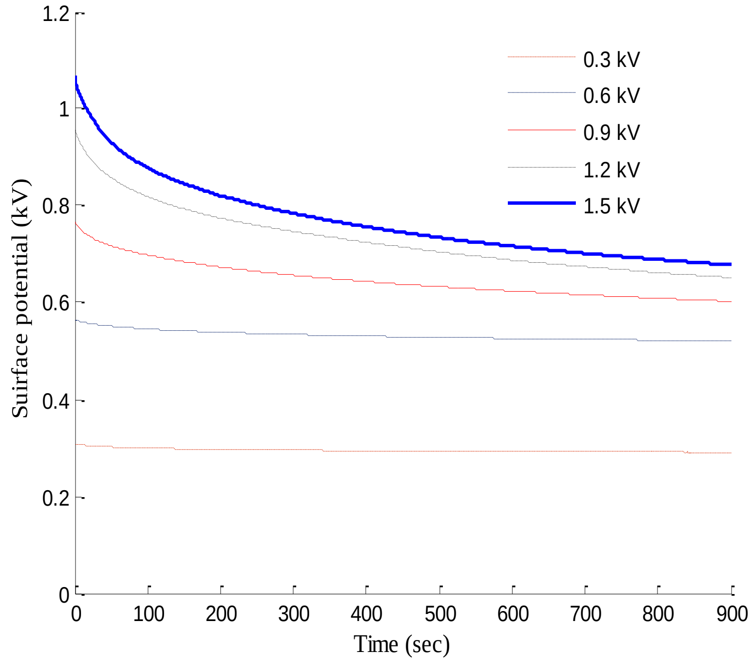

a)

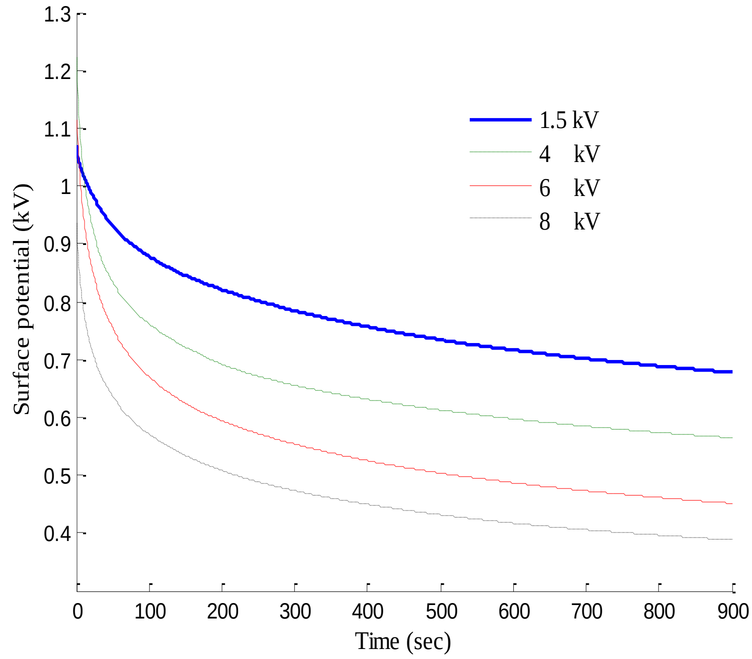

b)

Figure 4.1 Typical surface potential decay curves obtained at various grid potentials for the 0.3 mm thick sample, directly deposed on the surface of the grounded electrode; (a) $V_g \leq 1.5$ kV; (b) $V_g \geq 1.5$ kV.

The available amount of data on non-woven media is not large enough to attempt the elaboration of a specific model for this class of materials. It can be assumed that, similar to what happens in films, there are more deep charge traps at the surface of the media. At low grid voltage, most of the charges are captured in these traps. As the grid voltage increases, more charges are captured in the swallow energy band. When the high voltage that generated the corona discharge is turned off, these charges can be more easily anealed by the ions of oposite polarity in ambiant air.

When in contact with the grounded plate electrode, the capacity of a sample that carries a charge Q, has a surface S and a thickness d, can be expressed as:

$$C = \varepsilon \frac{S}{d} = \frac{Q}{V} \tag{4.1}$$

The surface density, σ, of the sample can be calculated with the following formula:

$$\sigma = \frac{Q}{S} = V \frac{\varepsilon}{d} \tag{4.2}$$

Considering ε = 10^{-11} F/m and d = 0.4 mm, which should be a rather adequate assumption, as the media is very porous (PP represented only 15% of the volume of the sheet) and deposed un-stretched on the plate electrode, the surface charge density corresponding to the maximum potential V = 1100 V would be σ = 27 μC/m^2. This value, which is in good agreement with what is commonly accepted as the maximum allowable surface charge density in air σ = 26 μC/m^2, was confirmed by an experiment made on the 0.8 mm thick sample (Figure 4.2).

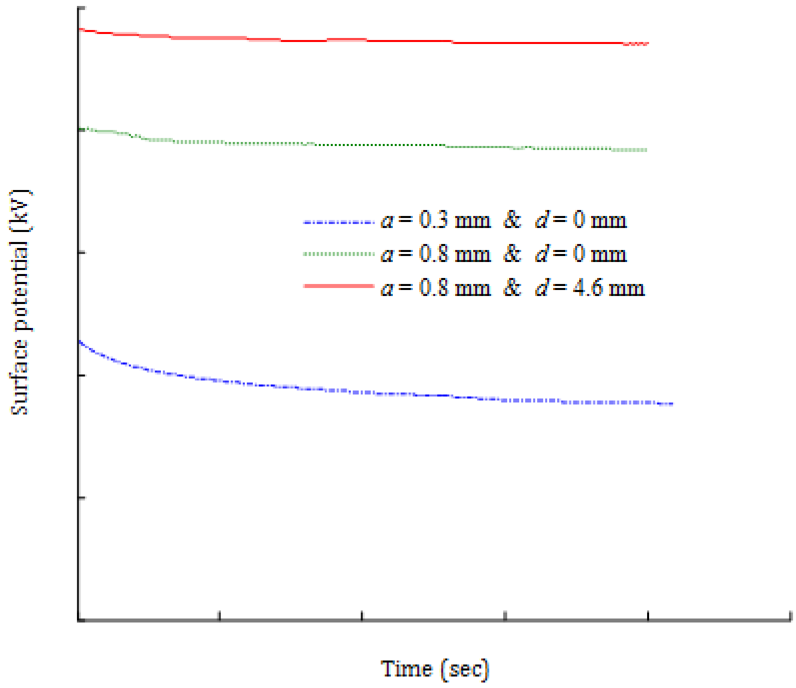

Figure 4.2. Typical surface potential decay curves obtained at a grid potential V_g= 2.4 kV for the *a* = 0.3 mm and *a* = 0.8 mm thick samples, in contact with the grounded electrode (*d* = 0) or suspended at *d* = 4.6 mm above it, at ambient temperature.

4.1.2 Samples at a distance from a grounded plate

For the second set of experiments, the 0.8 mm thick samples were suspended at 4.6 mm above the surface of the grounded plate electrode, using a PP grid, in order to avoid any direct or lateral charge leakage to the ground. The results of these experiments are shown in Figure 4.3.

The high voltage applied to the grid was limited to V_g = 10 kV by the technical features of the available experimental set-up. However, this value is probably not too far from the optimum, because the corresponding surface charge density, calculated for V = 10 kV, d = 5.4 mm, and ε = 8.85 10^{-12} F/m (the presence of the PP fibres has a negligible effect on the global dielectric constant of the media to plate gap) is σ = 16.37 μC/m^2.

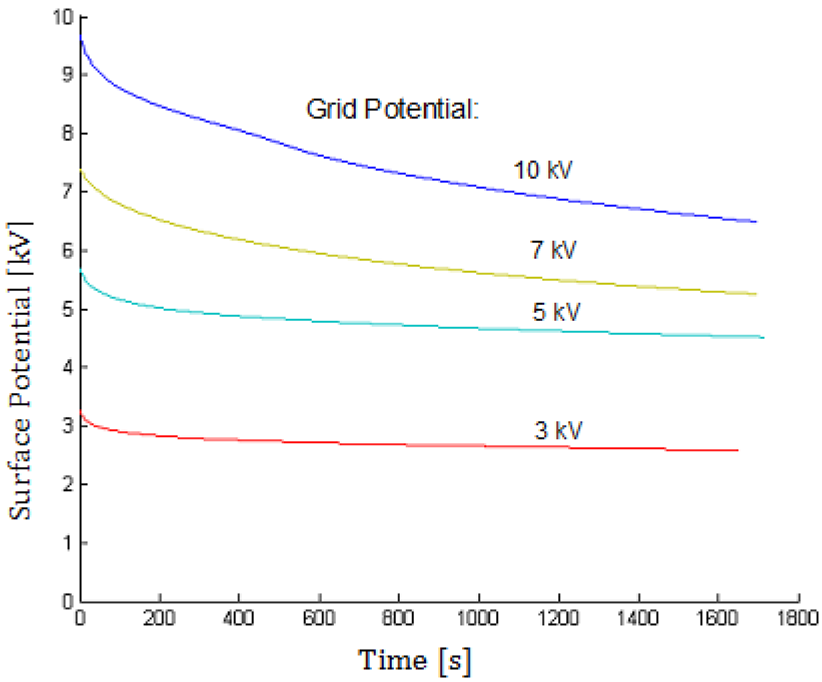

Figure 4.3. Typical surface potential decay curves obtained at various grid potentials for the 0.8 mm thick sample, suspended at 4.6 mm above the grounded electrode, at ambient temperature.

Surprisingly, at lower values of V_g, the potential V at the surface of the sample is slightly higher than that imposed by the grid. In addition to experimental errors (the grid potential was computed as $V_g = RI$, and neither R nor I were measured by precision instruments), this might be explained by several aéro-electro-dynamic phenomena. The corona wind exerts a pressure on the sample and bends downwards the PP grid on which it is suspended. As a consequence, the spacing between the sample and the grounded electrode reduces from s to s^*. At the same time, the space charge that is present in the air gap between the grid and the surface of the sample tends to repel the charges that are deposited on the PP sheet, producing a compression effect on the non-woven medium, which changes its thickness from d to d^*, $d^* < d$. As V is measured several seconds after the high-voltage is turned off, there is no more corona wind and space charge in the air gap. With no more aerodynamic and electrostatic forces in action, the spacing between the upper face of the non-woven medium and the grounded electrode increases from $s^* + d^*$ to $s + d$. At constant surface charge density σ, this increase causes a decrease of the capacitance C and hence an increase of the potential at the surface of the sample, which can thus surpass that of the grid electrode.

The effect of the temperature on the curves of surface potential decay is double: an increase of the value measured at the initial instant and a diminution of the slope of its decay in time, as shown by the results displayed in Figure 4.4. These observations can be explained by several physical mechanisms. Thus, at higher temperature, the charge injected at the surface of the media may move to deeper traps. Heating would also produce an increase of charge mobility, which could lead to the crossing of the sample by most of the charges during the charging phase, therefore making the decay more stable during this short 900 s period. Finally, the diminution of the moisture content of the heated sample slows down the charge decay, as water increases the electrical conduction and favourites charge neutralisation.

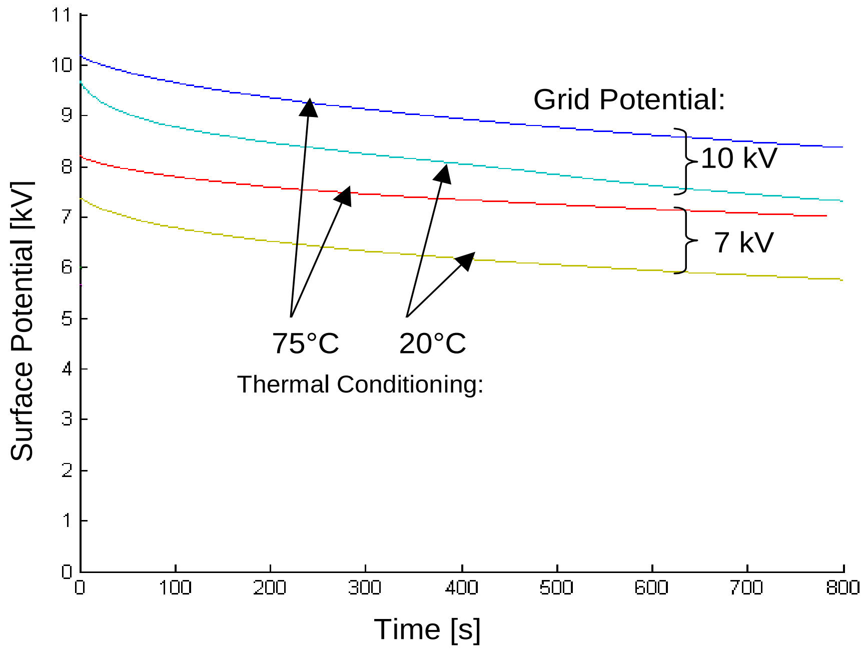

Figure 4.4. Effect of thermal conditioning on the surface potential decay curves obtained at various grid potentials for the 0.8 mm thick sample, suspended at 4.6 mm above the grounded electrode.

4.2 Accelerated discharge of non-woven fabrics using a commercial ion generator

The charge accumulated on non-woven fabrics due to tribocharging effects inherent to the manufacturing process might be harmful either to the operator or to the electronic equipment of the production line. Whenever charge build-up cannot be avoided, it is important to dispose of effective means to rapidly discharge the materials.

4.2.1 Materials and methods

The experiments were performed on 165 x 117 mm^2 samples of non-weaved sheets of PP and PE, at ambient air temperature (19°C to 22.5°C) and relative humidity (35% to 43%). The sheet thickness for both samples was 300 μm; the average fiber diameter was 28 μm for PP and 19 μm for PE, as shown in Figure 4.5.

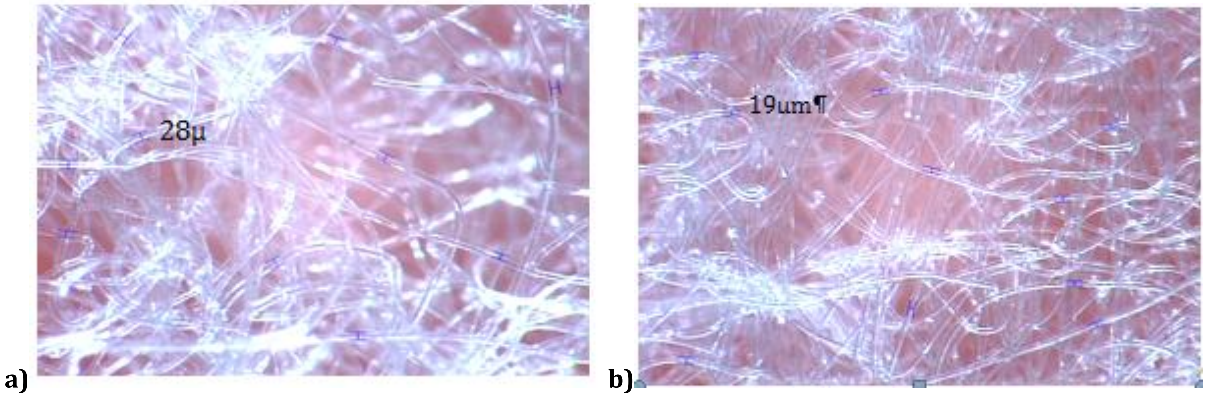

Figure 4.5. Photograph of the non-woven (a) polypropylene and (b) polyester media.

The samples were charged for 10 seconds using a triode electrode system (Figure 4.6) that consists of a high-voltage wire-type dual electrode [93], facing a grounded plate electrode (aluminium; 120 mm x 90 mm), and a grid electrode. The surface potential on the charged media was then measured for 10 minutes with an electrostatic voltmeter (model 341B), equiped with an electrostatic probe (model 3450, Trek Inc., Medina, NY). The measured potential was monitored via an electrometer (model 6514, Keitheley Instruments, Cleveland, OH), connected to a PC. The acquisition and processing of the experimental data was performed using an ad-hoc virtual instrument, developped in LabView environment. After 10 minutes, the media was moved beneath the neutralizer (model 6430, Ion Systems, Berkeley, CA) and it was exposed to both negative and positive ions, for either 4 or 10 seconds. Finally, the surface potential after neutralisation was measured using the previously-described method.

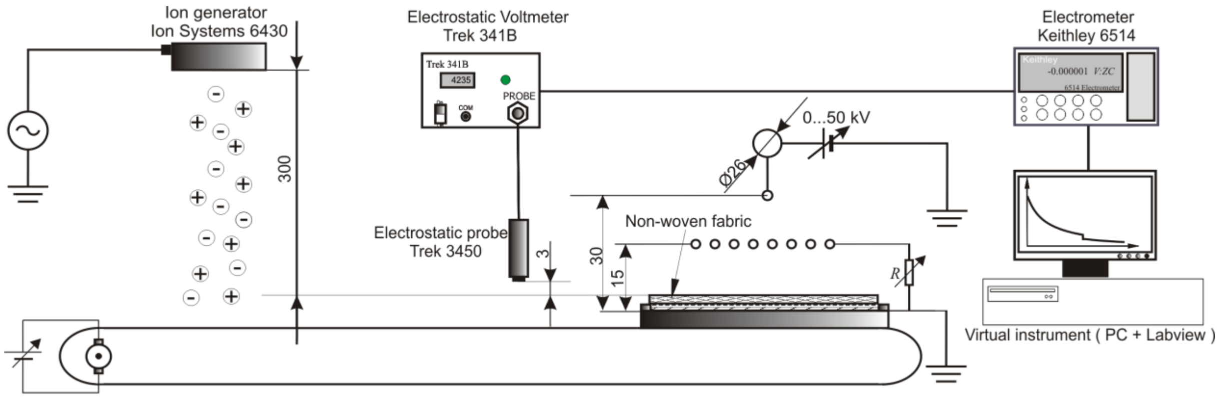

Figure 4.6. Experimental set-up.

4.2.2 Discharging of PP samples

In a first set of experiments, the PP samples, laid on the grounded electrode, were charged using several values of the grid potential V_g, then neutralized using the operating conditions recommended by the manufacturer of the ion generator: neutralization time t_N = 4 s, and neutralizer – sample spacing d_N = 300 mm (Figure 4.7).

When the sample was charged using a grid potential V_g = 0.6 kV, the potential at the surface of the media V_m measured after 10 min was of about 670 V, and decreased to about 540 V after neutralization. In all the other cases, i.e. V_g = 0.8 kV, 1 kV, and 2 kV, the surface potential remained relatively high: V_m ~ 700 V. During the first 60 s after neutralization turn-off, the potential V_m at the surface of the PP sample increases with several volts (Figure 4.8). Then V_m decreases at roughly the same rate (i.e., 0.01 V/s) as before neutralization.

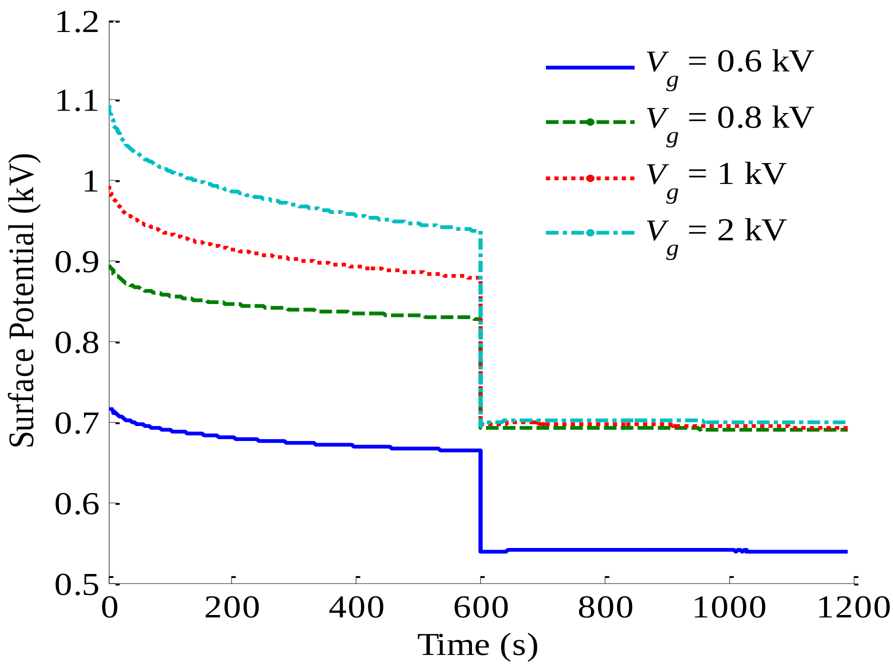

Figure 4.7. Typical surface potential decay curves, obtained for PP samples in contact with the ground electrode and corona-charged at various potentials of the grid electrode V_g. The neutralization was performed 600 s after corona-charging turn-off, for a duration t_N = 4 s.

A possible explanation is the following: after the media was exposed for t_N = 4 s to both negative and positive ions generated by the neutralizer, part of the charge that was initially at the surface of the sample was eliminated. This created a possibility for the charges trapped deeper in the structure of the fibrous media to climb up to the surface and increase the potential measured by the electrostatic probe.

Another explanation may be formulated in relation to the compression exerted on the fibrous media by the air flow generated by the fan of the neutralizer . When the action of the air flow ceases, the fibrous material decompresses; the distance between the charges at the surface of the media and the grounded electrode increases, and the electrostatic probe measures a higher potential at the surface of the sample.

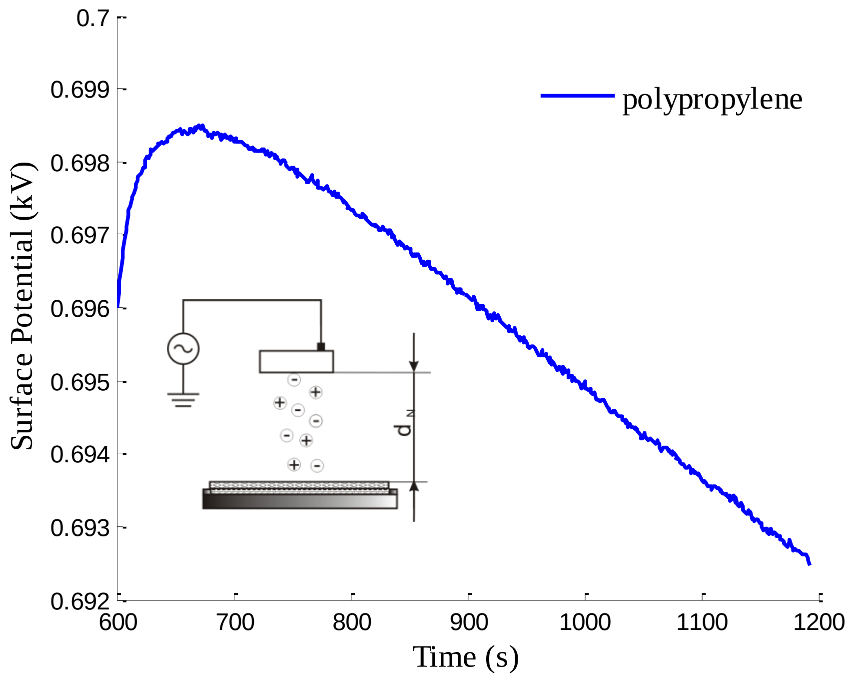

Figure 4.8. Zoom on the surface potential decay curve obtained after neutralization in the case of a PP sample in contact with the ground electrode, corona-charged using a grid potential V_g= 1 kV. The neutralization was performed 600 s after corona –charging turn-off, for a duration t_N = 4 s.

For a fixed distance d_N, by increasing the duration t_N of the neutralization process, and hence the amount of charge provided by the ion generator, it is possible to reduce the potential at the surface of the sample (Figure 4.9). However, neutralization durations t_N > 10 s are likely to be considered unacceptable for most situations of practical interest.

Figure 4.10 shows that decreasing the spacing d_N between the ion generator and the samples quite significantly improves the discharge effect of the neutralizer. As a matter of fact, by reducing d_N, more ions generated by the neutralizer will be able to cross the spacing to the sample without recombination, and contribute to the discharge of the non-woven PP media.

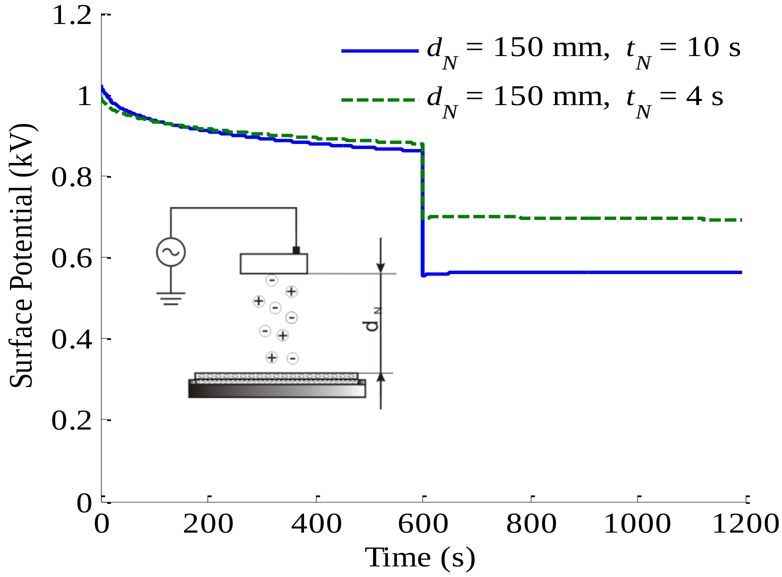

Figure 4.9. Typical surface potential decay curves obtained for two neutralization durations t_N in the case of PP samples in contact with the ground electrode and corona-charged using V_g = 1 kV. The neutralization was performed 600 s after corona-charging turn-off.

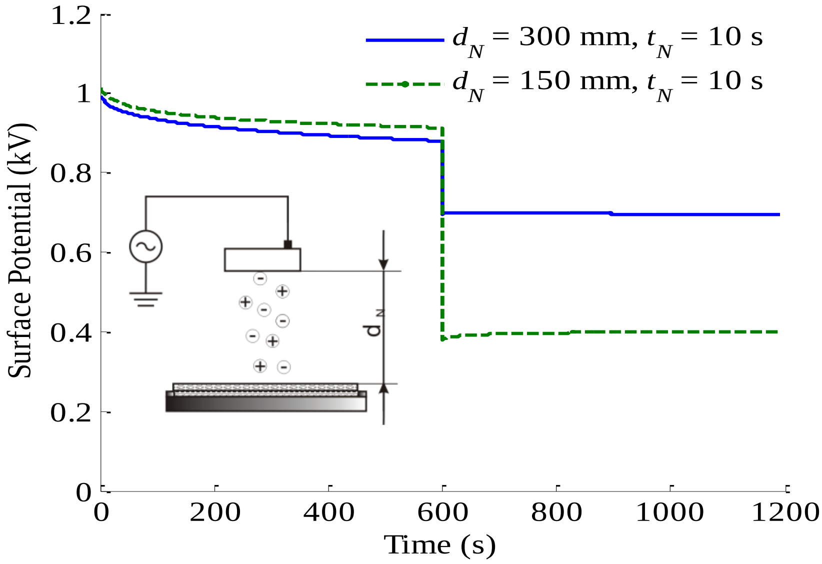

Figure 4.10. Typical surface potential decay curves obtained for two values of the spacing d_N between the neutralizer and the non-woven media, in the case of PP samples in contact with the ground electrode and corona-charged using V_g = 1 kV. The neutralization was performed 600 s after corona-charging turn-off, for a duration t_N = 10 s.

The neutralization is more effective when the sample is suspended on an insulating grid located at d_N = 4.6 mm above the grounded plate (Figure 4.11). This result can be explained by the fact that the air flow generated by the fan of the neutralizer can pass through the sample, which was not the case when the non-woven fabric was laid directly on the grounded electrode. The ions can penetrate much deeper and neutralize a larger number of charges accumulated in the texture of the fibrous media. This hypothesis might be confirmed by the following observation (Figure 4.12): after neutralization, the potential at the surface of the samples located at d_N = 4.6 mm increases for a much longer time (600 s and more) than in the case when the non-woven media were in contact with the grounded electrode (about 60 s). Indeed, the redistribution of the charges needs a longer time in case when the neutralization affected the whole depth of the non-woven media, than in the case when the ion penetration was limited to a thin sheath at the surface of the samples.

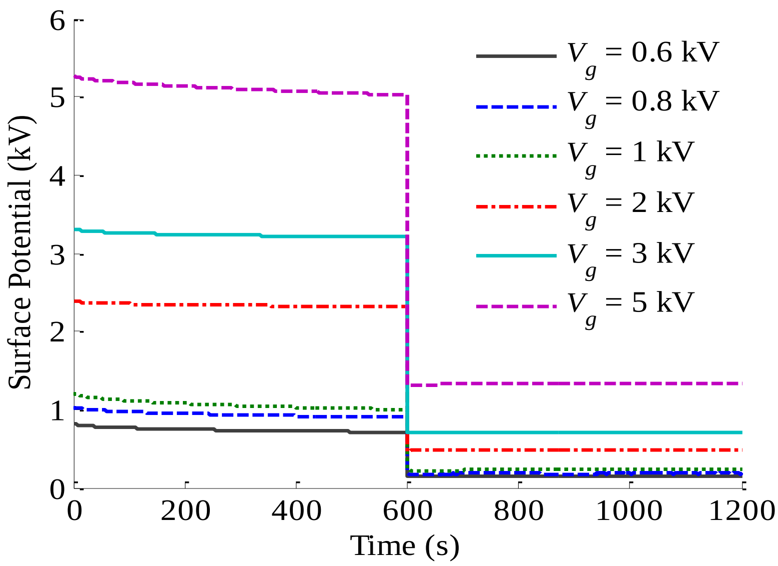

Figure 4.11. Typical potential decay curves obtained for PP samples suspended at a distance d_N = 4.6 mm from the grounded electrode, and corona-charged at various potentials of the grid electrode V_g. The neutralization was performed 600 s after corona-charging turn-off, for t_N = 4 s.

This hypothesis might be confirmed by the following observation (Figure 4.12): after neutralization, the potential at the surface of the samples located at d_N = 4.6 mm increases for a much longer time (600 s and more) than in the case when the non-woven media were in contact with the grounded electrode (about 60 s). Indeed, the redistribution of the charges needs a longer time in case when the neutralization affected the whole depth of the non-woven media, than in the case when the ion penetration was limited to a thin sheath at the surface of the samples.

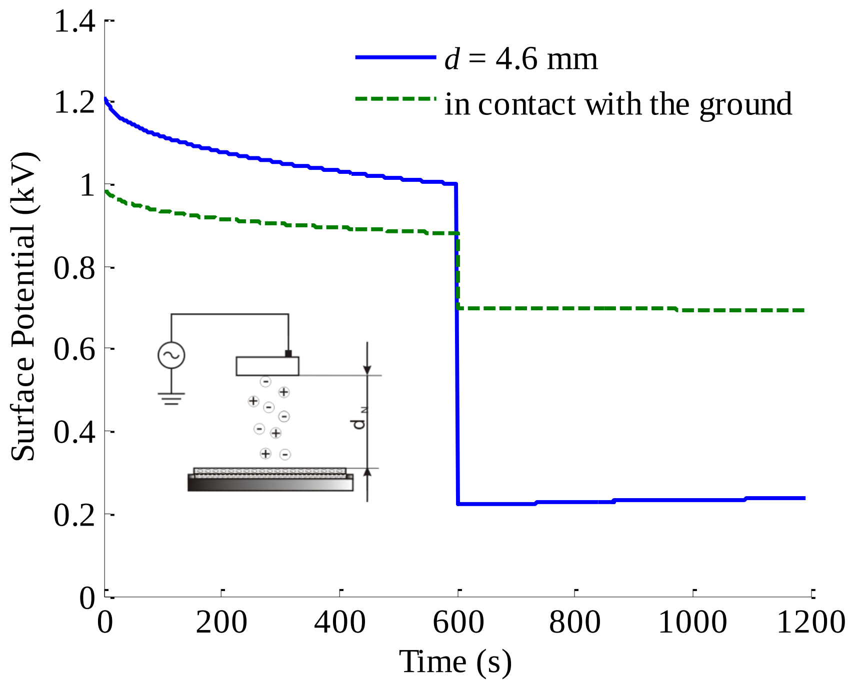

Figure 4.12. Typical surface potential decay curves obtained for PP samples at a distance d_N = 4.6 mm or in contact with the ground electrode. The samples were corona-charged using V_g = 1 kV. The neutralization was performed 600 s after corona-charging turn-off, for a duration t_N = 4 s.

4.2.3 Discharge of PET samples

The ability of polyester to preserve the charge acquired by corona discharge is poor (Figure 4.13). Thus, the surface potential decays to about 200 V in 600 s after the corona-charging of the sample using a grid potential V_g = 1 kV. The neutralization applied at that moment has a rather small effect: it reduces the surface potential by less than 15%.

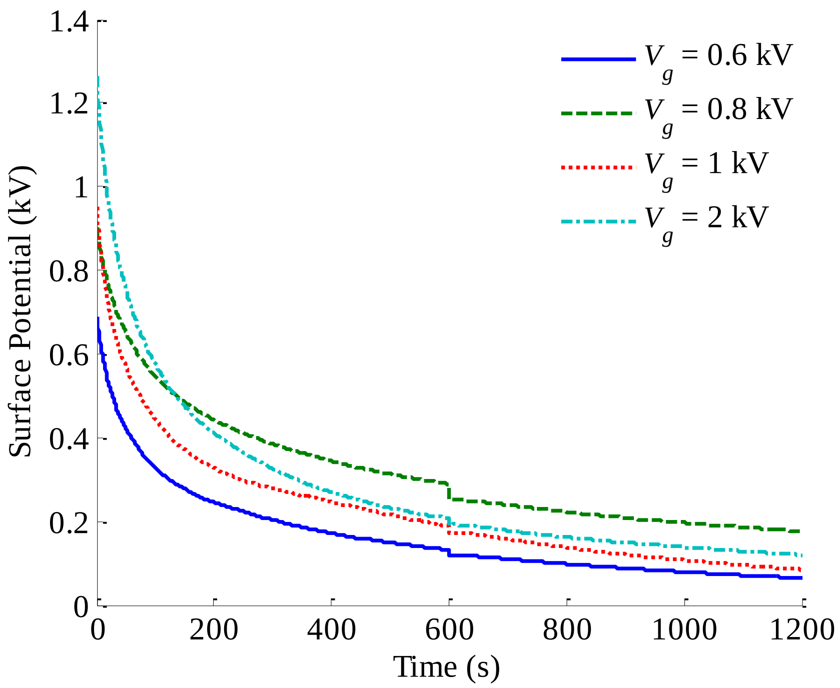

Figure 4.13. Typical surface potential decay curves obtained for PE samples in contact with the ground electrode, and corona charged at various potentials of the grid electrode V_g. The neutralization was performed 600 s after corona-charging turn-off, for a duration t_N = 4 s.

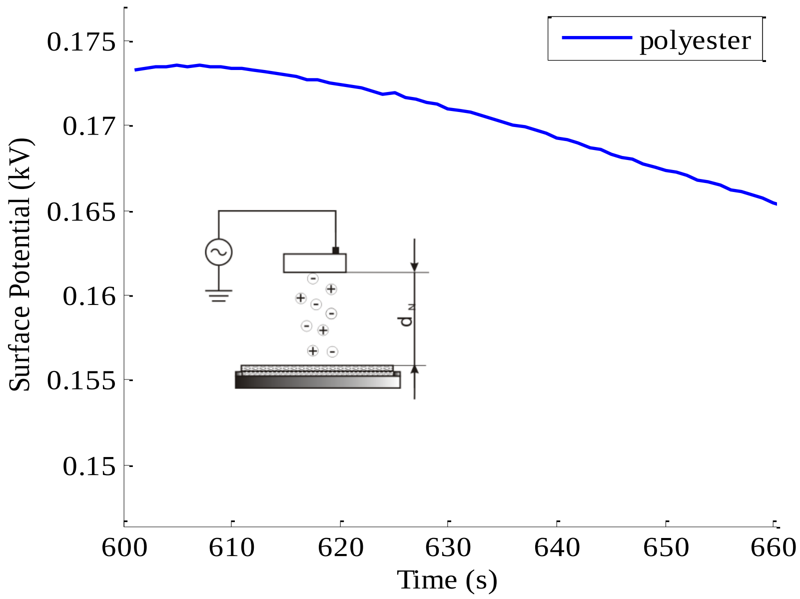

Figure 4.14. Zoom on the surface potential decay curve obtained after neutralization in the case of a PE sample in contact with the ground electrode, corona-charged using a grid potential V_g= 1 kV. The neutralization was performed 600 s after corona – charging turn-off, for a duration t_N = 4 s.

Same as for the PP samples, a slight potential increase is observed at the surface of PET samples after neutralization turn-off, but only for less than 10 s (Figure 4.14). After that, the potential continued to decay rather steeply.

When the PE samples are suspended at a distance at d_N = 4.6 mm above the grounded plate, their surface potential decreases much slower and the effect of the neutralization is much more significant (Figure 4.15), though less important than with PP samples. The comparison between the surface potential decay curves obtained for PE and PP samples clearly point out the different behavior of these two non-woven media (Figure 4.16).

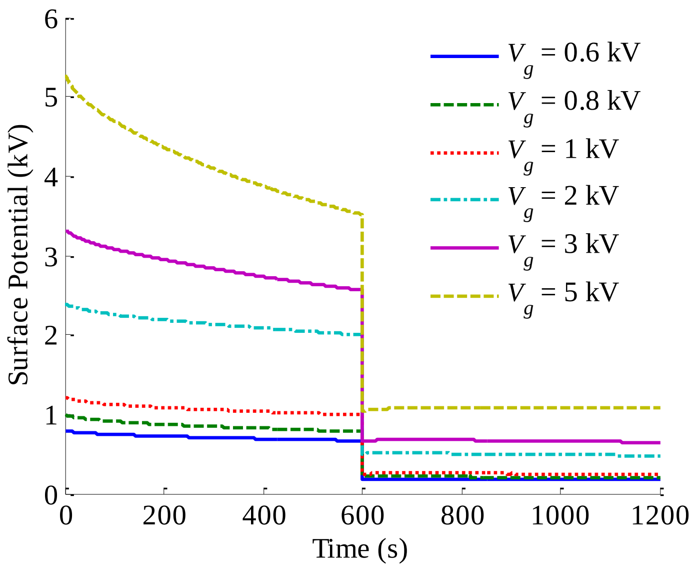

Figure 4.15. Typical surface potential decay curves obtained for PE samples suspended at a distance *d* = 4.6 mm from the grounded electrode, and corona-charged at various potentials of the grid electrode V_g. The neutralization was performed 600 s after corona-charging turn-off, for a duration t_N = 4 s.

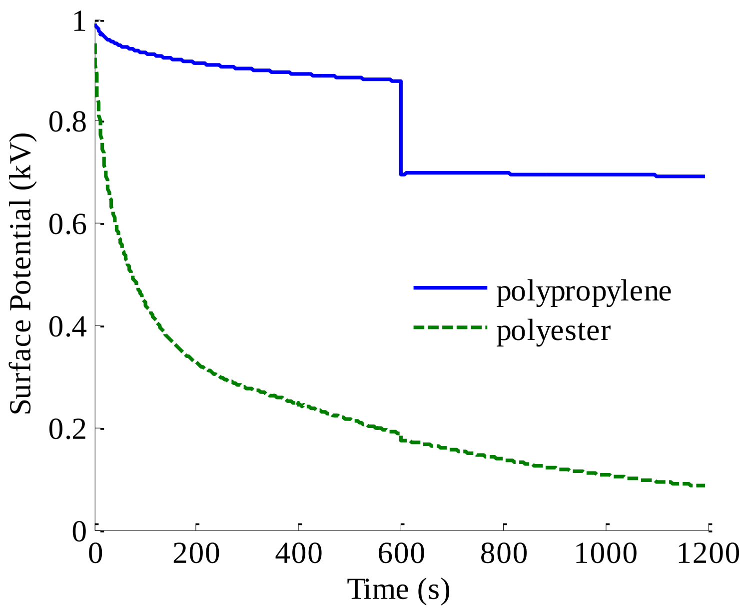

Figure 4.16. Comparison between two typical surface potential decay curves obtained for PP and PE samples in contact with the ground electrode, and corona charged using a grid electrode potential V_g = 1 kV. The neutralization was performed 600 s after corona-charging turn-off, for a duration t_N = 4 s.

4.3 Factors that influence the accelerated discharge of non-woven PP and PET

The present subchapter reports the results of an experimental study aimed at evaluating two factors that influence the charge elimination on non-woven PP and PET fabrics: the frequency and the amplitude of sinusoidal or triangular high-voltage neutralizers.

4.3.1 Materials and methods

The experiments were performed on 100 x 100 mm^2 samples of non-weaved sheets of PP and PET, at ambient air temperature (19.9°C to 24°C) and relative humidity (27% to 44%). The sheet thickness for both samples was 400 μm; the average fiber diameter was 28 μm for PP and 19 μm for PET. The samples were charged for 10 seconds using a triode electrode system (subchapter 2.4) that consists of a high-voltage wire-type dual electrode, facing a grounded plate electrode (aluminum, 165 mm x 115 mm), and a grid electrode.

The surface potential on the charged media was then measured for 10 minutes with an electrostatic voltmeter (model 341B), equipped with an electrostatic probe (model 3450, Trek Inc., Medina, NY). The measured potential was monitored via an electrometer (model 6514, Keitheley Instruments, Cleveland, OH), connected to a PC. The acquisition and processing of the experimental data was performed using an ad-hoc virtual instrument. After 10 minutes, the media was moved beneath a neutralizing electrode, connected to a high-voltage amplifier 30 kV, 20 mA (model 30/20A, Trek Inc., Medina, NY). In all the experiments the neutralization time was t_N = 4 s, and the neutralizer – sample spacing d_N = 50 mm (Figure 4.17).

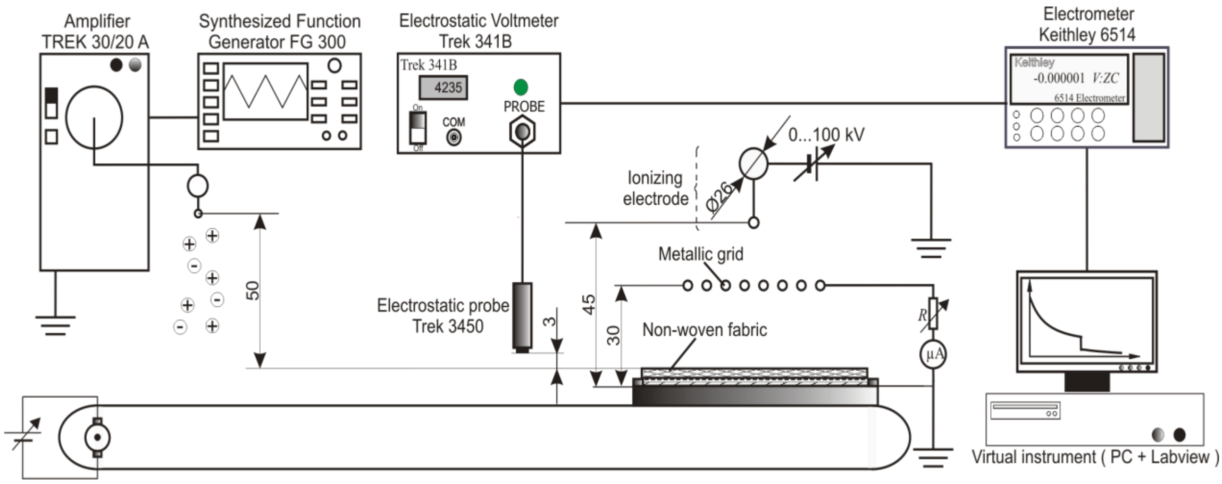

Figure 4.17. Schematic representation of the experimental set-up.

The efficiency of the neutralization was quantified by the ratio between the surface potential after (V_2) and prior to (V_1) the exposure of the charged sample to the AC corona discharge. The amplitude U_m and the frequency f of the high-voltage was adjusted using a synthesized function generator (model FG 300, Yokogawa, Japan).

The experimental methodology design [157]-[158] was employed to evaluate the effects of two factors: amplitude U (range: 16 to 24 kV) and frequency f (range: 20 to 400 Hz) of the neutralization voltage. A normalized centered value x_i was defined for each factor u_i (i = 1, 2) as follows:

$$x_i = (u_i - u_{ic})/\,\Delta u_i = u_i^*, \tag{4.1}$$

where

$$u_{ic} = (u_{imax} + u_{imin})/2;\ \Delta u_i = (u_{imax} - u_{imin})/2. \tag{4.2}$$

4.3.2 Discharging of PP samples

In a first set of experiments, the PP samples, laid on the grounded electrode, were charged using a grid potential V_g = 5.2 kV, then neutralized using sinusoidal high-voltages of various frequencies, amplitudes and frequencies, selected in accordance with a composite factorial design (Figures 4.18 and 4.19, Table 4.I). The potential at the surface of the media V_m measured after 10 min was of about V_1 = 1250 V. When U = 20 kV, f = 20 Hz, the surface potential decreased to about V_2 = 170 V after neutralization (Figure 4.18).

During the first 60 s after neutralization turn-off, the potential V_m at the surface of the PP sample increases with several volts (Figure 4.19). Then V_m decreases at roughly the same rate (i.e., 0.01 V/s) as before neutralization. A possible explanation was given in 4.2.2.

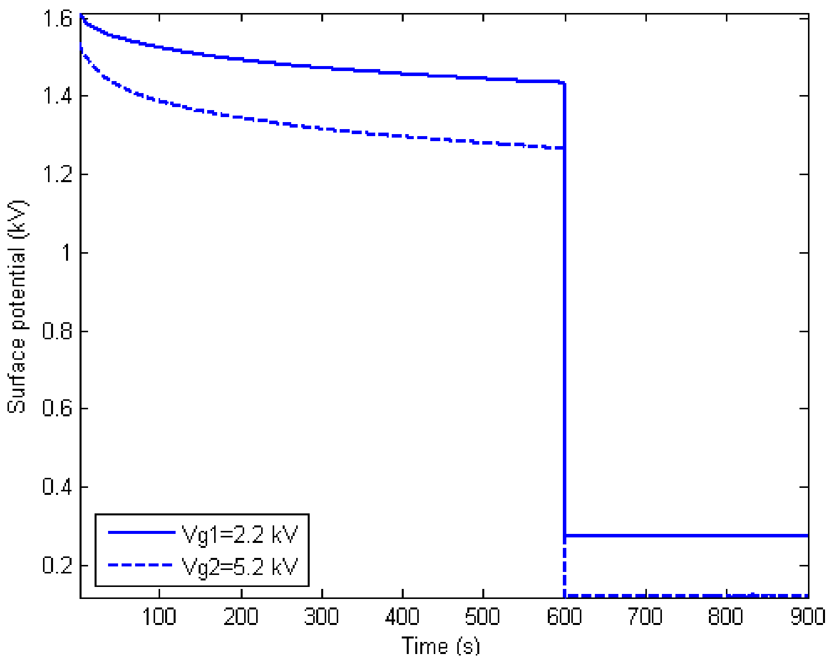

Figure 4. 18. Typical surface potential decay curves, obtained for PP samples in contact with the ground electrode and corona-charged at various potentials of the grid electrode V_g. The neutralization was performed 600 s after corona-charging turn-off, for a duration t_N = 4 s, , using a sinusoidal high-voltage of amplitude U_m = 20 kV and frequency f = 20 Hz.

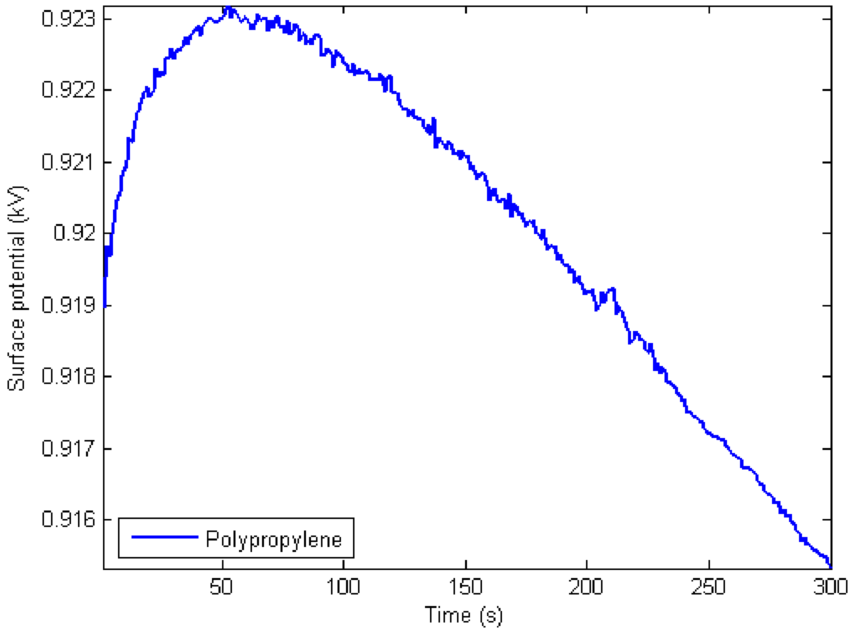

Figure 4.19. Zoom on the surface potential decay curve obtained after neutralization in the case of a PP sample in contact with the ground electrode, corona-charged using a grid potential V_g= 5.2 kV. The neutralization was performed 600 s after corona–charging turn-off, for a duration t_N = 4 s, using a sinusoidal high-voltage of amplitude U_m = 16 kV and frequency f = 20 Hz.

The ratio V_2/V_1 could be modeled by a second order polynomial of the central normalized values of the frequency f^* and of the voltage U^*:

$$V_2/V_1 = 2.27 - 14.9f^* - 10.3U^* + 22.8f^{*2} + 13.9U^{*2} + 6.2\, f^*U \tag{4.3}$$

The model is characterized by an excellent “goodness of fit”: R^2=0.999, and a fairly high “goodness of prediction”: Q^2=0.911. The predicted equal V_2/V_1 contour plots (Figure 4.20) indicate that the efficiency of the neutralization increases with both f and U. The surface potential after neutralization represents less than 5% of the value recorded for the charged sample for practically any U > 18 kV and f > 200 Hz.

<u>Table 4.I</u>. Results of three series of charge-elimination experiments performed on corona-charged non-woven PP fabrics.

Case I: V_g = 5.2 kV; U: sinusoidal

Case II: V_g = 5.2 kV; U: triangular

Case III: V_g = 2.2 kV; U: triangular

Exp. No	f [Hz]	U [kV]	V_2/V_1 [%]		
			Case I	Case II	Case III
1	20	16	70.82	96.79	98.43
2	400	16	9.23	20.98	24.07
3	20	24	36.9	36.3	15.15
4	400	24	18.93	2.43	-14.29
5	20	20	9.34	5.16	-17.98
6	400	20	11.04	-9.89	-28.96
7	210	16	25.96	84.91	32.19
8	210	24	7.26	1.21	-29.6
9	210	20	1.66	-6.23	-22.81
10	210	20	2.33	-6.83	-28.65
11	210	20	1.87	-6.79	-34.78

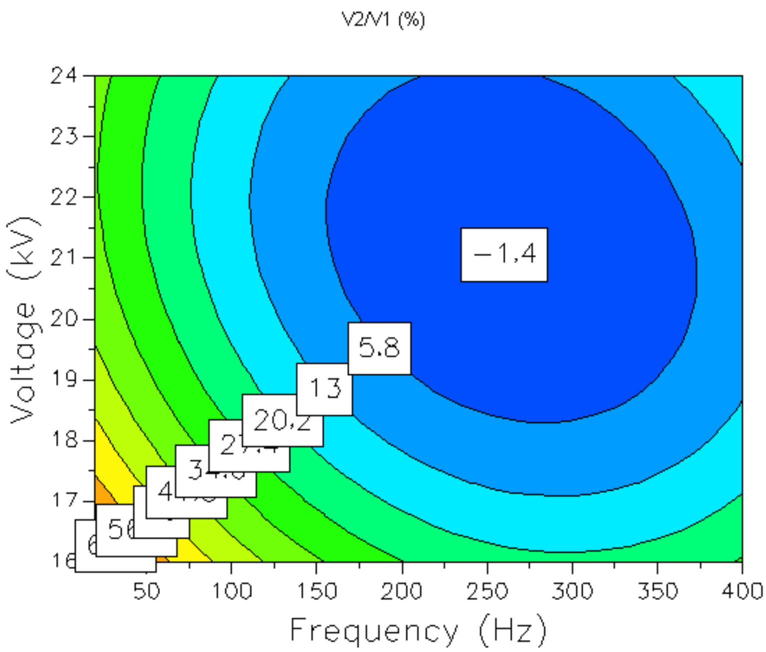

Figure 4.20. MODDE 5.0 – predicted equal V_2/V_1 contour plots (case I: V_g = 5.2 kV; U: sinusoidal).

The second set of experiments (case II in Table 4.I) were performed on similarly-charged non-woven PP fabrics (V_g = 5.2 kV), but the neutralizing voltage was triangular. The V_2/V_1 ratio could be expressed by a quadratic model similar to the one obtained in case I:

$$V_2/V_1 = -6.62 - 6.8f^* - 41.2U^* + 4.2f^{*2} + 49.7U^{*2} + 2.3\, f^*U \quad (4.4)$$

According to this model, which has excellent statistical indexes (R^2=1, and Q^2=0.992), the V_2/V_1 ratio varies with the frequency as shown in Figure 4.21. The negative values of the V_2/V_1 ratio indicate that when using f > 200 Hz, the potential at the surface of the sample after neutralization is likely to change the polarity. The minimum V_2/V_1 predicted by the "Optimizer" function of MODDE 5.0 is -17.14% and is obtained for f = 344.84 Hz and U= 21.61 kV.

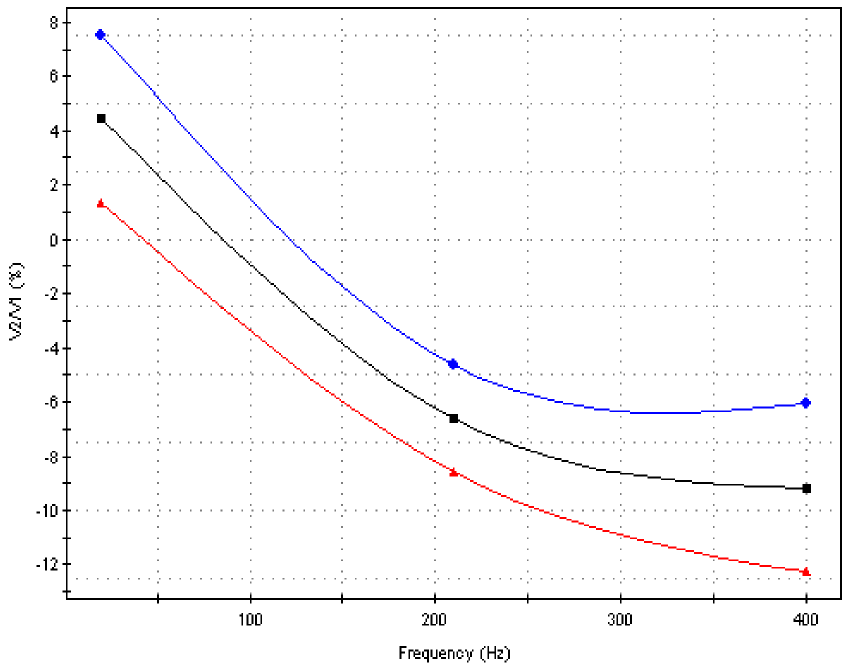

Figure 4.21. MODDE 5.0 – predicted variation of V_2/V_1 with the frequency f (case II: V_g = 5.2 kV; U: triangular).

The third set of experiments (case III in Table 1) pointed out that the neutralizing technique under investigation is equally effective with samples that were charged at lower grid potential V_g = 2.2 kV. The equal V_2/V_1 contours in Figure 4.22 were plotted using the following quadratic model (R^2=0.995, Q^2=0.987):

$$V_2/V_1=-29.3-26.4f^*-30.6U^*+28.3f^{*2}+31.4U^{*2}+11f^*U \qquad (4.5)$$

They clearly show that the best results (i.e., $V_2/V_1 \cong 0$) are obtained at lower f and U than in the previous case. This observation points out the need to adapt the neutralization conditions to the charging state of the non-woven fabric.

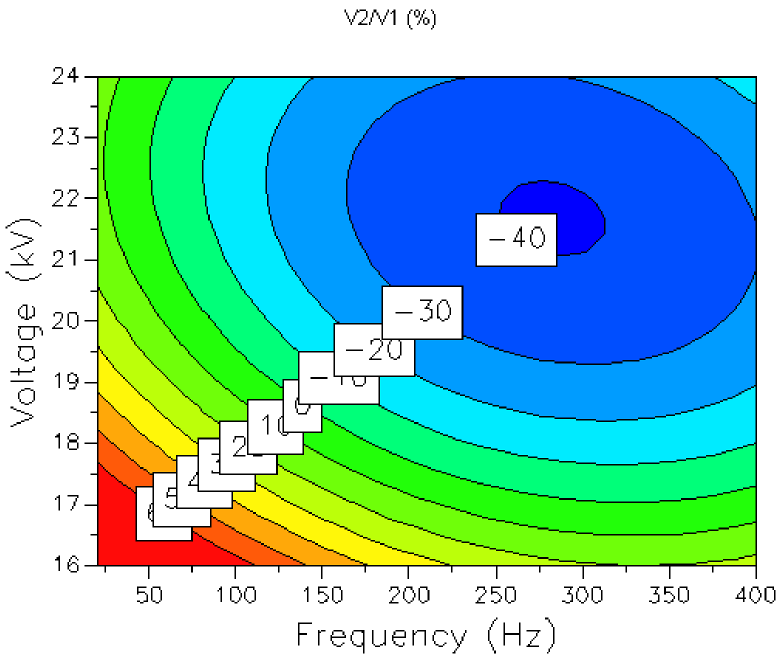

Figure 4.22. MODDE 5.0 – predicted equal V_2/V_1 contour plots (case III: V_g = 2.2 kV; U: triangular).

4.3.3 Discharging of PET samples

The surface potential of non-woven PET samples decays much faster than that of PP fabrics (Figure 4.23). The frequency f and the amplitude U that ensured best neutralization of PP samples proved to be effective also in the case of fibrous PET.

After neutralization turn-off, the potential V_m at the surface of the PET samples increases much more than in the case of PP. Then the surface potential decreases at roughly the same rate (i.e., 0.05 V/s) as before neutralization. This observation validates the considerations exposed before regarding the de-trapping of the charges in the depth of the samples as an explanation for this particular behavior. The charge carriers can penetrate faster in the depth of the PET samples, which explains the steeper surface potential decay curve after corona charging. They can also more easily climb to the surface of the materials, after the elimination of the superficial charge.

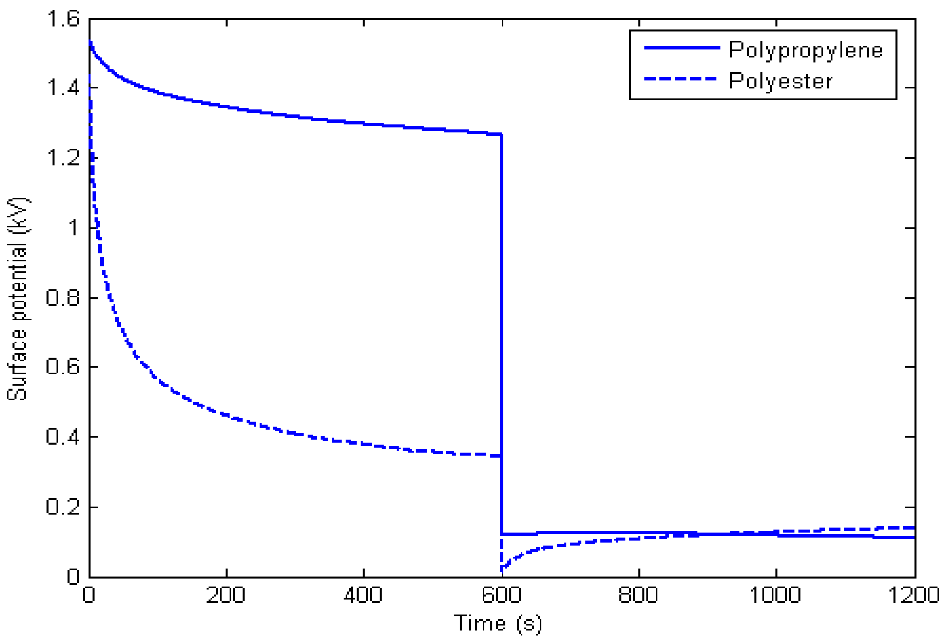

Figure 4.23. Comparison between the surface potential decay curves of PET and PP, similarly-charged at V_g=5.2 kV, and neutralized using a sinusoidal voltage f=20 Hz, U=20 kV.

The neutralization process is strongly dependent on the characteristics of the non-woven fabrics, as pointed out by the experiments carried out on two types of PET samples: Polyester 1 and Polyester 2. The latter has a more porous structure than the former, and this might explain the much faster surface potential decay, as shown in Figure 4.24.

Thermal conditioning of the samples (warm air at 60°C was blown onto the samples for 20 min, prior to corona-charging) has little effect on the neutralizing conditions (Figure 4.25). However, this aspect will need further investigations, under better controlled environmental conditions.

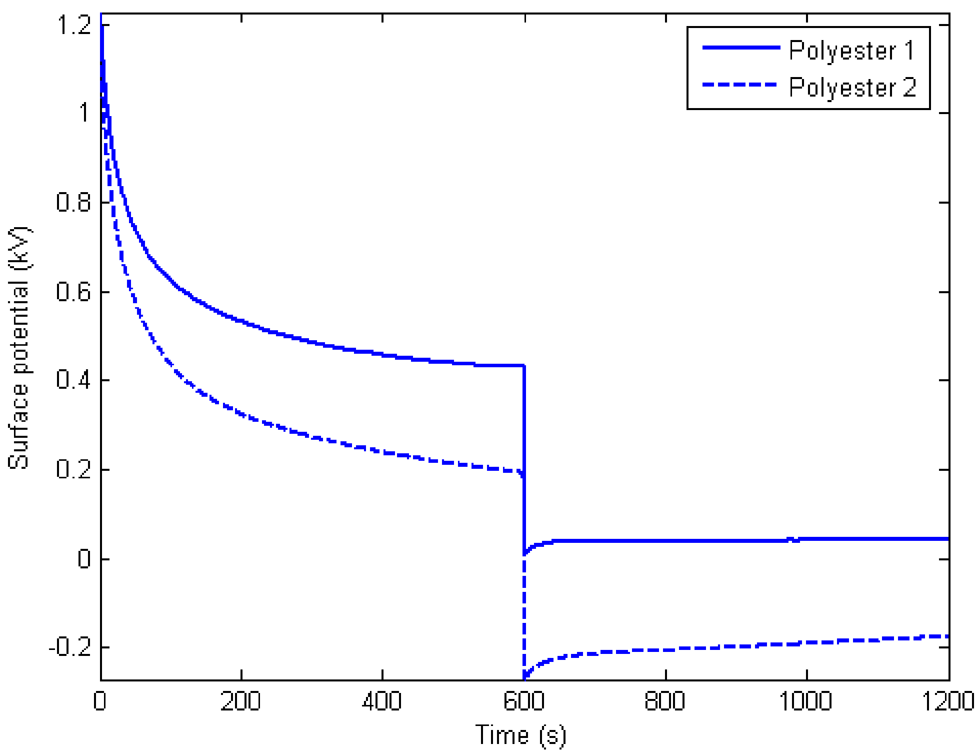

Figure 4.24. Comparison between the surface potential decay curves of two different PET samples, similarly-charged at V_g=5.2 kV, and neutralized using a sinusoidal voltage *f*=210 Hz, *U*=20 kV.

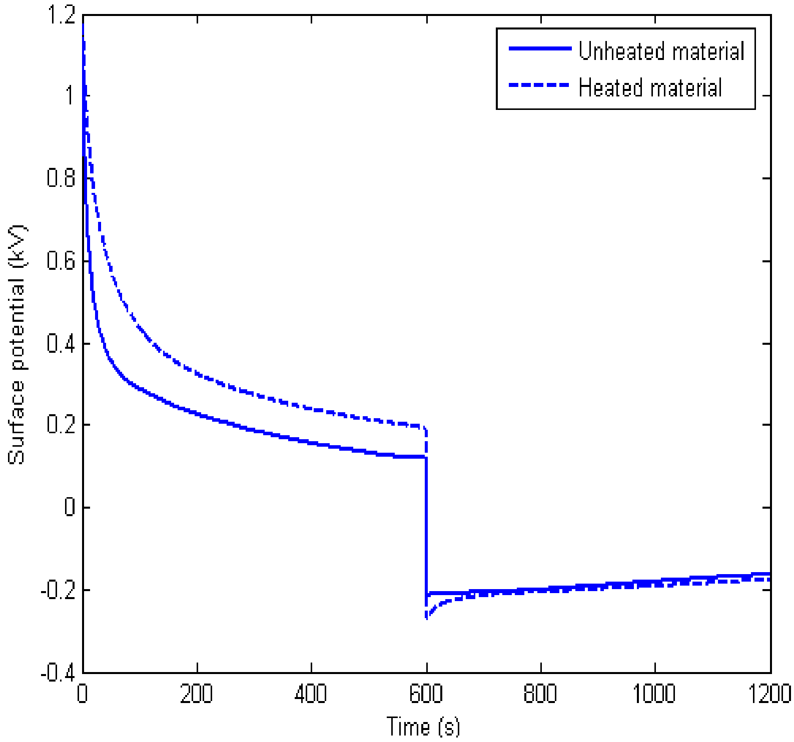

Figure 4.25. Comparison between the surface potential decay curves of two different PET samples, similarly-charged at V_g=5.2 kV, and neutralized using a sinusoidal voltage f=210 Hz, U=20 kV.

4.4 Conclusions

(1) The estimated surface charge density on non-woven PP fabrics is close to the Gauss limit in atmospheric air (26 μC/m^2), but it decreases to less than 2/3 of this value in less than 30 min. When heated to 75°C prior to corona-charging, the PP media lose less than 20% of their initial charge in 30 min.

(2) Surface potential decay measurement is an effective technique for assessing the neutralization of corona-charged non-woven media.

(3) The efficiency of the neutralization achieved with a commercial ion generator depends on the nature of the processed materials, the distance between the neutralizer and the substrate, the duration of exposure and the position of the sample with respect to the grounded electrode.

(4) The charge build-up on fibrous dielectrics, such as PP or PET, can be effectively eliminated by the use of corona electrodes energized from either sinusoidal or triangular AV high-voltage supplies.

(5) Within the experimental domain investigated in this paper, the efficiency of the neutralization typically increases with both the frequency and the amplitude of the neutralizing voltage.

(6) At similar amplitude and frequency, the sinusoidal high-voltage ensures a better elimination of the static charge than the triangular one, probably due to higher energy transfer in the discharge.

5 STUDY OF SOME ELECTROSTATIC HAZARDS

The important thing is not to stop questioning.

Curiosity has its own reason for existing.

Albert Eistein

Effects of electrostatic accumulation, that can cause negative effects of electrostatic attraction (ESA) of particles during MEMS fabrication, will be demonstrated in this chapter. Results that show such effects due to static charge accumulated on the silicon wafers and MEMS devices during non-automated micro and nanofabrication processes will be presented.

An example of the effects of such phenomena is exposed for the case of an electrostatic comb drive, where parts of the device are contaminated through ESA. The results of the electrostatic field measurements performed during the fabrication process of MEMS devices are shown and a solution for overcoming the ESA effects is proposed.

5.1 Rationale and method

Though focused on a peculiar application, the present study aims to point out the importance of ESD risk evaluation in a rapidly growing field of semiconductor industry: MEMS manufacturing.

5.1.1 Investigation rationale

During the last two decades, specialists from corporations such as Intel, Texas Instruments, IBM, National Semiconductors, Ion Systems, etc., have been joining their efforts through working groups and standards committees, such as ESDA and SEMATECH, to establish reliable static control programs that minimize the device damage and malfunctions during automated processing. Of particular actuality is the ESD protection research for deep-submicron technologies (low-k technology included), System On a Chip (SOC), SOI (SOInsulator), new CMOS RF circuits and interconnects [8], [10], [46]-[47], [50], [53], [69], [78]-[79].

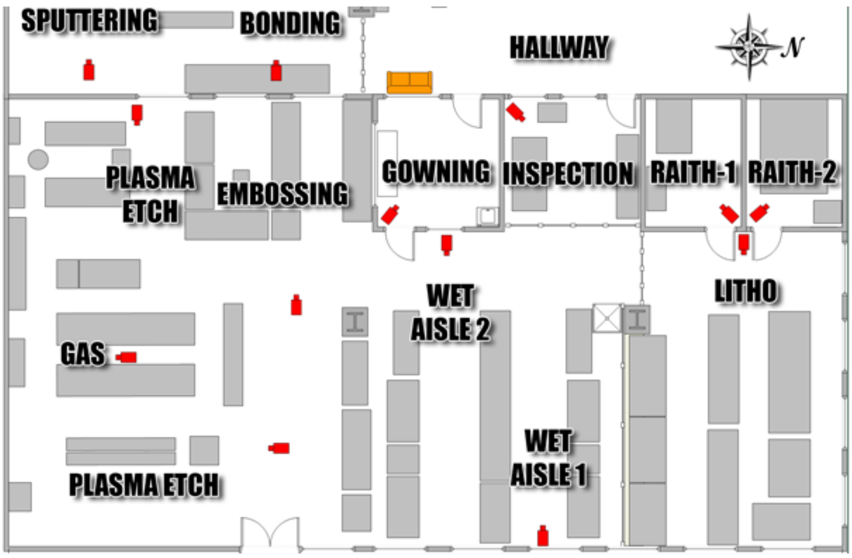

Figure 5.1. Typical plan of a nanofabrication facility

However, the fabrication and experimentation units for Micro and Nano Electro Mechanical Systems (MEMS, and NEMS), rarely involve automated processing and less demanding static requirements are commonly accepted. The level of static control in these small volume prototyping units (e.g. Figure 5.1) generally serves the purpose. Nevertheless, the rate of failure in such non-automated micro and nanofabrication units is high. The outcome of applying the same process sequence, the same recipe, is sometimes different and in many cases no scientific or methodological explanation can be found to the observed manufacturing failure. This does not suggest that static electricity is at the origin of all these failures. It first suggests that there is still much research to be done in order to list all the factors that impede experimentalists from obtaining better repeatability rate. Secondly, from the static electricity researchers' point of view, it incites to evaluating the role of static charge in some of these failures and to finding effective and inexpensive solutions to overcome static problems where they exist.

The present work is focused on evaluating the static electricity acquired by a set of silicon wafers during a very simple and common starting process in MEMS fabrication: cleaning with piranha solution. The relationship between the level of static electricity at the end of the cleaning process and the particle contamination level after some of the silicon wafers were exposed close to the sputtering machine – a real life scenario – was also analyzed. We then present the effect of the electrostatic charge accumulated on a final product, a MEMS device.

5.1.2 ESA and the clean room

Reported work, [11], [13], [159], discussions with nanofabrication technologists and members of standards committees on electrostatic discharge control [6] as well as the authors' observations suggested that static electricity is at the origin of some of the defects in the fabrication of micro and nanosystems. Preliminary measurements were conducted in a prototyping nanofabrication unit (Figure 5.1) and resulted in electrostatic fields as high as tens of kV/in in the wet etch area (Figure 5.2.a), cleaning decks (Figure 5.2.b), plastic and Teflon wafer cassettes, as well as glass containers.

a) b)

Figure 5.2. Test environment a) wet isle; b) cleaning deck.

High levels of static electricity were observed on Silicon wafers in the process. While Si is a semiconductor, the wafer oxide coating transforms the wafer into an insulator and makes it prone to static charge accumulation. Due to the dielectric nature of these materials, grounding does not eliminate the static charge accumulated on the surface. However, these highly charged objects are indispensable during product processing and come in contact with the product. Therefore, charge transfer takes place. The product (Si wafer or device in process) becomes charged by triboelectrification after contact and separation with the dissimilar materials in these objects [13], [30].

Surpluses of either negative or positive charges are accumulated on the surface of the product and contamination due to the electrostatic attraction (ESA) occurs. The contamination due to ESA occurs at much higher deposition rate than the contamination through sedimentation, which in the nanofabrication units is controlled through vertical unidirectional airflow. In some cases, ESA can produce movement of charged materials [69]. This last effect, although possible in microsystems, is not demonstrated in this work.

5.1.3 Measurement method and instrumentation

The electrostatic attraction (ESA) of airborne particles occurs as a result of the electric field produced by the charge accumulated on the surface of an object. Figure5.3.a shows the electric field lines from a charged surface, for example a wafer with SiO_2 underside coating [69], [78], [113].

As mentioned in the background chapter, the electric field produced by the surface charge is typically measured at a fixed distance from the surface with an Electrostatic

Fieldmeter (Figure 5.3.b.). The distance between the surface and the instrument used in this particular set of experiments is established optically. The used fieldmeter (Ion Systems, M 775, 0 to + 50 kV with 100 V resolution, accuracy: +- 5%) exhibits the required characteristics : it is of small dimensions - hand held type - and can be oriented perpendicular to the surface; it is ground referenced, capable of measuring the field magnitude and indicates the field direction [87].

Although this is a standard electrostatic field measurement technique, one limitation was encountered in the experiments. This limitation comes from the mismatch between the size of the charged surface generating the electrostatic field to be measured and the field of view of the instrument. In the first experiment, with the Si wafers, four-inch diameter wafers were processed. The surface of the wafers exceeded the field of view of the electrostatic fieldmeter. In literature [69], [113], the value of the electrostatic field on a wafer is referenced at a distance equal to one radius from the wafer surface It results that the distance between the fieldmeter probe to the surface in our case should have been precisely two inches for accurate reading to be obtained. Our fieldmeter optical device allows precise establishing of a fixed distance of one inch between the instrument and the target surface.

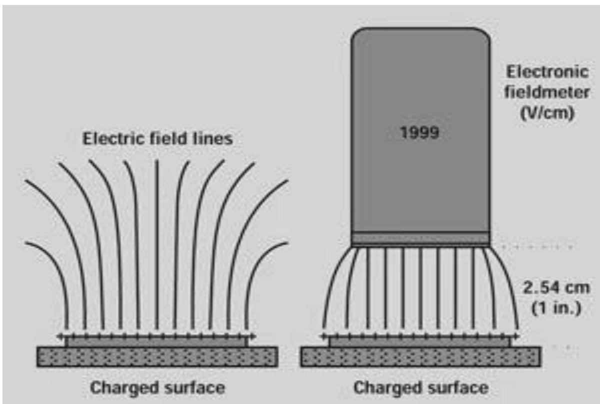

a) b)

Figure 5.3. Electric field produced by a charged surface. a) electric field lines. b) electric field measurement with an electrostatic fieldmeter. [112]

A method frequently used to overcome this limitation is linear extrapolation of the voltage at one inch from the center of the wafer [69]. At this stage of our research it was considered acceptable to measure the field at one-inch distance from the surface, scanned over the whole surface of the wafer, and average the values. The measurement error, considering a variation of 0.1 cm in distance while hand-holding the instrument is, for the 2.54 cm spacing, approximately 5 %.

Field measurements on a small product, a MEMS device, were not possible with this method. For measuring charge on the MEMS devices the Faraday cup charge measurement method, would have been more appropriate due to the size of the device. However, such instrument could not be brought into the facility.

To show the effect of static charge attraction on a final product as a result of processing, images with a Scanning Electron Microscope (SEM) were taken (Figure 5.4). The used SEM, LEO 1430, is equipped with a 4-quadrant backscattered electron detector.

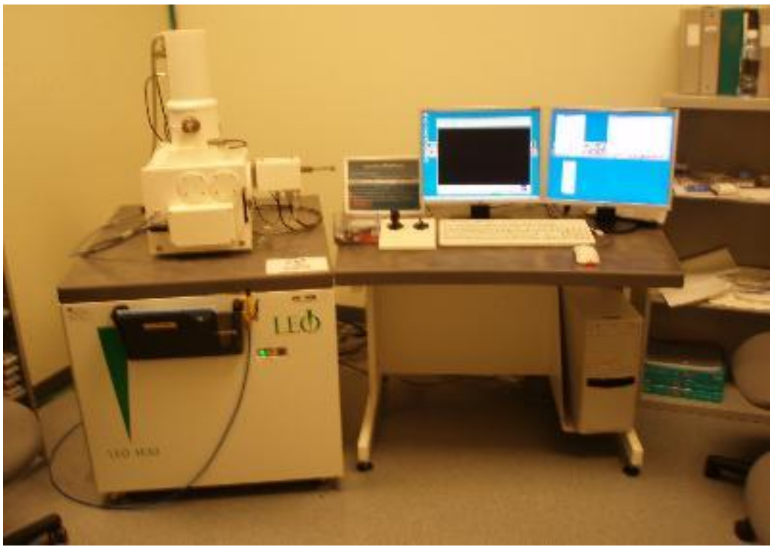

Figure 5.4. Setup for nanodevice photography

5.2 Measurements and ESA effects

Considering the high levels of electric field (of the order of tens of kV/in) preliminarily measured in the wet etching and cleaning area, the experimental approach [160] was to perform electrostatic field measurements on Si wafers during a simple and very frequent process, cleaning with piranha solution (Figure 5.2.b). The process also involved using plastic trays and glass containers from the metal shelf across the wet isle (Figure 5.2.a).

5.2.1 Voltage and particle measurements

Initially a set of ten new and manufacturer-cleaned silicon wafers was scanned in the cleanroom for contamination with particles over one micrometer diameter and the voltage on each wafer was measured using the method described in subsection 5.1.

Before processing, the number of particles on each Si wafer was insignificant: zero (on five wafers), one (on two wafers) and two (on three wafers). Only the results from five out of the ten wafers are shown in this work, the other five wafers were used as control, to verify the results. Before processing, the averaged absolute values of the voltages measured at a distance of one inch from the wafer surface are represented in Figure 5.5 in blue.

The electrostatic field on the plastic box holding the wafers was measured before and after unloading the wafers from the box. For measurements performed three inches apart on the box surface before unloading the wafers, the measured electrostatic field varied between −1.5kV/in and +12.5kV/in, whereas after unloading the wafers the field on the plastic box was measured between −6kV/in and −18kV/in. After unloading the tray, the electrostatic field on the tray surface was between −3kV/in and −19kV/in.

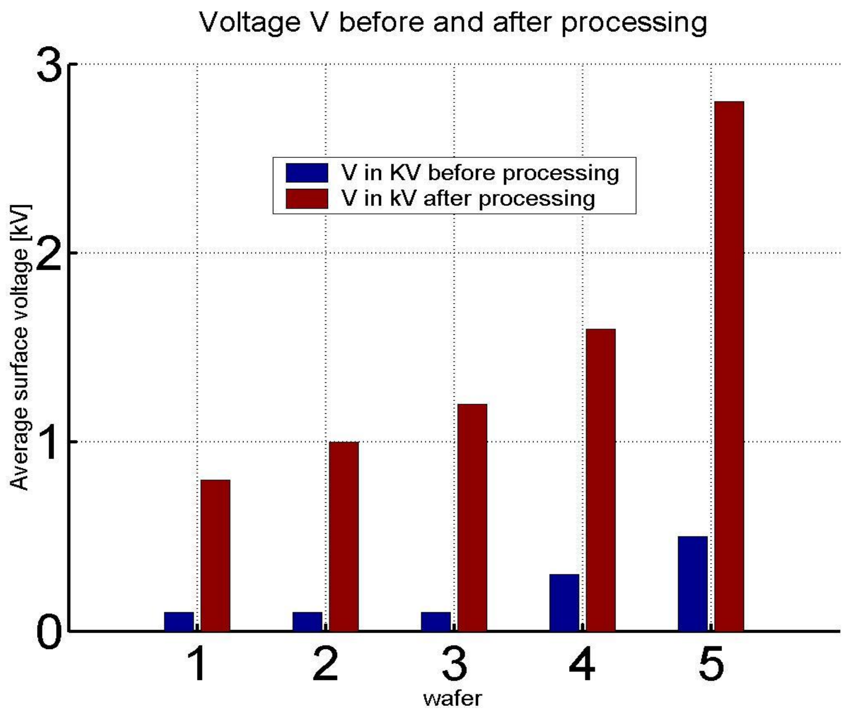

Figure 5.5. Comparison between the voltages measured at 1 in from the wafer surface before and after cleaning with piranha and drying.

The field on the Teflon cleaning cassette the wafers were transferred into and then submerged into the piranha solution was previously measured. Electrostatic fields between +6kV/in and +12kV/in were recorded prior to transferring the wafers to the Teflon cleaning cassette. The voltages at one inch distance from the trays and cassettes were monitored during handling the wafers from the cleaning tray to the storage trays after drying and then placing into the cassettes. The charge transfer phenomenon between the objects as a result of contact and separation was evident. However at this stage the charge transfer coefficients were not calculated. At the end of the process, the average of measured voltages at one inch from the wafers' surface varied between 800V and 13,000V, at least eight times higher than the initial voltage. The set of ten wafers was split in two subsets.

The first subset was formed from the wafers that displayed the lowest level of static electricity (800V to 2,800V) at the end of the process. Figure 5.5 compares the voltage at one-inch distance measured on the surface of these wafers at the end of the process with the voltage measured on the same wafers before the processing. In order to evaluate the wafer contamination due to the electrostatic charge accumulated during the process, these wafers were placed vertically, in order to avoid particle contamination through sedimentation, and then exposed out of the clean room close to the sputtering machine, – a real life scenario (Figure 5.1). The wafers were then scanned with a Tencor optical particle counter that was set successively to count particles of one microns, two microns and five microns. The result of particle counting on the five wafers, for which we compared the voltage in Figure 5.5, is represented in Figure 5.6.

In the case of the wafers that displayed smaller electrostatic fields the overall contamination is lower, whereas the contamination is considerably higher for the wafer of high static field, which is the case of wafer 5.

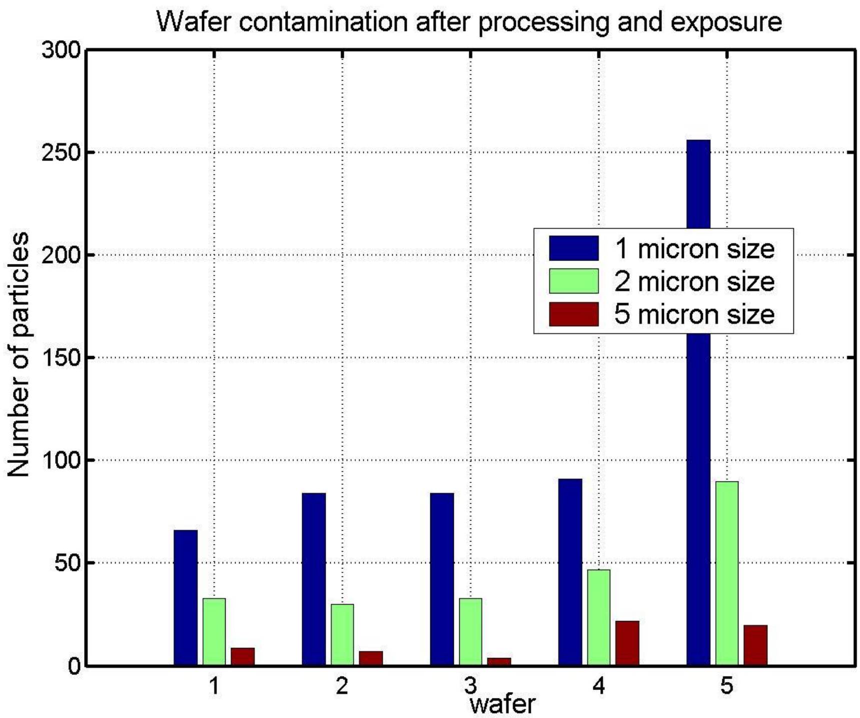

Figure 5.6. Number of particles on the wafer surface counted by size.

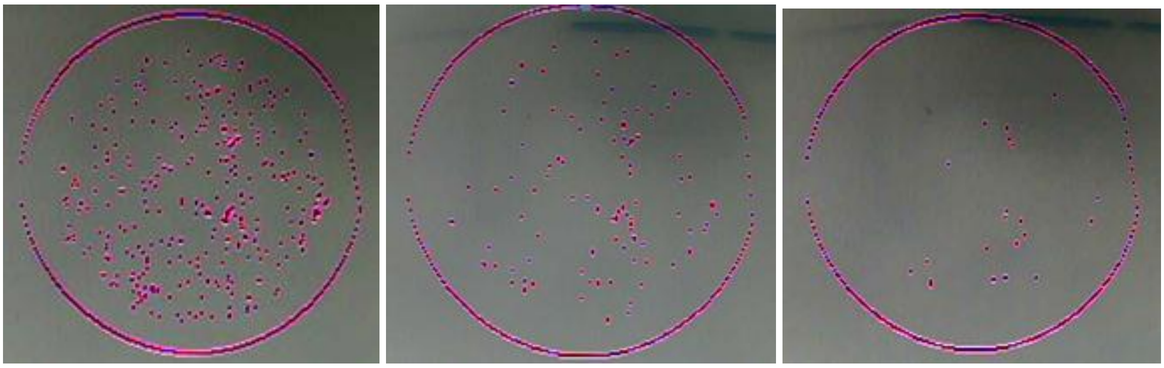

a) b) c)

Figure 5.7. Contamination count of wafer 5. a) one micron particles. b) two micron particles. c) five micron particles.

Figure 5.7 shows the contamination of wafer 5, which is represented also in Figure 5.6 by the last three bars of the graph. Figure 5.7.a represents the mapping of the contamination represented through the first bar of the last bar group in Figure 5.6. For this one-micron particle size 26 defect cells (clusters of particles) and 3 big areas of defects were identified. Figure 5.7.b is the map of the contamination represented in the next bar, for the two-micron particles, map in which two defect cells were found and no big area of defects. Figure 5.7.c shows the five-micron particles also represented in the very last bar of the Figure 5.6 graph. The scanner identified no big areas of defects at this particle size but one defect cell. It can also be observed that the wafer contamination is predominantly caused by electrostatic attraction, ESA, of smaller particles. From our experience and from published results [69], [113], [159], small particles create stronger bonds with the substrate and are then impossible to completely be removed from the surface. That is, once on the surface, they stay and will affect the following process, such as bonding, sputtering, etc.

In the beginning of this subsection, we mentioned that we measured and processed a set of ten wafers whereas we only showed the results from a subset of five wafers that exhibited the lowest electric field. The other set of wafers, on which we measured higher voltages (2.8kV to 13.5kV) after processing were also exposed vertically, not in the sputtering area but in the clean room. If the static electricity were not to be a factor in the wafer contamination, the level of contamination of the set exposed in the clean room would have been much lower than for the wafers exposed out of the clean room despite of the high static charge on their surface. The number of one-micron particles counted on the set of wafers exposed in the clean room for the same amount of time was 28, 31, 51, 76 and 85, which is smaller than in the previous case. However, for this particle size, a large number of defect cells were counted (78, 38, 3, 22, 21) on the wafers, numbers which are much higher than in the case of the wafers of lower static voltage exposed out of the clean room. The big areas of defects in the case of the wafers of higher static charge, exposed in the clean room, was also much higher (as high as 56) compared to the wafers exposed out of the clean room, where the maximum was 31. Considering the much lower concentration of airborne particles in the clean room, it results that the contamination was mainly due to electrostatic attraction of particles as a result of the electrostatic charge accumulated on the wafer, rather than sedimentation. Also, as the experiment indicated, a greater number of defective areas are present on a wafer when the static charge is higher even if the wafers are kept in the clean room.

5.2.2 ESA effects on MEMS

This subsection presents two examples of ESA contamination on MEMS devices as a result of charge accumulation during processing SOI (Silicon On Insulator) wafers into final products, two Electrostatic Comb Drives of different designs. The main processing steps will be outlined and images obtained with a scanning electron microscope will be shown in order to exemplify the effect of the ESA.

The SOI wafer was first cleaned with piranha solution. At the end of this process the field was measured at 6kV/in. No further field measurement were performed on this product. A SiO_2 layer was then grown on the cleaned wafer. We then divided the wafer in quarters, applied a layer of photoresist, transferred the mask pattern, developed, etched the SiO2 in the exposed areas, removed the photoresist with acetone and alcohol and spin-dried.

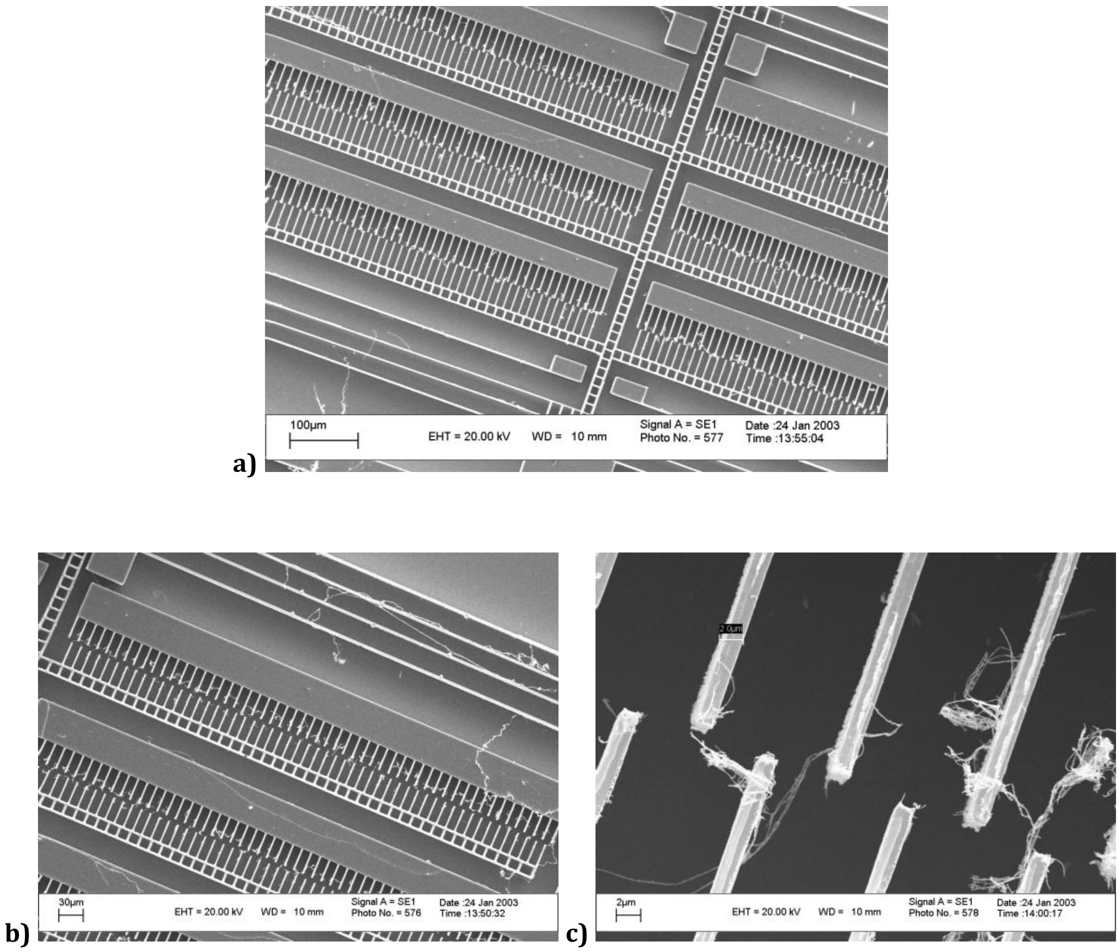

Figure 5.8. ESA on an electrostatic comb drive a) 100 micron scale, b) 30 micron scale, c) 2 micron scale

Figure 5.8 shows the electrostatic comb drive. Figure 5.8.a (on a 100 micron scale) images six comb pairs and shows that each of the pairs displays a quite significant contamination level towards the tips of the comb teeth. Figure 5.8.b (on a 30 micron scale) reveals that most of the contamination is attached to the immobile combs, effect also present in the second comb design in Figure 5.9.a. The immobile combs are solid with the large areas of insulator, which explains why charges accumulate on the surface of these comb teeth. As Figure 5.8.b and Figure 5.9. also show, a much lower number of particles, and smaller, are present on the mobile comb. This comb, of lighter structure, is of much lower surface and cannot accumulate as much charge as the surface of the fixed comb does. Laboratory analysis revealed that the material these devices were contaminated with is Teflon. The attracted Teflon frays are made more visible at 2 micron scale in Figure 5.8.cThis result makes sense knowing that Teflon is a material that MEMS devices frequently do come in contact with during processing. As charge accumulation can occur during SOI processing, the Teflon particles, at the bottom of the electrostatic series (§ 1.1.1), can be attracted to the device.

a) 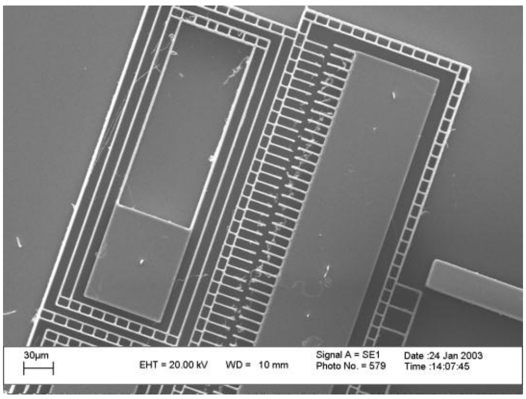

b) 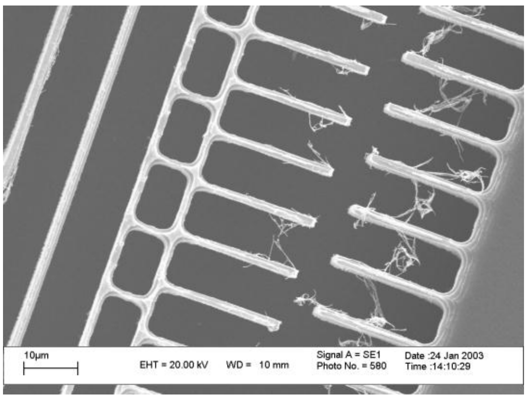

Figure 5.9. ESA on a different MEMS device a) 30 micron scale, b) 10 micron scale

The solution to these ESA problems is to ensure that the air conductivity is high enough to avoid the charge accumulation on the surface or to neutralize the charges accumulated on a surface. However, presently this is not part of the control program for the prototyping nanofabrication units. A more extensive study, involving the Ion Systems ionizers (subchapter 4.2) mounted on the wet deck and above the shelf across (Figure 5.2.a), was initially projected. However, this study could not be successfully carried on due to the drastic change in cleanliness quality, as well as price, of the manufacturer supplied wafers. The supplied wafers at the time of the planned second study were already highly contaminated, and a comparison with the presented study would have been irrelevant. On the other hand, as in the meantime the price-per-wafer had been significantly increased, the available number of wafers for the repetition of the study and the study in ionized air was not sufficient.

5.3 Conclusions

(1) Static electricity problems, particularly ESA, do occur during processing in MEMS prototyping units, and effective and economical solutions are required to overcome these problems.

(2) A more extensive study of the effects of ESA in prototyping units should be performed.

(3) Increasing the air conductivity in certain areas of the manufacturing unit is a possible solution to static electricity problems that should be tested in order to determine its effectiveness.

CONCLUSIONS AND PERSPECTIVES

On ne fait jamais attention à ce qui a été fait; on ne voit que ce qui reste à faire.

Marie Curie

The general conclusion of this work can be formulated as follows:

The refinement of the measuring methodology of the electrostatic charging of textile materials under various conditions is a prerequisite for the accurate evaluation of their ability to produce ESDs detrimental to electronic devices and systems.

The main scientific and technical contributions of this thesis are:

1. Accurate measurement of the static charge generated when walking on an insulating carpet

1.1. Increase the precision of the charge measurement by eliminating the parasitic capacitances, introduced by the long coaxial cable between the operator and the input of the electrostatic voltmeter.

1.2. Analyze and compare the charging of the operator in three practical situations: changing in protective clothing, walking on carpet, sitting at work bench.

1.3. Evaluate the efficiency of the new method to characterize the tribocharging levels of various combinations of carpet-shoe sole materials.

2. Design of a Faraday cage-based instrument for the measurement of the electric charge of textile materials

2.1. Improve the existing measurement techniques by eliminating the cable connection between the cup electrode and the electrometer instrument.

2.2. Elaborate the methodology for indirect measurement of the accumulated charge on the operator using the proposed Faraday instrument.

2.3. Characterize the accuracy of the indirect measurement versus the direct measurement of the accumulated charge on the human operator.

3. Critical analysis of two indirect methods of assessing the charging state of textile materials.

3.1. Establish an experimental protocol enabling the comparison between the electric field measurement and the surface potential monitoring, in relation with a variety of situations that can be encountered in industrial practice.

3.2. Characterize the accuracy of each of the two methods, in relation with a variety of situations that can be encountered in industrial practice.

3.3. Formulate recommendations of practical interest regarding the use of the two methods.

4. Evaluation of three methods of accelerated discharge of corona-charged non-woven fibrous dielectrics.

4.1. Analyze the factors that influence the efficiency of standard "AC ion generators" when used for the neutralization of textile materials.

4.2. Quantify the effects of wave shape and frequency of AC corona generators, when employed for the accelerated discharge of fibrous dielectrics.

4.3. Elaborate the methodology for the static control of filter materials on the production line.

5. Study of some electrostatic hazards in MEMS prototyping

5.1. Initiate, identify and evaluate static charge accumulation issues in research facility clean rooms during Si wafer processing for MEMS.

5.2. Measure the evolution of static charge level on Si wafers during chemical processing for MEMS.

5.3 Exemplify some damaging effects of undesirable charge accumulation during manufacturing of MEMS.

The present work pointed out some important aspects aimed at advancing the measuring methodology of the electrostatic charging of textile materials under various conditions, in view of determining their ability to produce detrimental ESDs. As a result of the experience gained during the completion of this study, future work should focus on the following issues:

1. Physical modeling of charge decay phenomena in fibrous dielectrics. By taking advantage of recent advancements in the modeling of planar, quasi-homogeneous polymer sheets, a specific physical model might be established for non-woven fibrous dielectrics. The model should take into account the ion-material interactions, the charge injection, the surface and volume conduction, as well as the effect of the non-homogeneous structure of these dielectrics, with the ultimate goal of rigorously controlling the charging state on such polymer structures during manufacturing.

2. Numerical modeling of charge build-up and dissipation in non-woven textile sheets. A three step approach is envisioned:

(1) construct a realistic geometrical model based on image acquisition from actual samples of various types of non-woven textiles;

(2) accurately describe the physical and electrical characteristics of each specific type of material;

(3) make use of appropriate physical models for the numerical simulation of charge dynamics on and within the material fibers.

3. Development of effective technical solutions for the reduction of ESD hazards in MEMS manufacturing. A more extensive study of the ESD phenomena in MEMS prototyping units should be performed, in order to achieve a much more comprehensive differentiation between the device failures due to the process itself and those due to the charge accumulation during manufacturing. One specific objective of such a study could be the evaluation of increasing the air conductivity in certain processing areas in clean rooms, as a solution to reduce ESD hazards.

BIBLIOGRAPHY

Homines dum docent discunt.

Seneca

[1] ESDA, *ESD Technology Roadmap*, Electrostatic Discharge Association www.esda.org/documents/2010ElectrostaticDischargeRoadmap.pdf, revised 2010.

[2] ESDA, *White Paper 1: A Case for Lowering Component Level HBM/MM ESD, Specifications and Requirements*, Electrostatic Discharge Association www.esda.org/IndustryCouncil.html, August 2008.

[3] ESDA, *White Paper 2: A Case for Lowering Component Level CDM ESD, Specifications and Requirements,* Electrostatic Discharge Association www.esda.org/IndustryCouncil.html, March 2009.

[4] Duvvury, C., "Paradigm shift in ESD qualification", *Proc. of 46th Annual IEEE International Reliability Physics Symposium* (April 27-May 1, Phoenix, AZ), IRPS 2008, pp. 1-2.

[5] Duvvury, C., private communication, Edmonton, CA, June 2005.

[6] Levit, L.B., private communication, Edmonton, CA, November 2002.

[7] Steinman, A., "Evaluating the Effectiveness of a CDM ESD Control Program*", Proc. ESA*, 2010, pp. 1-9.

[8] Amaresekera, A., Duvvury, C., *ESD in Silicon Integrated Circuits*. 2nd ed., John Wiley & Sons, New York, 2002.

[9] Boxleitner, W., *Electrostatic Discharge and Electronic Equipment: A Practical Guide for Designing to Prevent ESD Problems*, 1988.

[10] Dangelmayer, T.G., *ESD Program Management*, Kluwer Academic Publishers, Norwell, MA, 1999.

[11] Diaz, C.H., Kang, S.M., Duvvury, C., *Modeling of electrical overstress in integrated circuits*, Kluwer Academic Publishers, Norwell, MA, 1995.

[12] Gibson, N., "Static electricity — an industrial hazard under control?" *J. Electrostat.*, vol. 40-41, 1997, pp. 21-30.

[13] Greason, W.D., *Electrostatic Damage in Electronics: Devices and Systems,* Research Studies Press, Taunton, Somerset, UK, and, John Wiley & Sons, New York, 1987.

[14] Greason, W.D., *Electrostatic Discharge in Electronics*, John Willey & Sons, New York, 1992.

[15] Horvath, T., Berta, I., *Static Elimination*, Research Studies Press, Taunton, Somerset, UK, 1982.

[16] Kolyer, J. M., Watson, D. E., *ESD from A to Z*, 2nd ed., Kluwer Academic Publishers, Norwell, MA, 1999.

[17] Lacy, E.A., *Protecting Electronic Equipment from Electrostatic Discharge*, TAB Books Inc., Blue Ridge Summit, 1984.

[18] Lüttgens, G., Wilson, G., *Electrostatic Hazards*, Elsevier, Oxford, 1997.

[19] Mardiguian, M., *Electrostatic Discharge*, Interference Control Technologies Inc., Gainsville, 1993.

[20] McAteer, O.J., *Electrostatic Discharge Control*, McGraw Hill Publishing, New York, 1990.

[21] Oldervoll, F., "High electric stress and insulation challenges in integrated microelectronic circuits", *IEEE Electrical Insulation Magazine*, vol. 18-1, Jan.-Feb. 2002, pp. 16-20.

[22] Sclatter, N., *Electrostatic Discharge Protection for Electronics*, TAB Books, Blue Ridge Summit, 1990.

[23] Taylor, D.M., *Industrial Electrostatics*, John Willey & Sons, New York, 1994.

[24] Voldman, S., ESD: *Circuits and Devices*, John Wiley & Sons, New York, 2006.

[25] Dabral, S., Maloney, T.J., *Basic ESD and I/O Design*, Second Edition, John Wiley & Sons, 1998. (Intel)

[26] Feng, H.G., Zhan, R.Y., Wu, Q., Chen, G., Wang, A.Z., "Circular under-pad multiple-mode ESD protection structure for ICs", *Electronics Letters*, vol. 38, no.11, 2002, pp. 511-513.

[27] Golo, N.T., Kuper, F.G., Mouthaan, T.J., "Analysis of the electrical breakdown in hydrogenated amorphous silicon thin-film transistors", *IEEE Transactions on Electron Devices,* vol. 49, no. 6, 2002, pp. 1012-1018.

[28] Golo, N.T., van der Wal, S., Kuper, F.G., Mouthaan, T., "Estimation of the impact of electrostatic discharge on density of states in hydrogenated amorphous silicon

thin-film transistors", *Applied Physics Letters,* vol. 80, no. 18, 2002, pp. 3337-3339.

[29] Gong, K., Feng, H., Zhan, R., Wang, A.Z.H., "A study of parasitic effects of ESD protection on RF ICs"*, IEEE Transactions on Microwave Theory and Techniques,* vol. 50, no. 1, Jan. 2002, pp. 393-402.

[30] Greason, W.D., "Analysis of the Charge Transfer of Models for Electrostatic Discharge (ESD) and Semiconductor Devices", *IEEE Transactions on Industry Applications*, vol. 32, no. 3, May/June 1996, pp. 726-734.

[31] Ito, C., Banerjee, K., Dutton, R.W., "Analysis and design of distributed ESD protection circuits for high-speed mixed-signal and RF ICs"*, IEEE Transactions on Electron Devices,* vol. 4, no.8, 2002, pp. 1444-1454.

[32] Ker, M. D., Chen, T.Y., "Layout design to minimize voltage-dependent variation on input capacitance of an analog ESD protection circuit", *Journal of Electrostatics,* vol. 54, no. 1, 2002, pp 73-93.

[33] Kraz, V., Gagnon, J.E.P., "How good is your ground", *EE Evaluation Engineering*, vol. 41, no. 1, 2002, pp. 50-58.

[34] Kwang-Hoon, O., Duvvury, C., Banerjee, K., Dutton, R.W., "Analysis of gate-bias-induced heating effects in deep-submicron ESD protection designs", *IEEE Transactions on Device and Materials Reliability,* vol. 2. no 2, 2002, pp. 36-42.

[35] Maradei, F., Raugi, M., "Analysis of upsets and failures due to ESD by the FDTD-INBCs method", *IEEE Transactions on Industry Applications*, vol. 38, no. 4, 2002, pp.1009-1017.

[36] Markus P., Mergens J., Wilkening W., Kiesewetter G., Mettler S., Wolf H., Hieber J., Fichtner W., "ESD-level circuit simulation impact of interconnect RC-delay on HBM and CDM behavior", *Journal of Electrostatics*, vol. 54, no. 1, 2002, pp 105-125.

[37] Ming-Dou, K., Chien-Hui, C., "Electrostatic discharge protection design for mixed-voltage CMOS I/O buffers", *IEEE Journal of Solid-State Circuits*, vol. 37, no. 8, 2002, pp. 1046-1055.

[38] Ming-Dou, K., Chyh-Yih, C., "ESD protection design for CMOS RF integrated circuits using polysilicon diodes", *Microelectronics Reliability,* vol. 42, no. 6, 2002, pp. 863-872.

[39] Mohamedi, M., Takahashi, D., Itoh, T., Umeda, M., Uchida, L., "ESD fabricated thin films of spinel LiMn/sub 2/O/sub 4/ for lithium microbatteries: I. Effects of thickness", *Journal of the Electrochemical Society*, vol. 149, no. 1, 2002, pp. A19-25.

[40] Nagy, T.G., "Protect your high-speed circuits from ESD transients", *Electronic Design*, vol. 50, no. 14, 2002, pp. 53-56.

[41] Nikolaidis, T., Papadas, C., "Transmission gate switch for ESD protection of RF pad", *Electronics Letters*, vol. 38, no. 7, 2002, pp. 318-319.

[42] Parthasarathy, V., Khemka, V., Zhu, R., Whitfield, J., Bose, A., Ida, R., "A double RESURF LDMOS with drain profile engineering for improved ESD robustness", *IEEE Electron Device Letters*, vol. 23, no. 4, April 2002, pp. 212-214.

[43] Richier C., Salome P., Mabboux, G., Zaza I., Juge A., Mortini P., "Investigation on different ESD protection strategies devoted to 3.3 V RF applications (2 GHz) in a 0.18 µm CMOS process", *Journal of Electrostatics,* vol. 54, no. 1, 2002, pp. 55-71.

[44] Rouvroye, J.L., van den Bliek, E.G., "Comparing safety analysis techniques", *J. Reliability Engineering & System Safety*, vol. 75, no. 3, 2002, pp. 289-294.

[45] Tosic, G., N., Kuper, F.G., Mouthaan, T., "Zapping thin film transistors", *Microelectronics Reliability*, vol. 42, no. 4-5, 2002, pp. 747-765.

[46] Voldman, S.H., "Building an ESD Strategy: Bulk CMOS to SOI, Copper, Low-k, and SiGe", (Fourth Quarter 2000), *MicroNews* [IBM Online], vol. 6, no. 4, Available: http://www-3.ibm.com/chips/micronews/vol6_no4/voldman.html

[47] Voldman, S.H., "The state of the art of electrostatic discharge protection: physics, technology, circuits, design, simulation, and scaling", *IEEE Journal of Solid State Circuits*, vol. 34, no. 9, 1999, pp. 1272-1282.

[48] Voldman, S.H., Hui, D., Young, D., Williams, R., Dreps, D., Howard, J., Sherony, J., Assaderaghi, F., Shahidi, F., "Silicon-on-insulator dynamic threshold ESD networks and active clamp circuitry", *Journal of Electrostatics*, vol. 54, no. 1, January 2002, pp. 3-21.

[49] Wang, A.Z.H., *On-Chip ESD Protection for Integrated Circuits*, Kluwer, Dordrecht, 2002.

[50] SEMATECH 98013452A-TR - *Technology Transfer #, Test Structures for Benchmarking the Electrostatic Discharge (ESD) Robustness of CMOS Technologies*, SEMATECH Standard, February 1998.

[51] ESDA, *ESD Technology Roadmap*, Electrostatic Discharge Association www.esda.org, 2005.

[52] Horenstein, M.N., "Applied Electrostatics", in *Handbook of Engineering Electromagnetics,* R Bansal, Ed., Marcel Dekker, New York, 2004.

[53] Voldman, S.H., "Lightning Rods for Nanoelectronics", (2002, October issue), *Scientific American* [Feature Article - Online], 09/16/2002, Available: www.sciam.com/article.cfm?articleID=0005EE17-BE00-1D7F-90FB809EC5880000&pageNumber=1&catID=2.

[54] Barth, J., Richner, J., "Correlation considerations: real HBM to TLP and HBM testers", *Microelectronics Reliability*, vol. 42, no 6, 2002, pp. 909-917.

[55] Berndt H., "Studies on ESD- flooring material, especially the comparison of the measurement methods Walking test with normal resistance methods, microscopically explorations", *Proc. ESA*, Laplacian Press, 2004, pp. 271-279.

[56] Ficker, T., "Charging by walking", *J. Phys. D: Appl. Phys.,* vol. 39, 2006, pp. 410.

[57] Fujiwara, O., Kawa, T., "Numerical calculation of human-body capacitance by surface charge method", *Electronics and Communications in Japan*, vol. 1, 2002, pp. 38-44.

[58] Greason W. D., "Generalized model of electrostatic discharge (ESD) for bodies in approach: analyses of multiple discharges and speed of approach", *Journal of Electrostatics,* vol. 54, no. 1, 2002, pp. 23-37.

[59] Greason, W.D., "Investigation of potential differences for a three-body problem", *IEEE Transactions on Industry Applications*, vol. 38, no 4, 2002, pp. 996-1000.

[60] Greason, W.D., "Electrostatic discharge characteristics for the human body and circuit packs", *J. Electrostatics*, vol.59, 2003, pp. 285-300.

[61] Greason, W.D., "Analysis of the Charge Transfer of Models for Electrostatic Discharge (ESD) and Semiconductor Devices", *IEEE Trans. on Industry Applications*, vol. 32, no. 3, 1996.

[62] Jonassen, N., *Electrostatics*, 2nd ed., Kluwer Academic Publishers, Norwell, MA, 2002.

[63] Mayer, J.H., "Revised waveform drives ESD standards", *Test & Measurement World*, vol. 22, no. 3, 2002, pp. 43-44.

[64] Ono, H., Ohsawa, A., Tabata, Y. "New method for evaluating antistatic effect on floor coverings", *Journal of Electrostatics.,* vol. 57, no. 3-4, 2003, pp. 355-362.

[65] Seaver, A.E., "A mathematical justification for the simple HBC model", *Proceedings of ESA 2001*, Michigan State University, East Lansing, USA, June 2001.

[66] Antoniu, A., "Localization of the sources of the electroencephalogram", master's thesis, Dept. Electrical and Computer Engineering, University of Alberta, Edmonton, Canada, 2000. pp. 85.

[67] Antoniu, M., *Măsurări electronice,* Satya: Iasi, Romania, vol. 1 and 3, 2001 and 2002.

[68] Henry, L.G., Barth, J., Hyatt, H., Diep, T., Stevens, M., "Charged device model metrology: limitations and problems", *Microelectronics Reliability*, vol. 42, no 6, 2002, pp. 919-927.

[69] SEMI E78-0998, *Electrostatic Compatibility – Guide to Asses and Control Electrostatic Discharge (ESD) and Electrostatic Attraction (ESA) for Equipment,* SEMI Standard, 1998.

[70] *Protection of electrical and electronic parts, assemblies and equipment (excluding electrically initiated explosive equipment),* ESD Association standard ANSI/ESD S20.20, www.esda.org, 2007.

[71] *Electrostatics* Part 5-1*: Protection of electronic devices from electrostatic phenomena – general requirement,* International Electrotechnical Commission (IEC) Standard IEC 61340 5-1, www.iec.org, 2007-2008.

[72] *ESD sensitivity testing, charged device model, component level*, ESDA standard ANSI/ESD S5.3.1, www.esda.org, 2009.

[73] Caccavo, G., Cerri, G., Primiani, V.M., Pierantoni, L., Russo, P*.,* "ESD field penetration into a populated metallic enclosure a hybrid time-domain approach", *IEEE Transactions on Electromagnetic Compatibility,* vol. 44, no. 1, 2002, pp. 243-249.

[74] Cerri, G., Chiarandini, S., Costantini, S., De Leo, R., Mariani Primiani, V., Russo, P*.,* "Theoretical and experimental characterization of transient electromagnetic fields radiated by electrostatic discharge (ESD) currents", *IEEE Transactions on Electromagnetic Compatibility,* vol. 44, no. 1, 2002, pp. 139-147.

[75] Cerri, G., De Leo, R., Primiani, V.M., Pennesi, S., "Modeling of electromagnetic interference induced by electrostatic discharge (ESD) inside resonant structures", *IEEE Transactions on Electromagnetic Compatibility*, vol. 44, no.1, 2002, pp. 192-202.

[76] Hamada, L., Otonari, N., Iwasaki, T., "Measurement of electromagnetic fields near a monopole antenna excited by a pulse", *IEEE Transactions on Electromagnetic Compatibility*, vol. 44, no.1, 2002, pp. 72-78.

[77] Mayer, J.H., “Link EMI to ESD events", *Test & Measurement World*, vol. 22, no.3, 2002, pp. 39-40.

[78] Steinman, A., Bernie, J.C., Boehm, D., Albano, T., Tan, W., Pritchard, D.L., "Detecting ESD Events in Automated Processing Equipment", *Compliance Engineering,* Canon Communications LLC, Los Angeles, USA, September/October 2000.

[79] Steinman, A., Levit, L.B., "It’s the Hardware. No, Software. No, It’s ESD!", *Solid State Technology,* vol. 42*,* no.5, 1999.

[80] Vladimir, K., Albert, W., "The effects of EMI from cell phones on GMR magnetic recording heads and test equipment", *Journal of Electrostatics*, vol. 54, no. 1, 2002, pp. 39-53.

[81] Levit, L.B., Henry, L.G., Montoya, J.A., Marcelli, F.A., Lucero, R.P., "Investigating FOUPs as a source of ESD-induced electromagnetic interference"*, Micro*, vol. 20, no. 4, 2002, pp. 41-48.

[82] Antoniu, A., Manne, J., Tulip, J., Jaeger, W., "Challenges and Packaging Solutions in Portable QC Laser Systems for Open Path Atmospheric Gas Detection", *Proceedings of the Electrostatics Society of America* - University of Alberta – June 2005, Laplacian Press, Morgan Hill, CA, ISBN 1-885540-17-5, 2005, pp 143-144.

[83] Rudack, A.C, Pendley, M., Levit, L., "Measurement technique developed to evaluate transient EMI in a photo bay", *Journal of Electrostatics*, vol. 54, no. 1, 2002, pp. 95-104.

[84] Horenstein, M.N. "Measurement of Electrostatic Fields, Voltages, and Charges", in *Handbook of Electrostatic Processes*, J.S. Chang and J. Crowley, eds. Marcel Dekker, New York, 1995.

[85] Osei, K.N. "Measurement of Electrostatic Charge on Protective Clothing on Low Humidity", master's thesis, Dept. of Human Ecology, University of Alberta, Edmonton, Canada, 1992.

[86] Child, A., Deangelis, A.R., "*Static dissipative textile*", US Patent 20070270063, 2007.

[87] Vosteen, W.E., "A Review of Current Electrostatic Measurement Techniques and their Limitations", Presented at the Overstress Exposition, San Jose, CA, April 24-26, 1984.

[88] Wobschall, D., *Circuits For Electronic Instrumentation*, New York (McGraw-Hill) 1987.

[89] Horenstein, M.N., "Measuring isolated surface charge with a noncontacting voltmeter", *Journal of Electrostatics*, 35, 1995, 203-214.

[90] Noras, M.A., "Non-contact surface charge/voltage measurements. Fieldmeter and voltmeter methods", *Trek Application Note 3002*, 2002.

[91] Noras, M.A., "Non-contact surface charge/voltage measurements. Capacitive probe – principle of operation," *Trek Application Note 15001*, 2002.

[92] Molinié, P., Llovera, P., "Surface potential measurements: implementation and

interpretation," *Dielectric Materials, Measurements and Applications. IEE Conference Publication No. 473*, 2000, pp. 253 – 258.

[93] Llovera, P., Molinie, P., Soria,A., Quijano,A., "Measurements of electrostatic potentials and electric fields in some industrial applications: Basic principles", *J. Electrostat.,* vol. 67:2-3, pp. 457-461, 2009.

[94] Chen, G., Xu, Z., Zhang, L.W., "Measurement of the surface potential decay of corona-charged polymer films using the pulsed electroacustic method," *Meas. Sci. Technol.*, vol. 18, pp. 1453-1458, 2007.

[95] Chubb, J.N., "The assessment of materials by tribo and corona charging and charge decay measurement," *IoP Conf Series 163- Electrostatics 1999*, Cambridge, March 1999, pp. 329-333.

[96] Coelho, R., "On the significance of charge decay measurements in insulators," *IEEE Proc. 3rd Int. Conf. on Conduction and Breakdown in Solid Dielectrics*, 1989, pp. 212-217.

[97] Das Gupta, D.K., "Surface charge decay on insulating films," *IEEE Int. Symp. on Electrical Insulation*, Boston, 1988, pp. 296-299.

[98] Davidson, J.L., Williams, T.J., Bailey, A.G., Hearn, G.L., "Characterization of electrostatic discharges from insulating surfaces", *J. Electrostatics*, vol 51-52, 2001, pp. 374-380.

[99] Debska, M., "Surface potential decay on triglycine sulfate crystal," *J. Electrostat*, vol. 63, pp. 1017-1023, 2005.

[100] Horenstein, M.N., "Surface charging limit for a woven fabric on a ground plane", *Journal of Electrostatics*, 35 (1995) 31-40

[101] Ieda , M., Sawa, G., Shinohara, I., "A decay process of surface electric charge across polyethylene film," *Jpn. J. Appl. Phys.*, vol. 6, pp. 793-794, 1967.

[102] Molinié, P., Goldman, M, Gatellet, J., "Surface potential decay on corona-charged epoxy samples due to polarization processes," *J. Phys D: Appl. Phys*., vol. 28, pp. 1601-1610, 1995.

[103] Molinié, P., Goldman, M., Gatellet, J. "Surface potential decay on corona-charged epoxy samples due to polarization processes," *J. Phys D: Appl. Phys*., vol. 28, pp. 1601-1610, 1995.

[104] Pouillès, V., Lebey, T, Castelan, P, "Determination of the very-low frequency characteristics of dielectric materials: A surface potential approach," *J. Appl. Phys*., vol. 79, pp. 8620-8628, 1996.

[105] Tabti, B., Mekideche, M., Plopeanu, M., Dumitran, L.M., Herous, L., Dascalescu, L., "Corona charging and charge decay characteristics of non-woven filter media," *Conf. Rec. IEEE/IAS Ann. Meet.,* Edmonton, Alberta, Canada, 5-9 Oct. 2008, pp. 1-6.

[106] Wintle, H.J., "Surface-charge decay in insulators with non-constant mobility and with deep trapping," *J. Appl. Phys.*, vol. 43, pp. 2927-2930, 1973.

[107] Kacprzyk, R., Mista, W., "Back corona in fabrics," *Fibers and Textiles in Eastern Europe*, vol. 14, pp. 35 – 38, 2006.

[108] Greason, W.D., Beyer, B.H., "Corona charging method for controlled production of

film electrets," *IEEE Trans. Ind. Appl.*, vol. 20, 1984, pp. 687-693.

[109] Young, R.H., "Kinetics of xerographic discharge by surface charge injection," *J. Appl. Phys*, vol. 72, pp. 2993-2999, 1992.

[110] Lewis, T.J., "Charge transport, charge injection and breakdown in polymeric insulators," *J. Phys. D: Appl. Phys*., vol. 23, pp. 1469-1478, 1990.

[111] Molinié, P., "Charge injection in corona-charged polymeric films: potential decay and current measurements," *J. Electrostat*., vol. 45, pp. 265-273, 1999.

[112] Levit L.B., Steinman, A., "Investigating static charge issues in photolithography areas", *Micro,* Cannon Communications LLC, Los Angeles, USA, June 2000.

[113] Levit, L.B., Hanley, T.M., Curran, F., "In 300mm Contamination Control Watch Out for Electrostatic Attraction", *Solid State Technology,* June 2000.

[114] Koch, D., Molinié, P., "Cavity detection on organic coatings by electrostatic measurements. A detailed study using FR4 fiberglass epoxy laminates," *J. Electrostat*., vol. 66, pp. 467-475, 2008.

[115] Antoniu, M., Antoniu, A., Fosalau, C., Matei, L., "A Capacitive Angular Speed Sensor with Electret", *Proc. ESA and IEEE IAS Electrostatics Process Committee Joint meeting* - University of Arkansas, Laplacian Press, Morgan Hill, California, USA, 2003.

[116] Antoniu, M., Matei, L., Munteanu, D., "A Simple Method for Range Switching of Electrostatic Fieldmeter", *Proc. ESA*, Laplacian Press, 2001, pp. 203-210.

[117] Matei, L., Antoniu, A., David, V., Istoc, R., "Two Solutions for Polarity Detector of Electrostatic Field Modulator", *Proceedings of the 2002 ESA-ESJ Joint Meeting* at Northwestern University, Laplacian Press, Morgan Hill, California, ISBN 1-885540-14-0, pp. 325-331, June 2002

[118] Inculeţ, I., "The Present Position of the Electrostatics in the Environment Protection and the Canadian Experience", Simpozionul Internaţional sub egida NATO "The Modern Problems of Electrostatics with Applications in Enviroment Protection", Bucureşti, 9-12 Nov. 1998.

[119] Luca E., Zet, G., *Fizica*, Interacţiuni, câmpuri şi unde, vol. 2, Ed. Ştiinţifică, Bucureşti, 1996.

[120] Rosman, H., *Bazele teoretice ale câmpului electromagnetic*, vol. 1 Electrostatica, Ed. "Gh. Asachi", Iaşi, 1997.

[121] Tănăsescu, F.T., Cramariuc, R., Munteanu, V., *Electrotehnologii. Electrostatica*, vol.1, Ed. Academiei Române, Bucureşti, 2000.

[122] ESD-STM 7.1, *"Resistance Characterization of Floor Materials",* ESDA Standard, 2001.

[123] ESD STM 97.2-1999 Floor Materials and Footwear – Voltage Measurement in Combination with a Person, 1999.

[124] ANSI/ESDA/JEDEC JS-001, *"Electrostatic Discharge Sensitivity (ESD) Testing – Human Body Model (HBM) – Component Level",* ESD Association and JEDEC Solid State Technology Association standard, 2010.

[125] McGonigle, D.F., Jackson, C.W., Davidson, J., "Triboelectrification of houseflies (Musca domestica L.) walking on synthetic dielectric surfaces", *Journal of Electrostatics*, vol. 54, (2), pp. 167-177. 2002.

[126] Antoniu, A., Antoniu, M., Fosalau, C., Matei, L., Forin, A., "Researches Regarding the Electrostatic Charge in Electronic Industry', Working Rooms', *Proceedings of 5th International Power Systems Conference*, Timisoara, Romania, 2003, pp. 27-38.

[127] Electrostatic Instrumentation Catalog, Monroe Electronics, 1998, pp. 12.

[128] Antoniu, M., Antoniu, A., "A measurement method of the electrostatic charge at garment removal off a human operator", *Proc. ESA*, Laplacian Press, Morgan Hill, CA, 2004, pp. 254-262.

[129] Antoniu, M., Antoniu, A., Antoniu, G., Cotnareanu, F., "Faraday Cup Based Instrument for the Triboelectric Charge Measurement in Textile Manufacturing", *Proc. ESA,* Laplacian Press, Morgan Hill, CA, USA, 2005, pp. 145-152.

[130] Dascalescu, L., Iuga, A., Morar, R., Neamtu, V., Saurasan, I., Samuila, A., Rafiroiu, D., "Corona and electrostatic electrodes for high-tension separators," *J. Electrostat*., vol. 29, pp. 211-225, 1993.

[131] Oda, T., Ochiai, J., "Charging characteristics of a non-woven sheet air filter," *Proceedings 6th Int. Symp. on Electrets*, 1-3 Sept. 1988, pp. 515 – 519.

[132] Giacometti, J.A., Oliveira, Jr., O.N., "Corona charging of polymers", *IEEE Trans. Electr. Insul.,* vol. 27, pp. 924–943, 1992.

[133] Dascalescu, L., Medles, K., Das, S., Younes, M, Caliap, L., Mihalcioiu, A., "Using Design of Experiments and Virtual Instrumentation to Evaluate the Tribocharging of pulverulent materials in compressed-air devices", *IEEE-IAS Transactions*, vol. 44, pp. 3-8, 2008.

[134] Tabti, B., Mekideche, R., Plopeanu, M., Dumitran, L.D., Antoniu, A., Dascalescu, L., "Factors that influence the Decay Rate of the Potential at the Surface of Non-woven Fabrics after Negative Corona Discharge Deposition", *IEEE Transactions in Industry Application*, vol. 46, no. 4, 2010, 1586-1592.

[135] Ji, Z.B., Xia, Z.F., Shen, L.L., An, Z.L., "Charge storage and its stability in corona charged polypropylene non-woven fabrics used as air filters," *Wuli Xuebao/Acta Physica Sinica*, vol. 54, no. 8, 2005, pp. 3799-3804.

[136] Dascalescu, L., Plopeanu, M.C., Tabti, B., Antoniu, A., Dumitran, L.M., Notingher, P.V., "Corona Charging of Composite Non-woven Media for Air Filtration", *Proceedings of the Electrostatics Society of America* – paper D3, June 22-24, 2010.

[137] Plopeanu, M.C., Tabti, B., Antoniu, A., Noţingher, P.V., Dumitran, L.M., Dăscălescu, L., "Surface Potential Decay of Charged Non-Woven Media for Air Filtration", *Proceedings of the 7th Conference of the French Society of Electrostatics SFE 2010*, Montpellier, France, 30 August – 1 Sept., 2010, pp; 238-242.

[138] Myers, D.L., Arnold, B.D., "Electret media for HVAC filtration applications," *INJ Winter*, 2003, pp. 43-54.

[139] Hutten, I.M., *Handbook of Nonwoven Filter Media.* Oxford: Elsevier, 2007.

[140] Kacprzyk, R., "Non-conventional application of unwoven fabrics," *J. Electrostat.*, vol. 56, 2002, pp. 111-119.

[141] Antoniu, A., Dascalescu, L., Vacar, I.V., Plopeanu, M.C., Tabti, B., Teodorescu, H.N., "Surface Potential vs. Electric Field Measurements as Means to Characterize the Charging State of Non-Woven Fabrics", *Proceedings of the IEEE IAS Annual Meeting, Houston*, USA, 3 – 7 Oct, 2010.

[142] Brown, R.C., *Air filtration—An Integrated Approach to the Theory and Applications of Fibrous Filters*, Oxford: Pergamon Press, 1993.

[143] Lathrache, R., Fissan, H., "Enhancement of particle deposition in filters due to electrostatic effects," *Filtration & Separation*, vol. 24, 1987, pp. 418-422,.

[144] Smith, P.A., East, G.C., Brown, R.C., Wake, D., "Generation of triboelectric charge in textile fibre mixtures and their use as air filters", *J. Electrostat.*, vol. 21, 1988, pp. 81-98.

[145] Holme, I., McIntyre, E., Shen, Z.J., *Electrostatic Charging of Textiles*, Manchester: Taylor and Francis, 1998, pp. 1-85.

[146] Harper, C.A., *Handbook of plastics, elastomers, and composites*, 4th Edition, New York: McGraw-Hill, 2002, pp. 53-862.

[147] van Turnhout, J., Hoeneveld, W.J., Adamse, J.W.C., van Rossen, L.M., "Electret filters for high efficiency and high flow air cleaning," *IEEE Trans. Ind. Appl.*, vol 17, no. 2, 1981, pp. 240–248,.

[148] Walsh, D.C., Stenhouse., J.I.T., "Parameters affecting the loading behavior and degradation of electrically active filter materials," *Aerosol Science and Technology,* vol. 29, 1998, pp. 419-432.

[149] Tabti, B., Dascalescu, L., Plopeanu, M., Antoniu, A., Mekideche, M., "Factors that influence the corona-charging of fibrous dielectric materials," *J. Electrostat.*, vol. 67, issues 2-3, 2009, pp. 193-197.

[150] Antoniu, A., Tabti, B., Plopeanu, C.M., Dascalescu, L. "Accelerated discharge of corona-charged non-woven fabrics," *IEEE Trans. Ind. Appl*., vol. 46, no. 3, 2010, pp. 1188-1193.

[151] Antoniu, A., Vacar, I.V., Plopeanu, M.C., Dascalescu, L., "Factors that Influence the Accelerated Discharge of Non-Woven PP and PET Fabrics", *Proceedings of the 7th Conference of the French Society of Electrostatics SFE 2010*, Montpellier, France, 30 August – 1 Sept., 2010, pp. 232-237.

[152] Baumgartner, U., "Particle collection in electret fibers filters; a basic theoretical and experimental study," *Filtration & Separation,* vol. 24, 1987, pp. 346-351,.

[153] Romay, F.J., Liu, B.Y.H., Chae, S.J., "Experimental study of electrostatic capture mechanisms in commercial electret filters", *Aerosol Sci. &Technol.*, vol. 28, pp. 1998, 224–234.

[154] Nifuku, M., Zhou, Y., Kisiel, A., Kobayashi, T., Katoh, H., "Charging characteristics for electret filter materials," *J. Electrostat.*, vol. 51-52, 2001, pp. 200-205.

[155] Hu, Z., and H. Von Seggern, "Air-breakdown charging mechanism of fibrous polytetrafluoroethylene films," *J. Appl. Phys.*, vol. 98, no. 1, 2005, pp. 1-4.

[156] Siag, A.M., Tennal, K.B., Mazumder, M.K., "Determination of fiber charge density of electret filters," *Particulate Sci. & Technol.,* vol. 12, no. 4, 1994, pp. 351-365.

[157] Frigon, N.L., Mathews, D., *Practical Guide to Experimental Design*. New York: Wiley, 1996.

[158] Eriksson, L., Johansson, E., Kettaneh-Wold, N., Wikström, C., Wold, S., *Design of Experiments. Principles and Application,* Stockholm: Learnways AB, 2000.

[159] Schmidt, M.A., "Wafer-to-Wafer Bonding for Microstructure Formation", *Proceedings of the IEEE,* vol. 86, No. 8, August 1998.

[160] Antoniu, A, Salomons, M., Reus, N., "Effects of Electrostatic Charge Accumulation During MEMS Fabrication Process", *Proceedings of* t*he 2003 International Conference on MEMS, NANO, and Smart Systems Proceedings,* Banff, Canada, 2003, pp. 69-75.

[

Contributions à l'étude de certains effets électrostatiques nuisibles dans le processus de fabrication des dispositifs et circuits électroniques

Les risques des décharges électrostatiques (DES) sur des dispositifs et systèmes électroniques dépend de l'état de charge de l'opérateur et des objets situés à proximité. Cette thèse a eu comme objectif de contribuer à la mise au point d'une méthodologie de mesure pour caractériser l'état de charge des opérateurs et des matériaux textiles, afin d'établir leur capacité de produire DES nuisibles. Des méthodes de mesure directes et indirectes ont été proposées pour l'évaluation de la charge des opérateurs dans trois situations d'intérêt pratique. D'autres techniques, telles que la mesure de potentiel de surface et de l'intensité du champ électrique ont été utilisées pour le monitoring de l'état de charge des matériaux textiles. Des modèles comportementaux ont été établis pour la charge et la décharge de ces matériaux, en faisant appel à la méthodologie des plans d'expériences. Les essais réalisés sur des échantillons de polypropylène et de polyester ont permis de valider aussi deux méthodes permettant d'accélérer la diminution de la charge des médias isolants non-tissés en utilisant des générateurs d'ions ou des décharges couronne produites par des électrodes alimentées à des hautes tensions sinusoïdales ou triangulaires, de fréquences allant jusqu'à 400 Hz. Un exemple d'accumulation d'électricité statique sur une plaquette de silicium est aussi discuté, en rapport avec une application à la fabrication des microsystèmes électromécaniques. L'amélioration de la méthodologie de mesure est un pré-requis pour l'adoption des meilleures stratégies destinées à maîtriser les risques électrostatiques dans un environnement industriel.

Contributions to the study of certain electrostatic hazards in the manufacturing process of electronic devices and circuits

The risk of electrostatic discharge (ESD) on electronic devices and systems depends on the charge state of the operator and nearby objects. This thesis aimed at contributing to the development of a measurement methodology to characterize the state of charge of the operators and textile materials, in order to determine their ability to produce harmful effects. Direct and indirect measuring methods have been proposed for assessing the charge of operators in three situations of practical interest. Other techniques, such as surface potential and electric field intensity measurements were used for monitoring the state of charge of textile materials. Behavioural models have been established for the charging and discharging of these materials, using the methodology of experimental design. Tests on samples of polypropylene and polyester have also validated two methods for accelerating the reduction of the charge of insulating nonwoven media using ion generators or corona discharge produced by electrodes energized from sinusoidal or triangular high voltage supplies, at frequencies up to 400 Hz. An example of static electricity on a silicon wafer is also discussed in relation with an application to the fabrication of mechanical and electronic micro-systems. Refinement of the measurement methodology is a prerequisite for the adoption of best strategies to control electrostatic risks in an industrial environment.